14. Outros métodos de detecção de exoplanetas

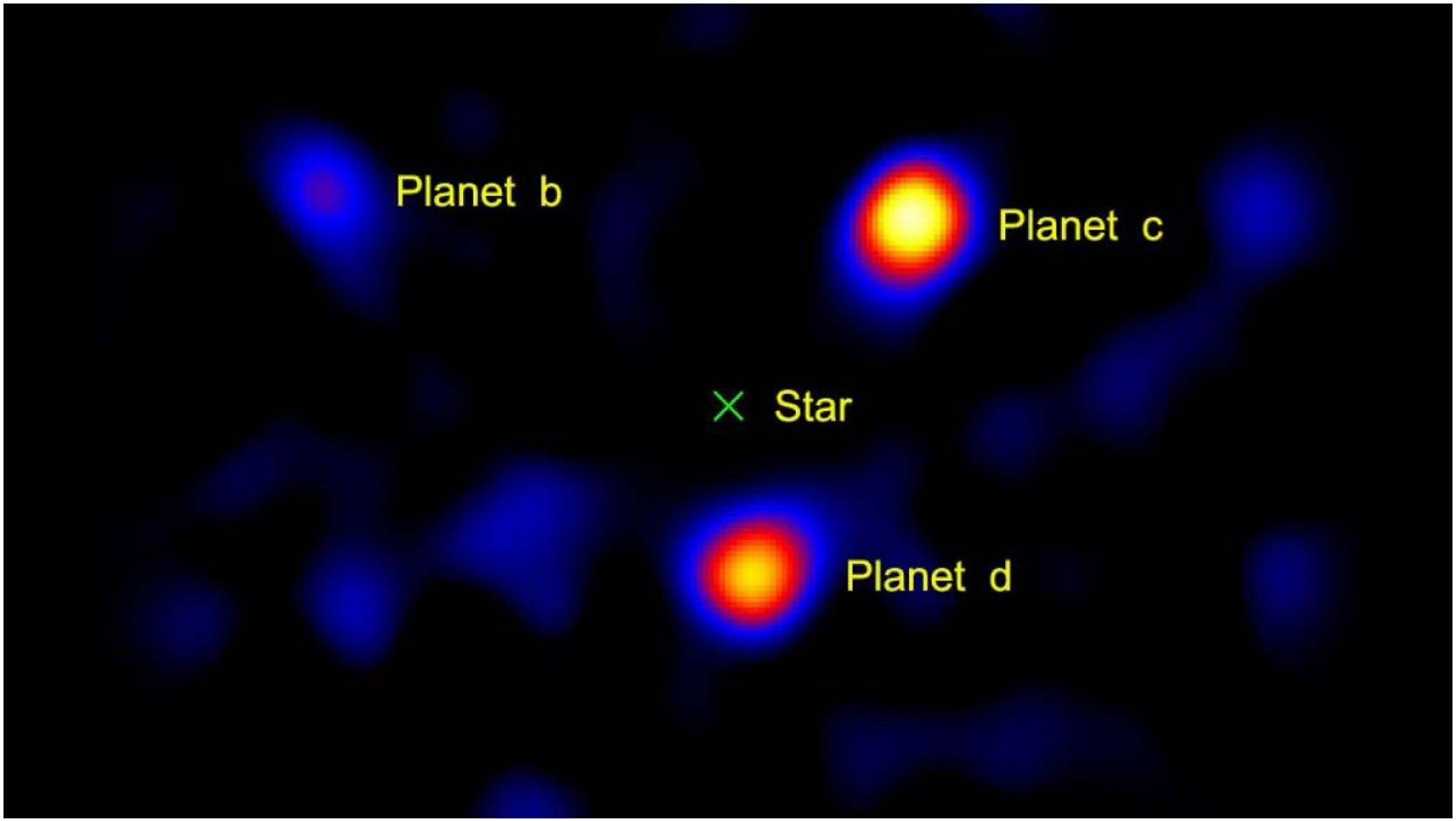

Direct image of exoplanets around the star HR8799 using a Vortex coronagraph on a 1.5m portion of the Hale telescope.
Credit: NASA/JPL-Caltech/Palomar Observatory

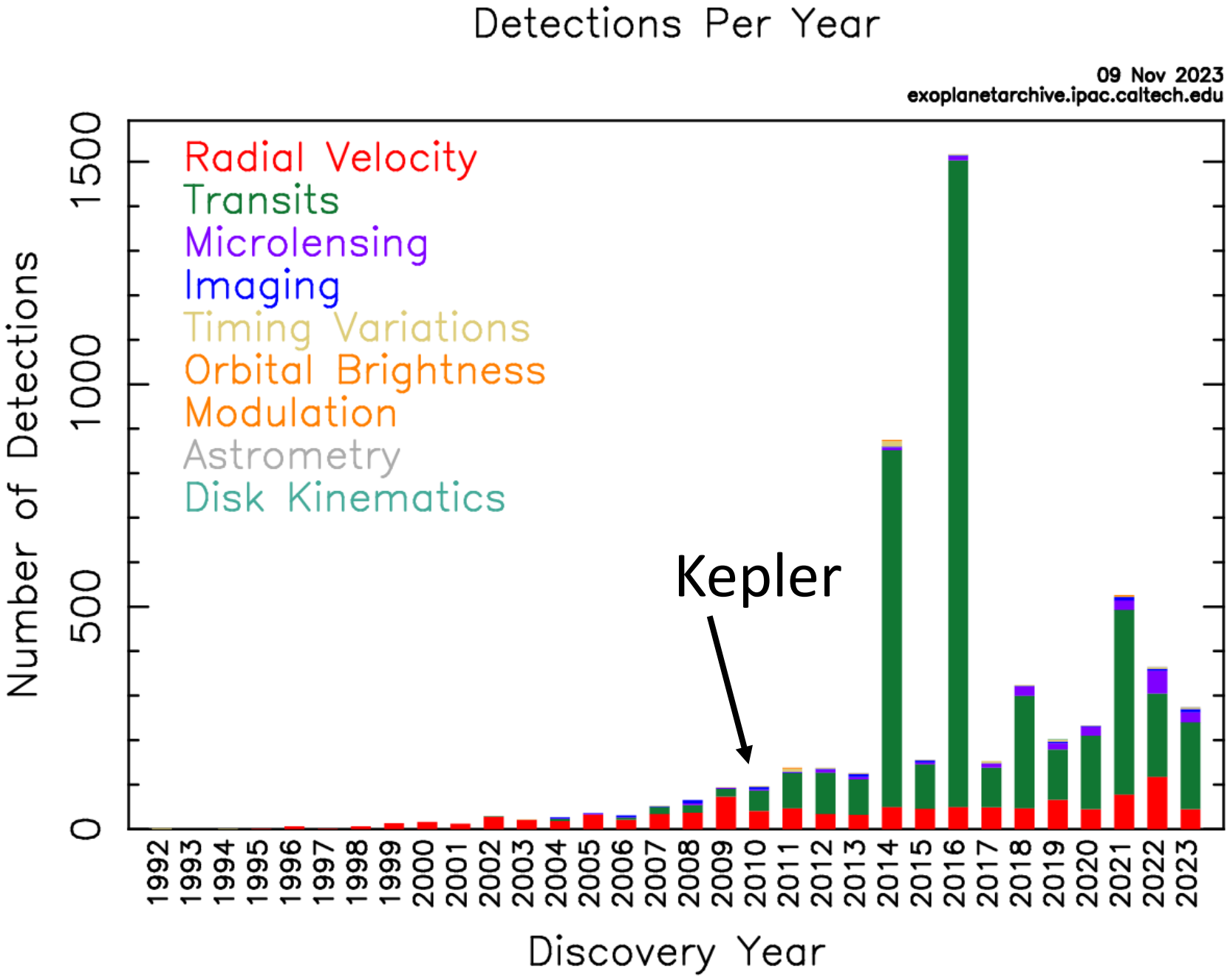
Detections Per Year
09 Nov 2023
exoplanetarchive.ipac.caltech.edu
Radial Velocity
Transits
Microlensing
Imaging
Timing Variations
Orbital Brightness
Modulation
Astrometry
Disk Kinematics
Kepler
Number of Detections
0
500
1000
1500
1992
1993
1994
1995
1996
1997
1998
1999
2000
2001
2002
2003
2004
2005
2006
2007
2008
2009
2010
2011
2012
2013
2014
2015
2016
2017
2018
2019
2020
2021
2022
2023
Discovery Year

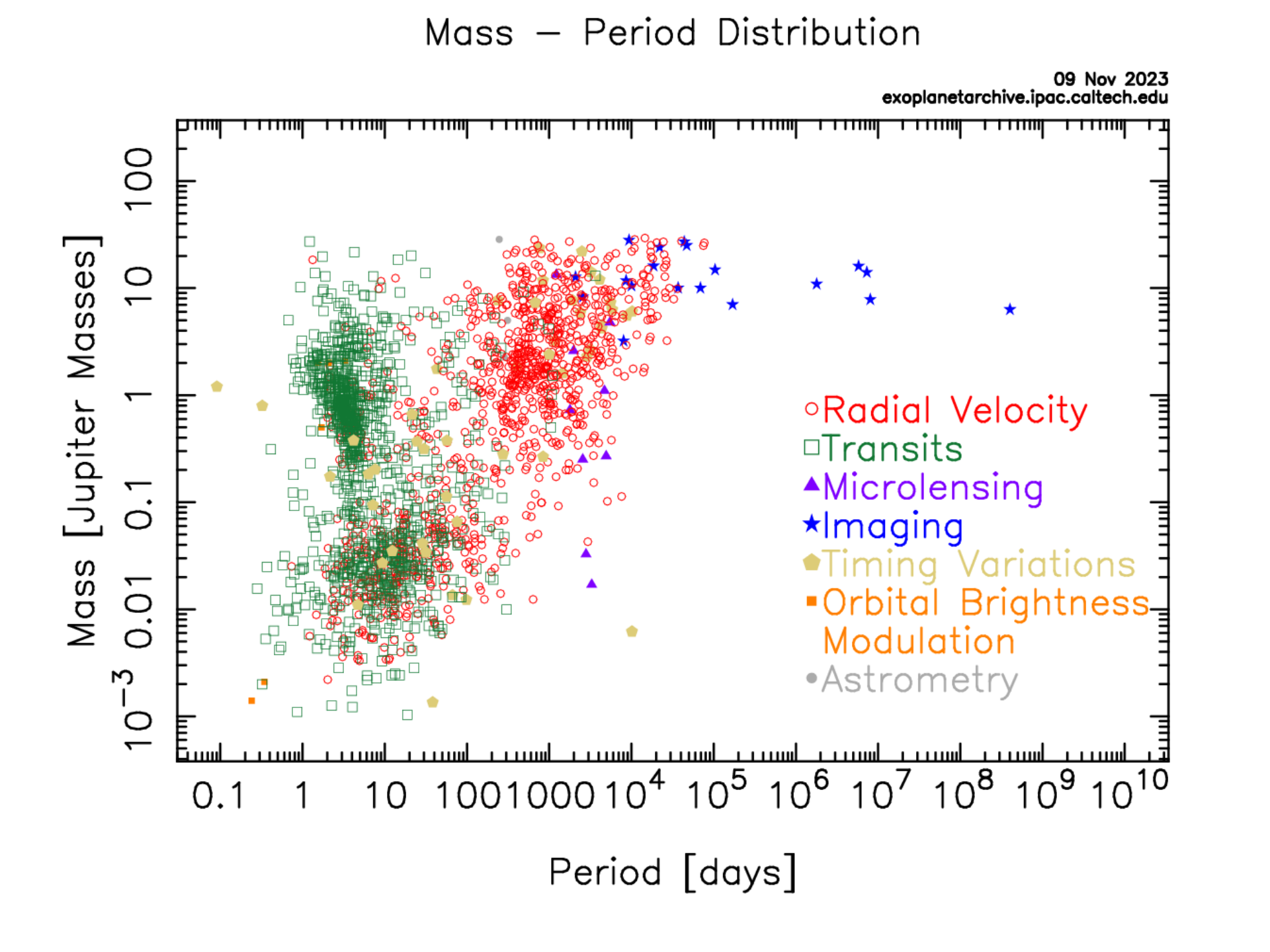
Mass – Period Distribution
09 Nov 2023
exoplanetarchive.ipac.caltech.edu
Mass [Jupiter Masses]
10^{-3}
0.01
0.1
1
10
100
0.1
1
10
100
1000
10^4
10^5
10^6
10^7
10^8
10^9
10^{10}
Period [days]
Radial Velocity
Transits
Microlensing
Imaging
Timing Variations
Orbital Brightness Modulation
Astrometry

Método de detecção: microlentes gravitacionais

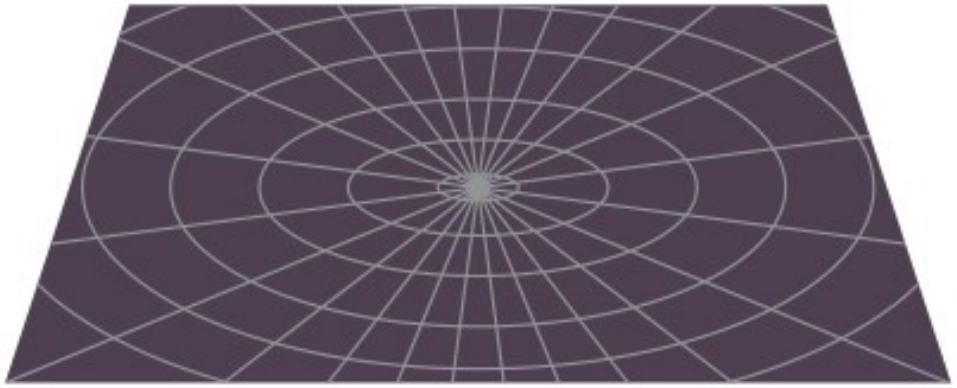

a A two-dimensional representation of "flat" spacetime. The distances between adjacent circles are the same.

Einstein, 1907 – 1915: Relatividade geral

Curvatura do espaço-tempo é causada pela massa.

Maior gravidade é devida à maior curvatura

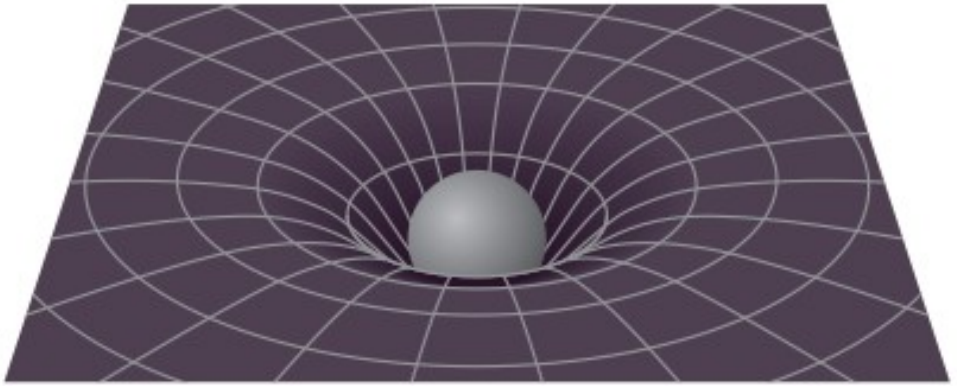

b Gravity arises from curvature of spacetime, represented here by a mass pushing down on the rubber sheet. Notice how the circles become more widely separated near the mass, showing that the curvature is greater as we approach the mass on the sheet.

A massa do Sol curva o espaço-tempo

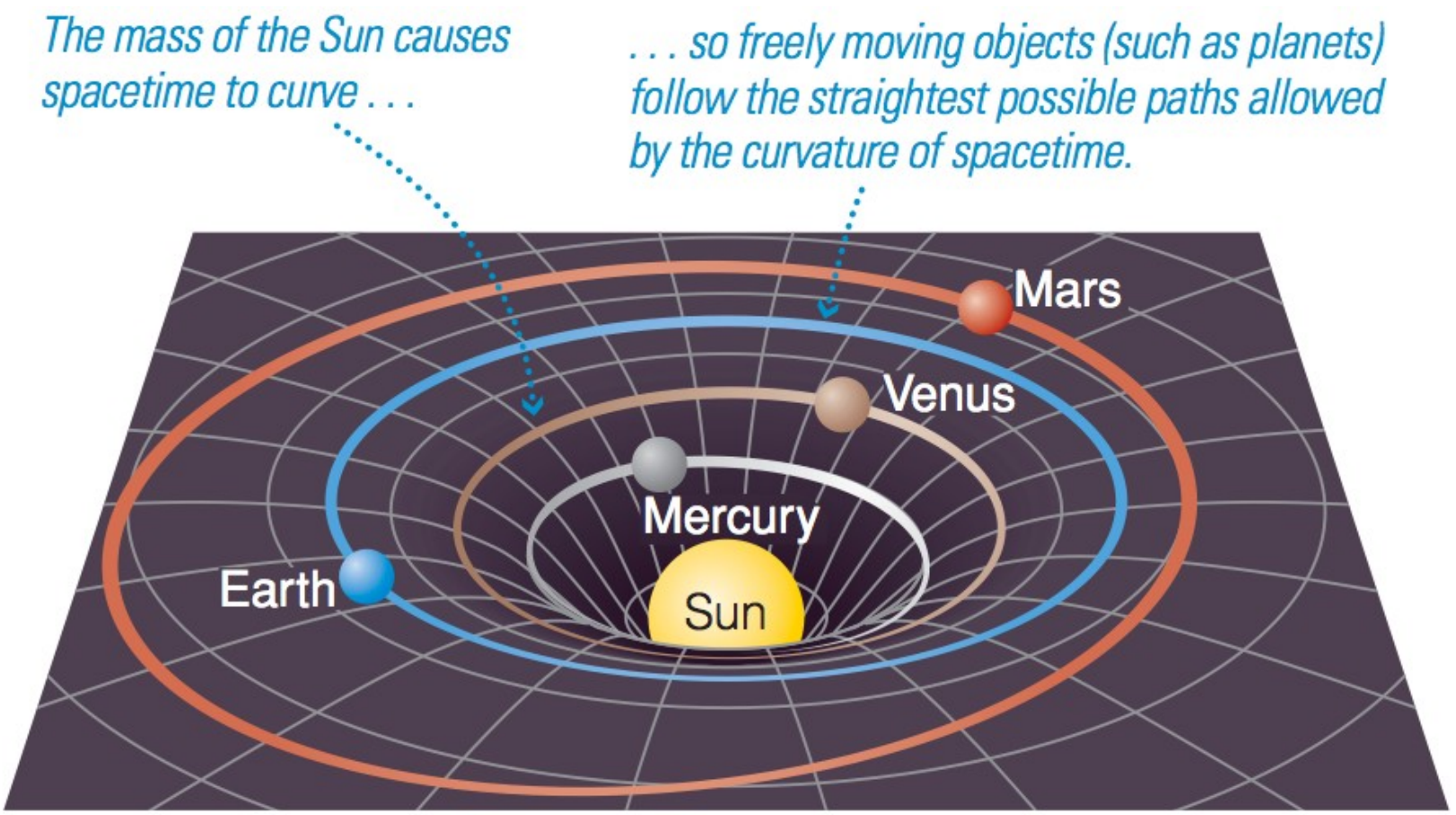

© The cosmic perspective

According to general relativity, planets orbit the Sun for much the same reason that you can make a marble go around in a salad bowl: The planet is going as straight as it can, but the curvature of spacetime causes its path through space to curve.

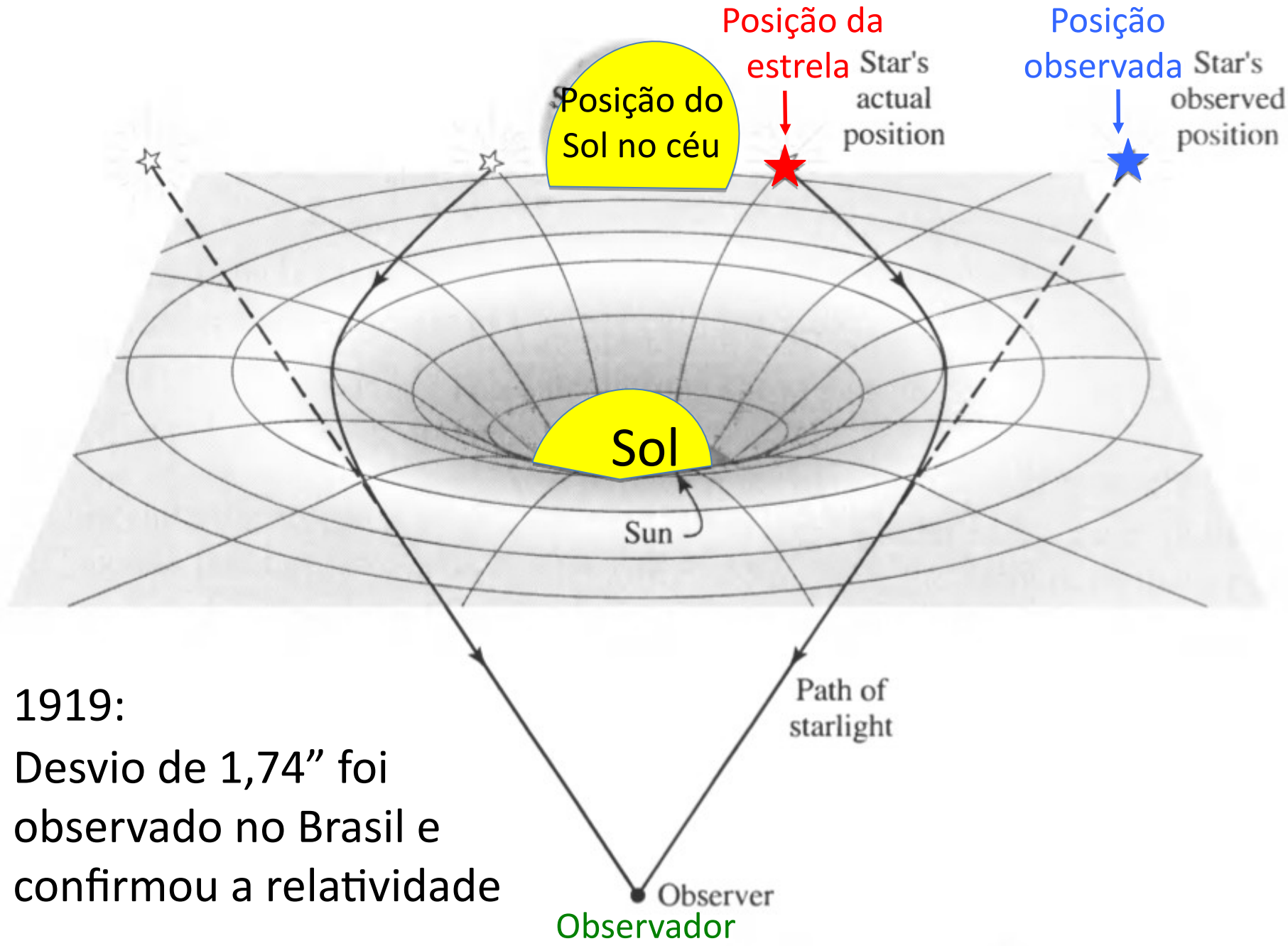

1919:

Desvio de 1,74” foi observado no Brasil e confirmou a relatividade

FIGURE 17.5 Bending of starlight measured during a solar eclipse.

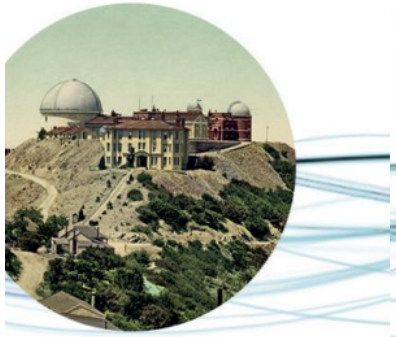

1911

O astrônomo alemão Erwin Finlay-Freundlich tentou medir a deflexão da luz com placas fotográficas de um eclipse solar obtidas pelo **Observatório Lick**, nos Estados Unidos

1912

Pesquisadores do Observatório Argentino liderados por **Charles Perrine** planejaram registrar um eclipse solar na serra da Mantiqueira, em Minas Gerais. Devido ao mau tempo, nada foi fotografado

1914

O início da **Primeira Guerra Mundial** novamente frustrou os planos de Finlay-Freundlich de registrar um eclipse na Crimeia, na Rússia

1916

O Observatório Argentino conseguiu registrar um eclipse solar em Tucacas, na Venezuela, mas nenhuma fotografia serviu para comprovar as ideias de Einstein

1918

A equipe do Observatório Lick não conseguiu fotografar o eclipse do Sol nos Estados Unidos porque seus equipamentos estavam presos na Rússia desde 1914

1919

O eclipse que confirmou a ideia de Einstein cruzou a linha equatorial. Foi observado em Sobral e na ilha do Príncipe, na África

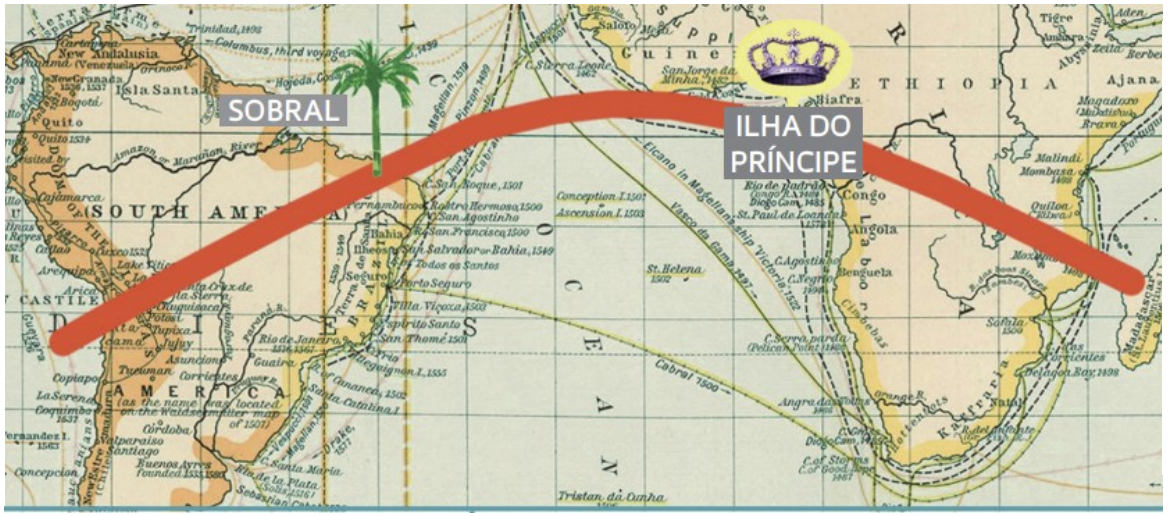

1922

Fotografias de um eclipse solar feitas na Ilha Christmas reforçaram os dados obtidos anos antes em Sobral

https://revistapesquisa.fapesp.br/quando-a-luz-se-curvou/

Difícil de medir. Pela Relatividade Geral, deslocamento de apenas 1,74”

Highest resolution image of the 1919 solar eclipse in Sobral. One copy of a plate from Sobral went to Landessternwarte Heidelberg-Königstuhl, who recently (2019?) scanned theirs as part of the Heidelberg Digitized Astronomical Plates project

https://www.eso.org/public/images/potw1926a/

Imagem composta do Eclipse e campo de estrelas na mesma região (em data diferente)

Foto do Eclipse Solar Total de 21/8/2017

I re-shot Regulus, Nu Leonis, and the surrounding regions on 28/12/2017 to merge them into the original totality shot. This image shows both those stars and many others as they were on the day of totality.

https://www.cloudynights.com/gallery/image/56791-2017-eclipse-with-background-stars/

Observação é difícil devido ao brilho da coroa

Deflexão da luz estelar passando a uma distância ξ de uma estrela de massa M (segundo a relatividade geral):

$$\hat{\alpha} = \frac{4GM}{c^2 \xi} = 1{,}74\,'' \left(\frac{M}{M_\odot}\right)\left(\frac{\xi}{R_\odot}\right)^{-1}$$

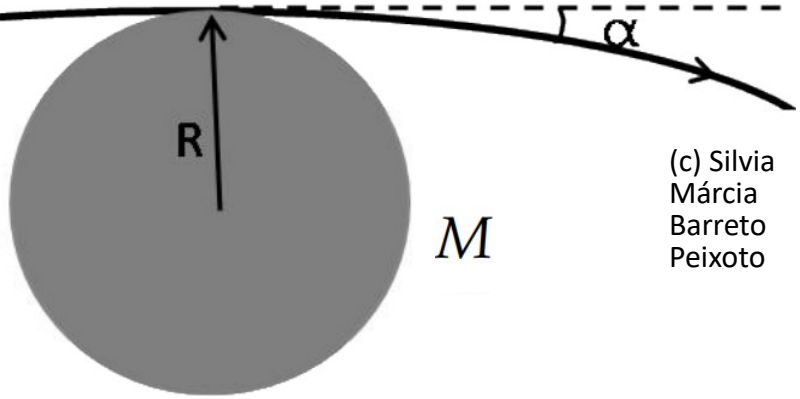

(c) Silvia Márcia Barreto Peixoto

Para o Sol, α = 1,74 ”

Ilustração do efeito de deflexão da luz em comparação com a posição “normal” das estrelas (quando o Sol não está na linha de visada)

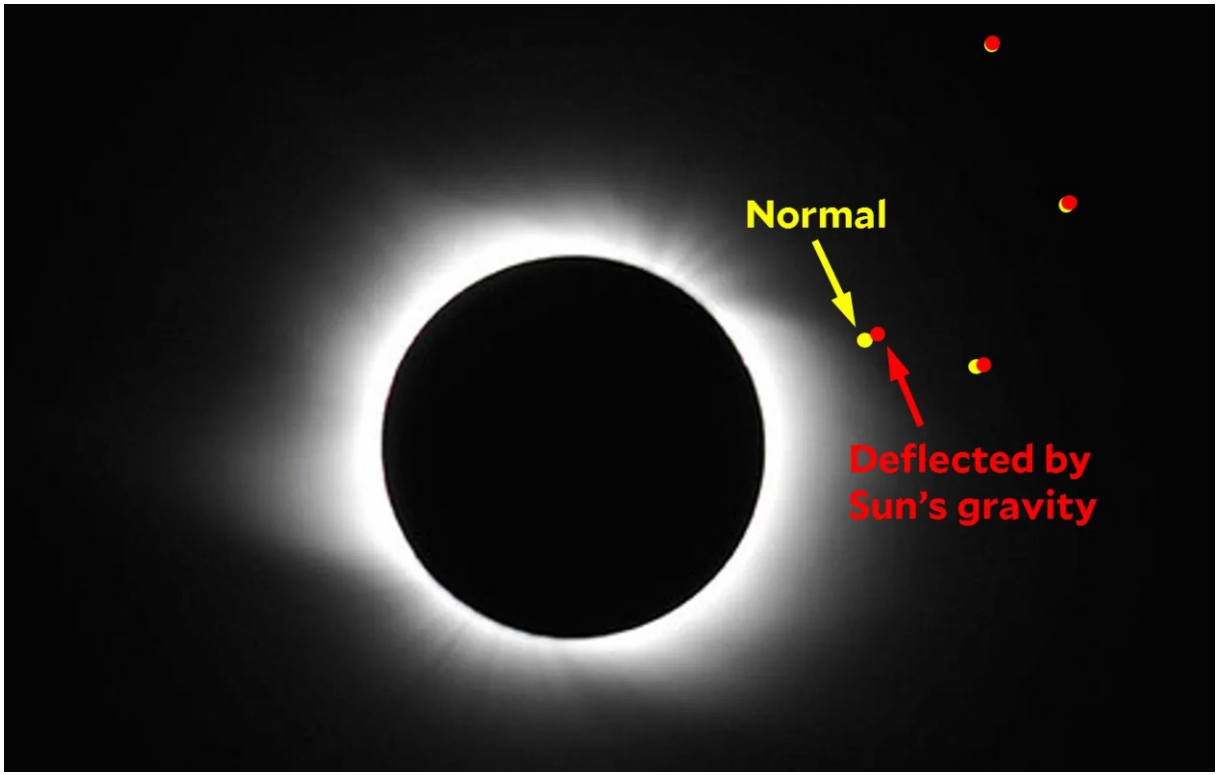

https://www.motherjones.com/kevin-drum/2019/05/did-an-eclipse-prove-einstein-was-right/

Observador distante de galáxia (fonte de luz) e de outra galáxia ou aglomerado de galáxias (lente) pode observar o efeito de lente gravitacional

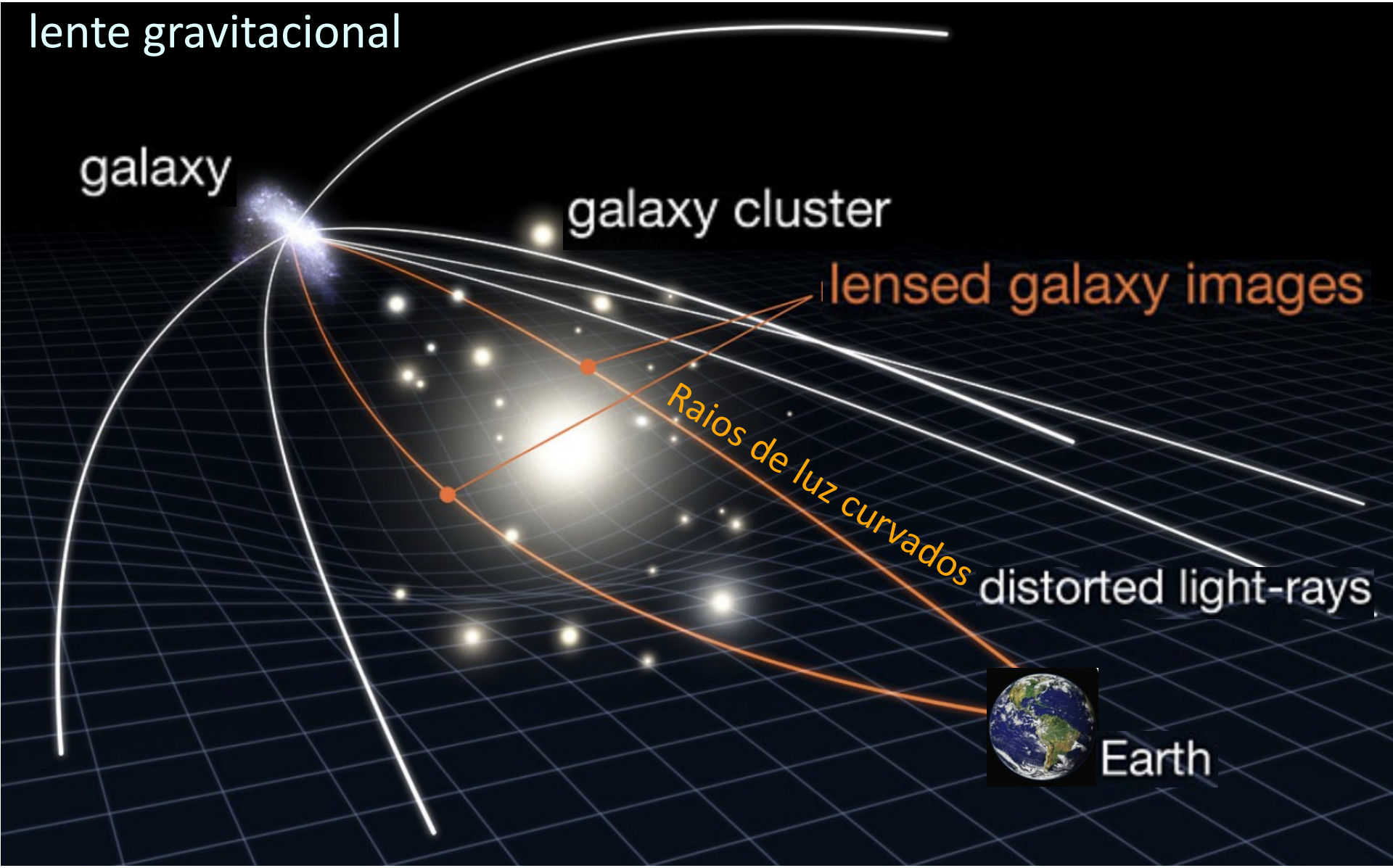

https://esahubble.org/images/heic1106c/

A galáxia luminosa vermelha (LRG 3-757) é a “lente” que distorce a luz de uma galáxia azul (“fonte”) muito mais distante, pelo efeito de lente gravitacional

APOD 21/12/2011: The gravity of a luminous red galaxy (LRG 3-757) has gravitationally distorted the light from a much more distant blue galaxy. More typically, such light bending results in 2 discernible images of the distant galaxy, but here the lens alignment is so precise that the background galaxy is distorted into a horseshoe -- a nearly complete ring. Since such a lensing effect was generally predicted by Einstein over 70 years ago, rings like this are now known as Einstein Rings. The image was taken with the Hubble Space Telescope

https://apod.nasa.gov/apod/ap111221.html

Aglomerado de galáxias Abell 370 é a “lente” que distorce a luz de ~100 galáxias (“fontes”) muito mais distantes

Galaxy cluster Abell 370, located ~ 4 billion light-years away, contains several hundred galaxies tied together by the mutual pull of gravity. Entangled among the galaxies are ~100 mysterious-looking arcs of blue light. These are actually distorted images of remote galaxies behind the cluster. These far-flung galaxies are too faint for Hubble to see directly. Instead, the gravity from the cluster acts as a huge lens that magnifies and stretches images of background galaxies

https://hubblesite.org/contents/articles/gravitational-lensing

Deflexão da luz a uma distância ξ de estrela de massa M :

$$\hat{\alpha} = \frac{4GM}{c^2 \xi} = 1{,}74\," \left(\frac{M}{M_\odot}\right)\left(\frac{\xi}{R_\odot}\right)^{-1}$$

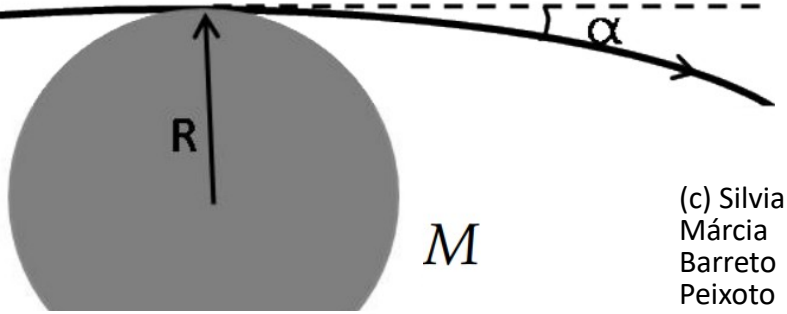

(c) Silvia Márcia Barreto Peixoto

Microlentes

Alinhamento perfeito:

θ_E, **raio** do anel de Einstein

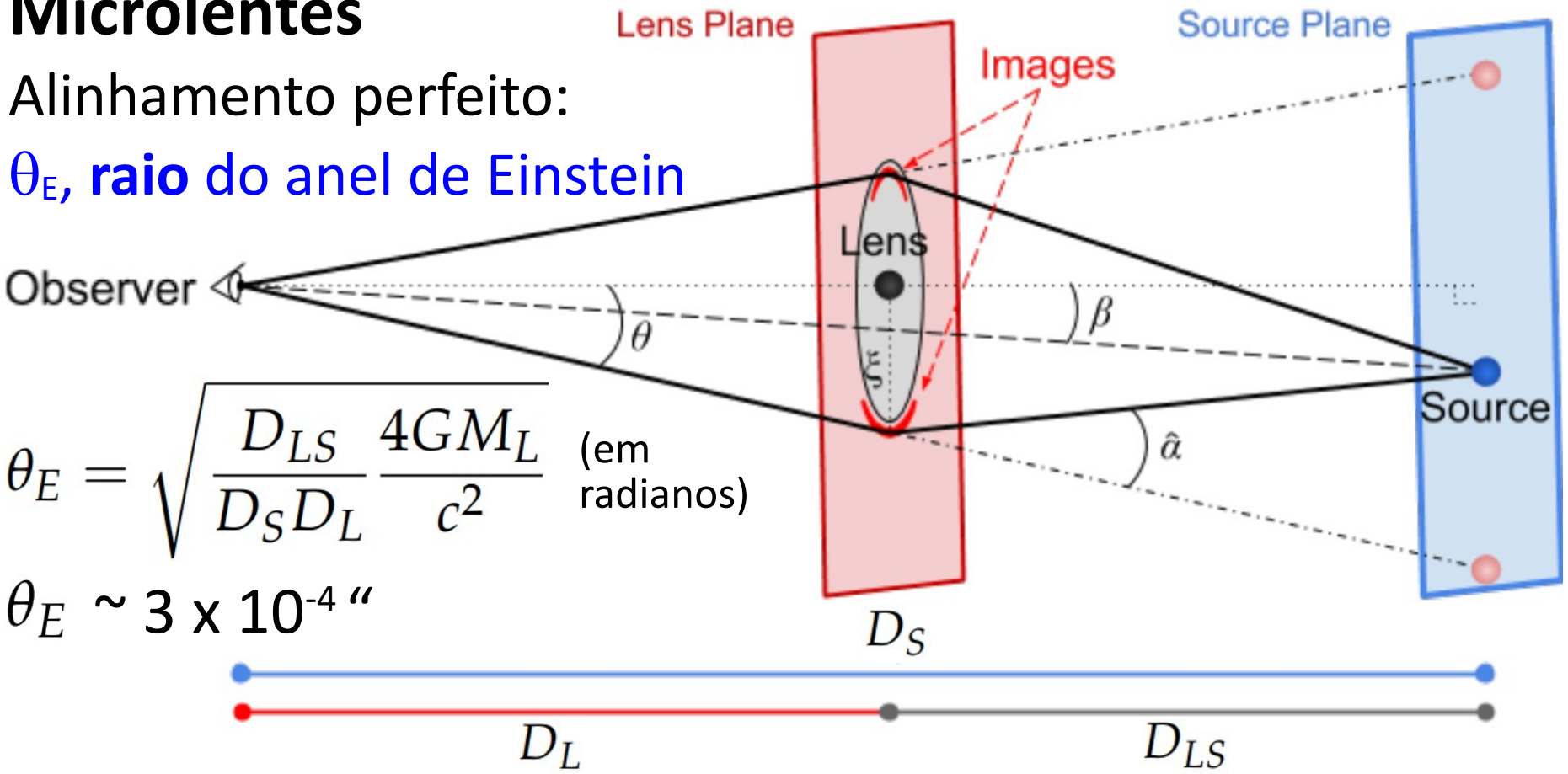

$$\theta_E = \sqrt{\frac{D_{LS}}{D_S D_L}\frac{4GM_L}{c^2}}$$ (em radianos)

θ_E ~ 3 x 10^{-4} "

Microlente gravitacional

Raio do anel de Einstein:

$$\theta_E = \sqrt{\frac{D_{LS}}{D_S D_L}\frac{4GM_L}{c^2}}$$ (em radianos)

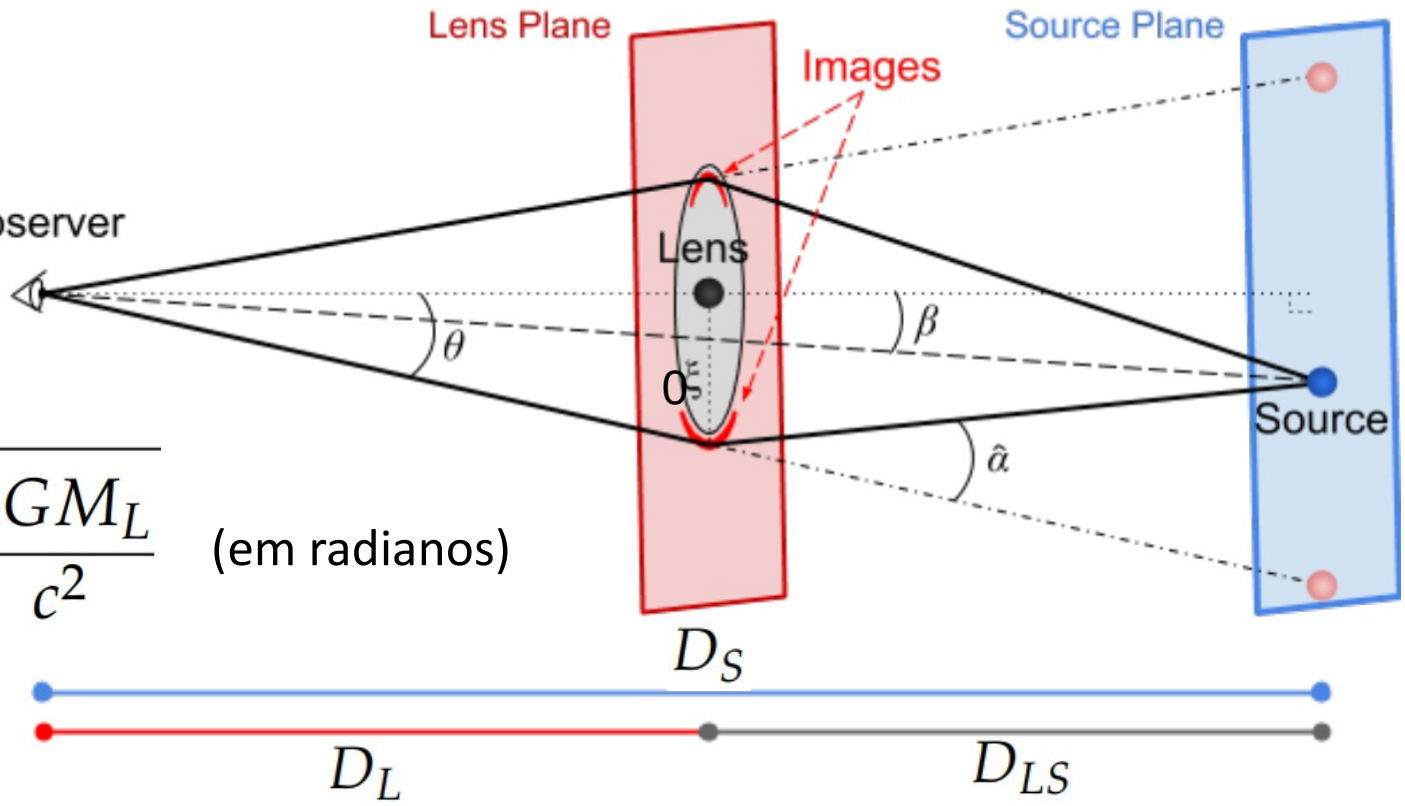

Consider an M-dwarf lens star ($M_L = 0.3M_\odot$) at a distance of $D_L = 6.5$ kpc from the Earth, and a source star at a distance $D_S = 8.5$ kpc. The angular Einstein ring radius is

$$\theta_E \approx 0.902\text{mas}\left(\frac{M_L}{M_\odot}\right)^{1/2}\left(\frac{10\text{kpc}}{D_L}\right)^{1/2}\left(1-\frac{D_L}{D_S}\right)^{1/2} \sim 300\mu\text{as} = 0{,}3\text{mas}$$

This corresponds to a physical distance on the lens plane of

$$r_E = \theta_E D_L \sim 3\text{AU}\left(\frac{M_L}{M_\odot}\right)^{1/2} \sim 1.6\text{AU}$$

(c) Yiannis Tsapras, 2018

Microlente gravitacional

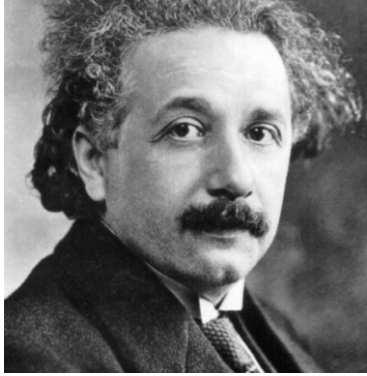

Albert Einstein

Science Vol. 84, No. 2188 (Dec. 4, 1936), pp. 506-507

LENS-LIKE ACTION OF A STAR BY THE DEVIATION OF LIGHT IN THE GRAVITATIONAL FIELD

Some time ago, R. W. Mandl paid me a visit and asked me to publish the results of a little calculation, which I had made at his request. This note complies with his wish.

The light coming from a star A traverses the gravitational field of another star B, whose radius is R_0. Let there be an observer at a distance D from B and at a distance x, small compared with D, from the extended central line $\overline{AB}$. According to the general theory of relativity, let α_0 be the deviation of the light ray passing the star B at a distance R_0 from its center.

not decrease like $1/D$, but like $1/\sqrt{D}$, as the distance D increases.

Of course, there is no hope of observing this phenomenon directly. First, we shall scarcely ever approach closely enough to such a central line. Second, the angle β will defy the resolving power of our instruments. For, α_0 being of the order of magnitude of one second of arc, the angle R_0/D, under which the deviating star B is seen, is much smaller. Therefore, the light coming from the luminous circle can not be distinguished by an observer as geometrically different from that coming from the star B, but simply will manifest itself as increased apparent brightness of B.

The same will happen, if the observer is situated at a small distance x from the extended central line $\overline{AB}$.

$\theta_E \sim 0{,}3$mas (segundo Einstein, sem esperança de medida)

Porem, tem efeito de aumento do brilho aparente!

Microlente gravitacional

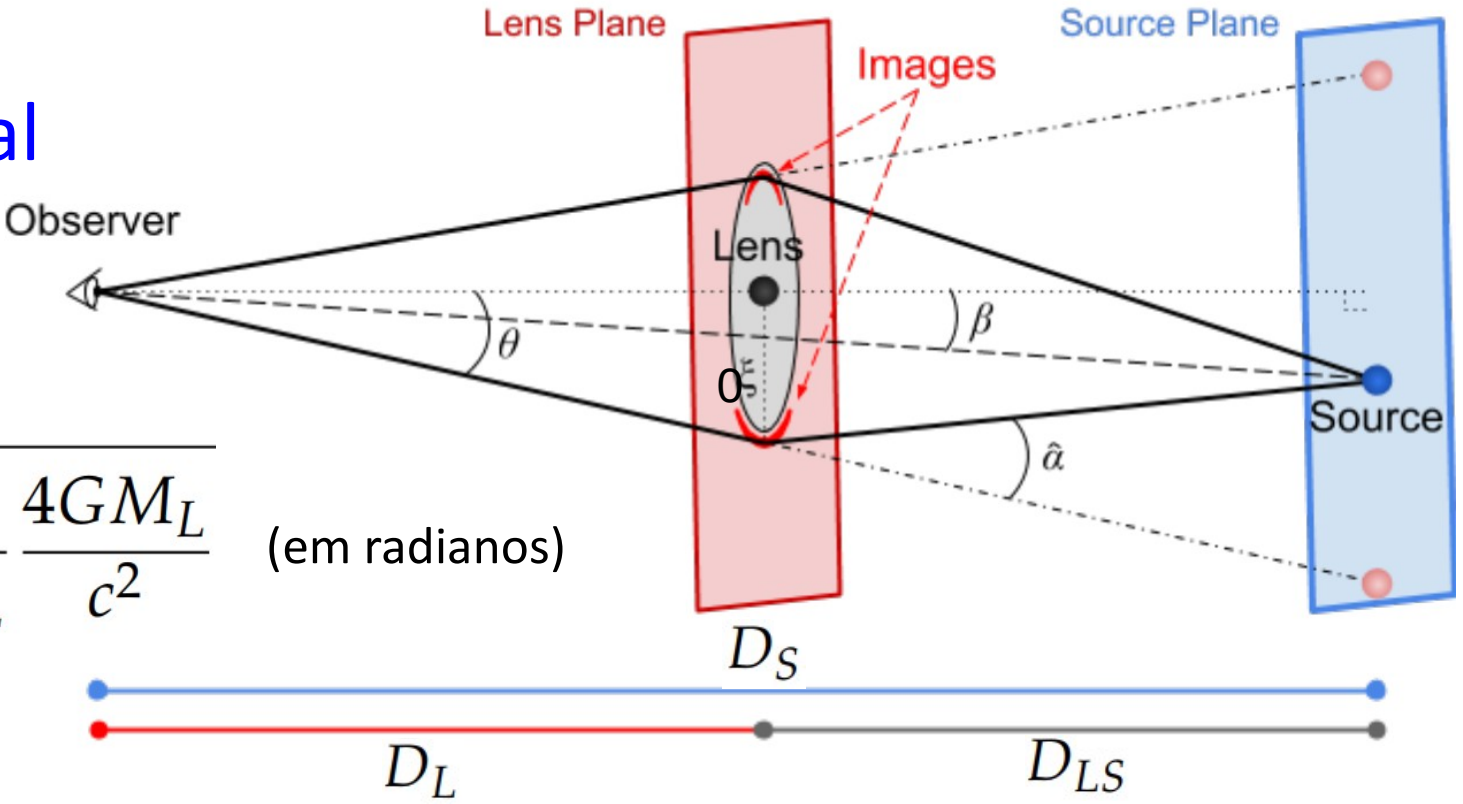

Raio do anel de Einstein:

$$\theta_E = \sqrt{\frac{D_{LS}}{D_S D_L}\frac{4GM_L}{c^2}}$$ (em radianos)

Magnificação do brilho:

$$A = \frac{u^2+2}{u\sqrt{u^2+4}} \qquad u = \beta/\theta_E$$

Exemplos

1) Magnificação mínima: $A = 3/\sqrt{5} \approx 1.34$

2) Magnificação para u = 0,1 → A ~ ...

(c) Yiannis Tsapras, 2018

Microlente gravitacional: efeito de apenas ~0,3 mas

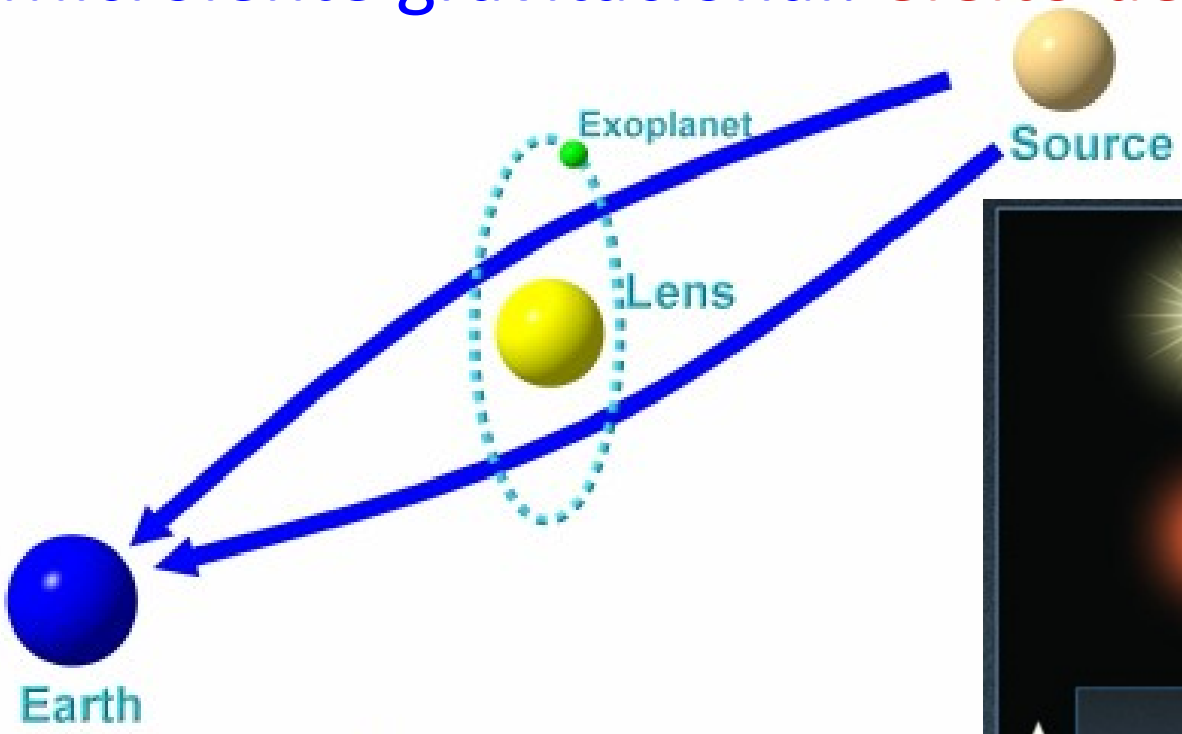

Desvio angular pequeno, mas também aumento de brilho

(1) Quando 1 estrela passa frente a outra, o brilho da estrela de fundo aumenta

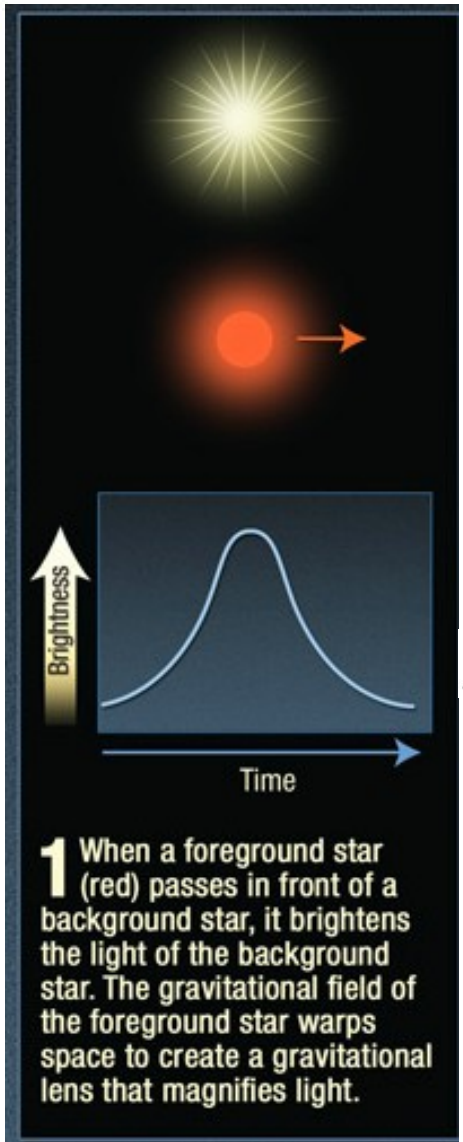

$$A = \frac{u^2 + 2}{u\sqrt{u^2 + 4}}$$

$$u = \beta / \theta_E$$

Microlente gravitacional

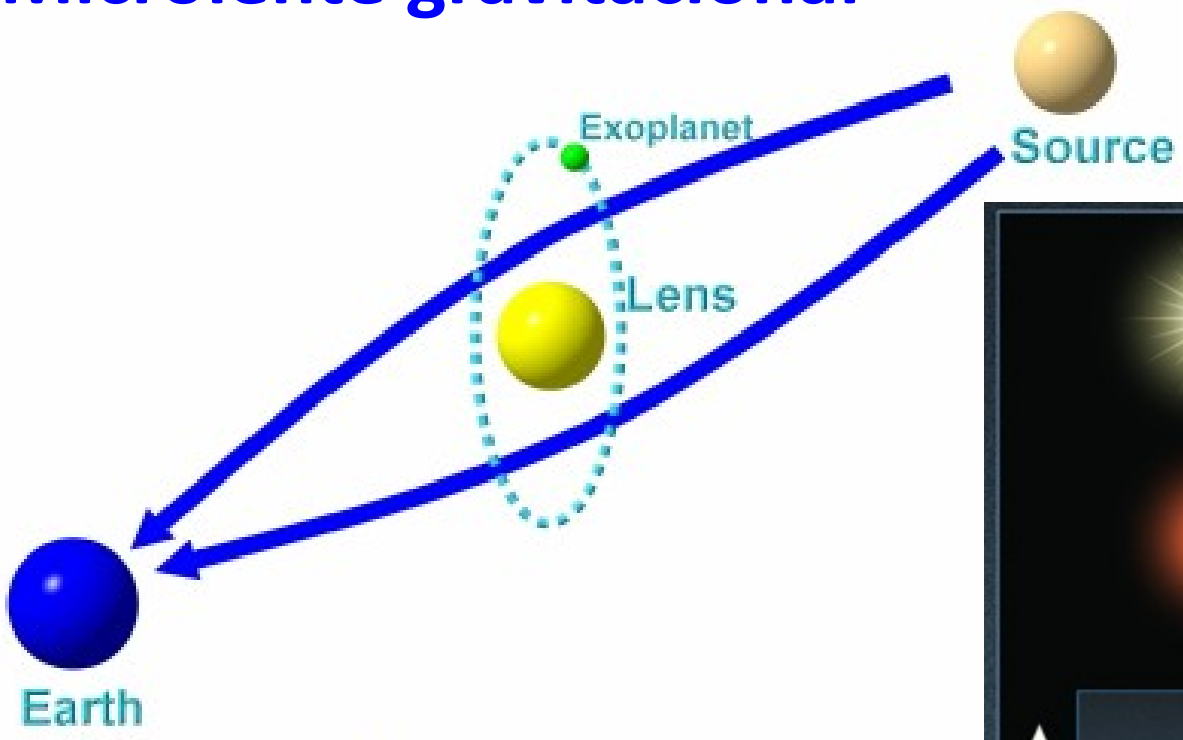

Desvio angular pequeno, mas também aumento de brilho

(1) Quando 1 estrela passa frente a outra, o brilho da estrela de fundo aumenta

(2) Se estrela "lente" tem planeta → magnificação adicional do brilho

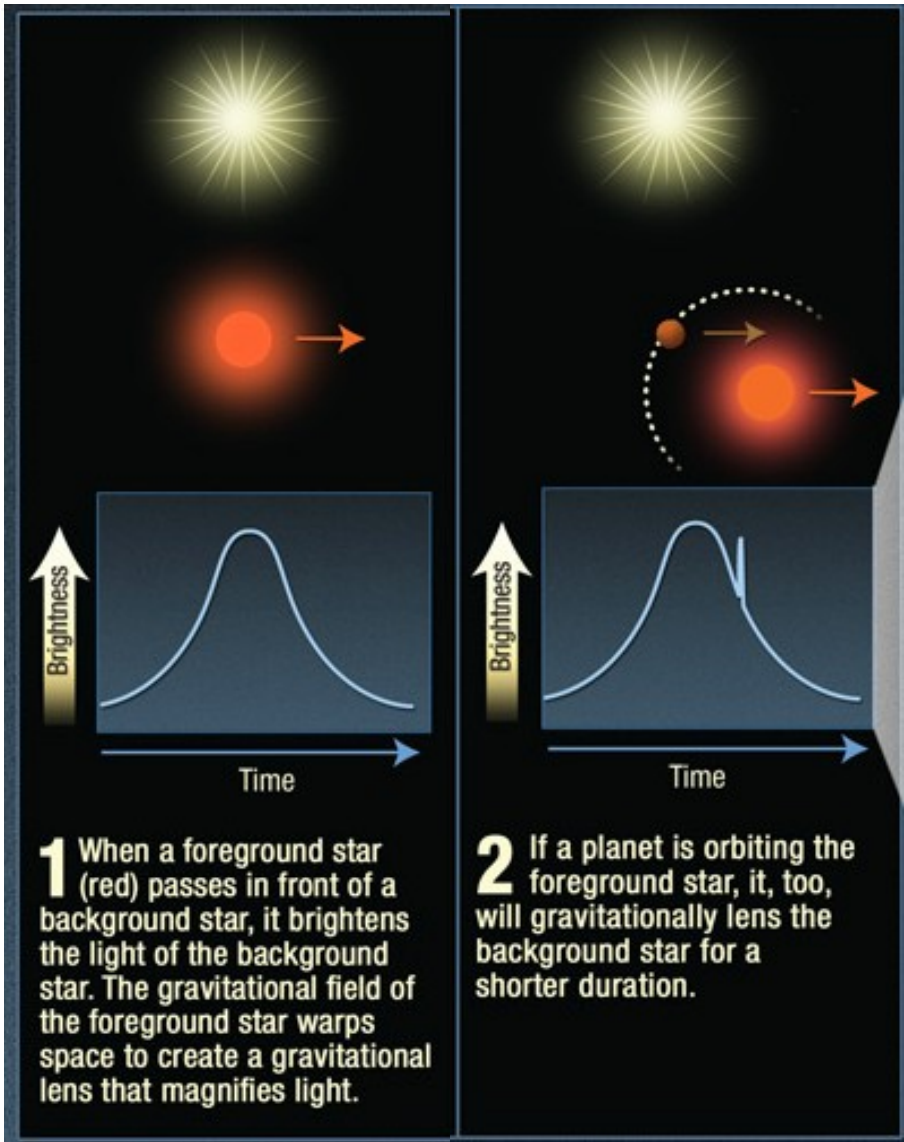

Microlente gravitacional

Magnificação de brilho pelo alinhamento com a estrela e aumento adicional devido ao planeta

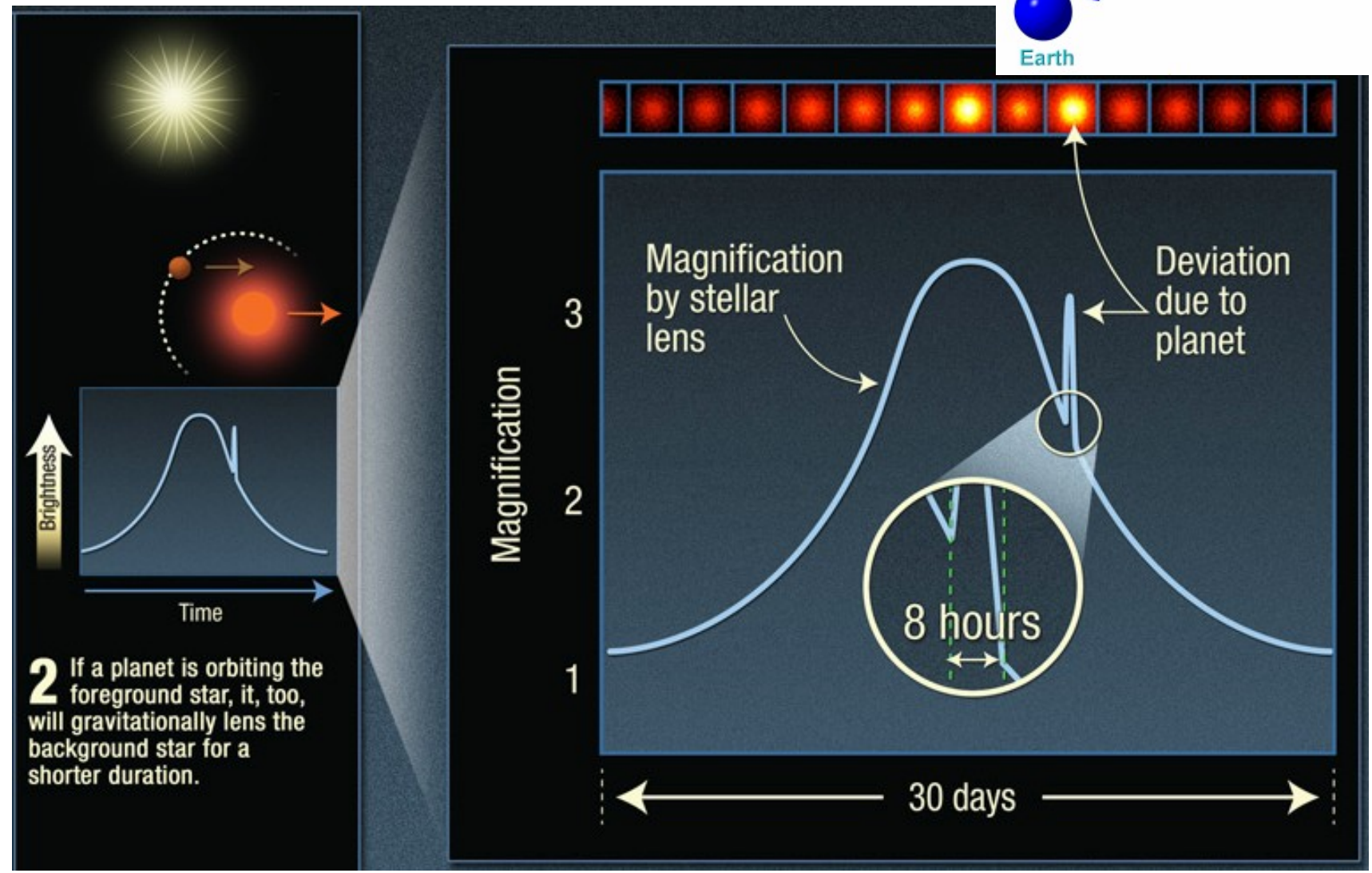

Microlente gravitacional: escalas de tempo

Escala de tempo $t_E = \dfrac{\theta_E}{\mu_{LS}}$

θ_E : raio do anel de Einstein

μ_{LS} : movimento próprio entre fonte *S* e lente *L*

$$\theta_E = \sqrt{\frac{D_{LS}}{D_S D_L}\frac{4GM_L}{c^2}} \approx 0.902\text{mas}\left(\frac{M_L}{M_\odot}\right)^{1/2}\left(\frac{10\text{kpc}}{D_L}\right)^{1/2}\left(1-\frac{D_L}{D_S}\right)^{1/2} \sim 300\mu\text{as}$$

Usando um mov. próprio típico

$\mu_{LS} \sim 15\mu\text{as/d}$

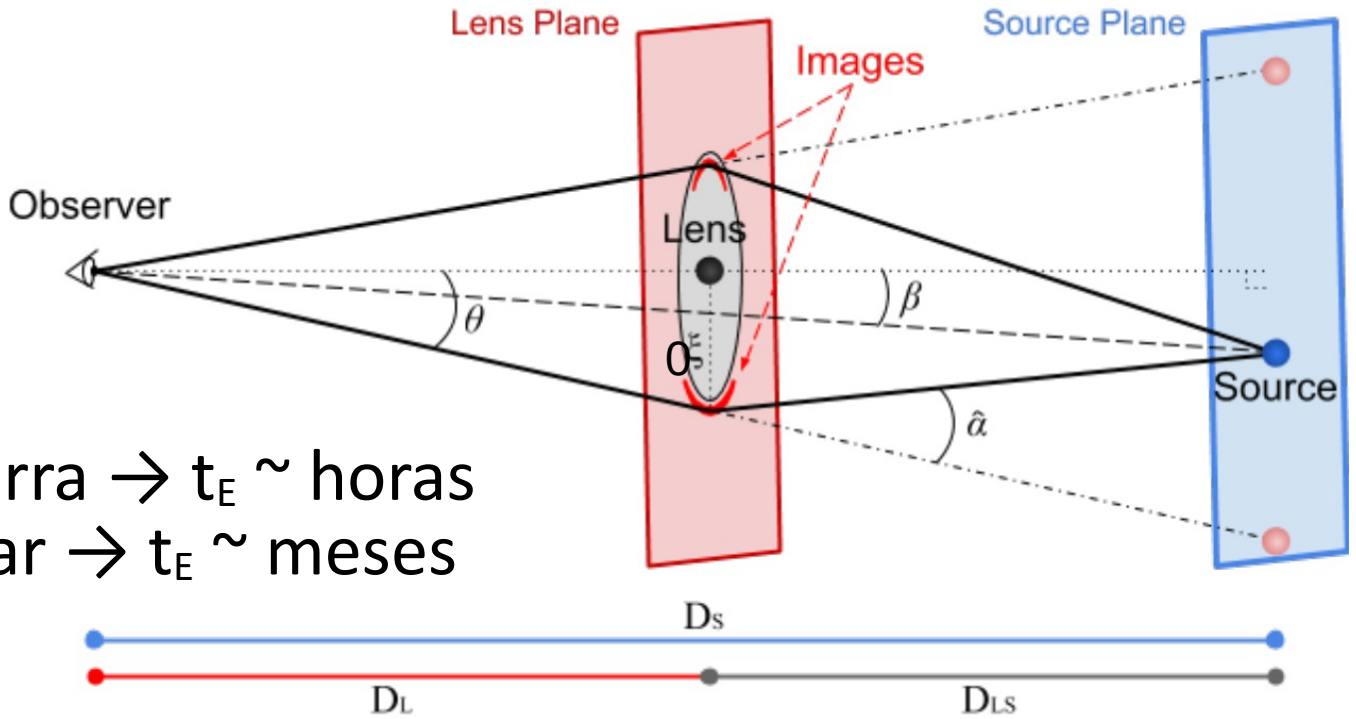

M_L = massa da Terra → t_E ~ horas

M_L = 1 massa solar → t_E ~ meses

(c) Yiannis Tsapras, 2018

Microlente gravitacional: escalas de tempo

$$t_E = \frac{\theta_E}{\mu_{LS}}$$

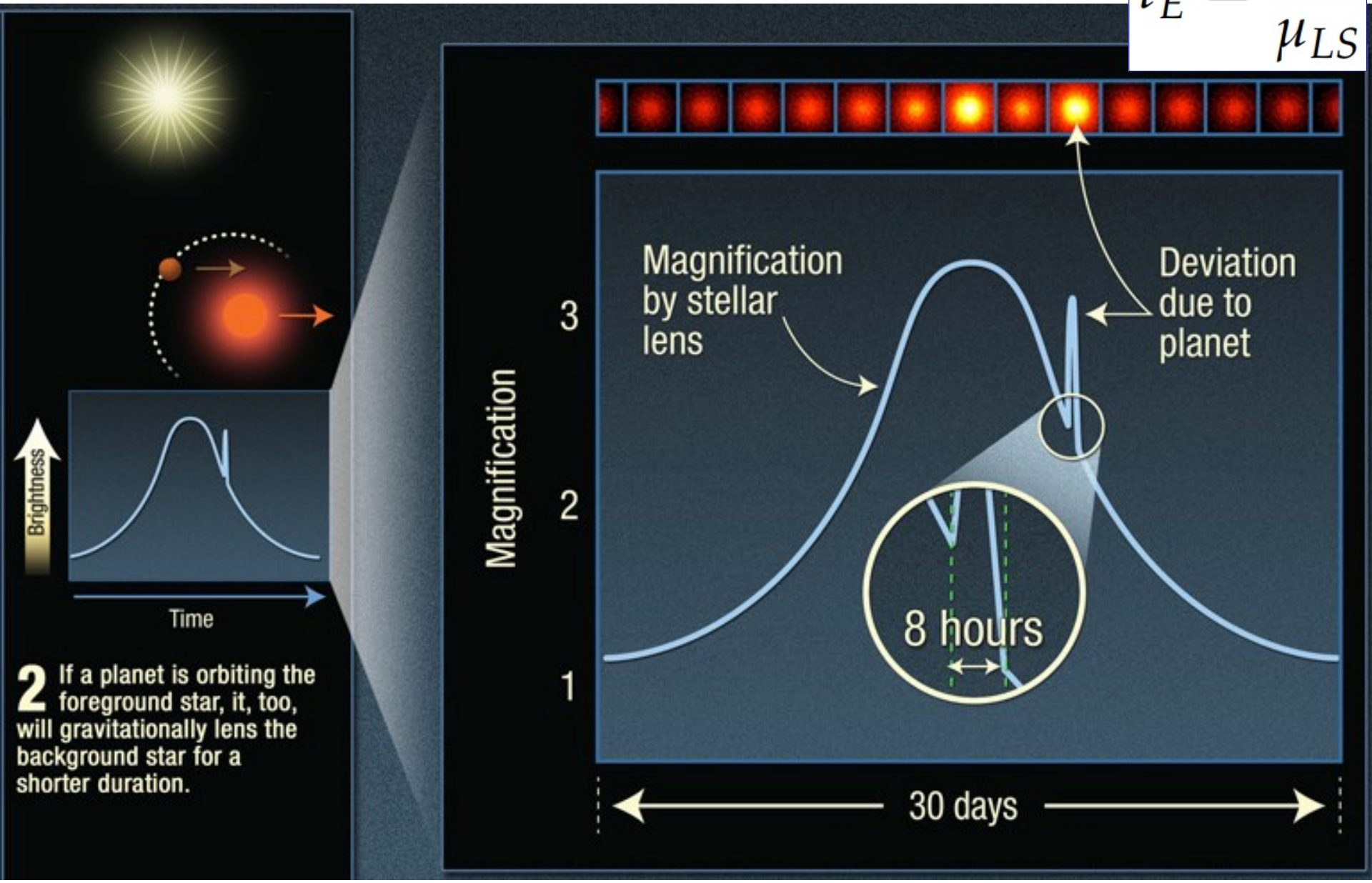

Estrelas são fontes quase pontuais → alinhamento perfeito é muito improvável (p.ex., nos próximos 1000 anos a *18 Sco* não ficará alinhada)

→ Procurar campos densos de estrelas

Imagem do *Digitized Sky Survey* de 0.5x0.5 graus (30x30 min de arco) ao redor da gêmea solar 18 Sco.

O movimento próprio da estrela é de 0,2” / ano em A.R. e -0,5” / ano em Declinação. O percurso nos próximos 1000 anos é mostrado pela seta.

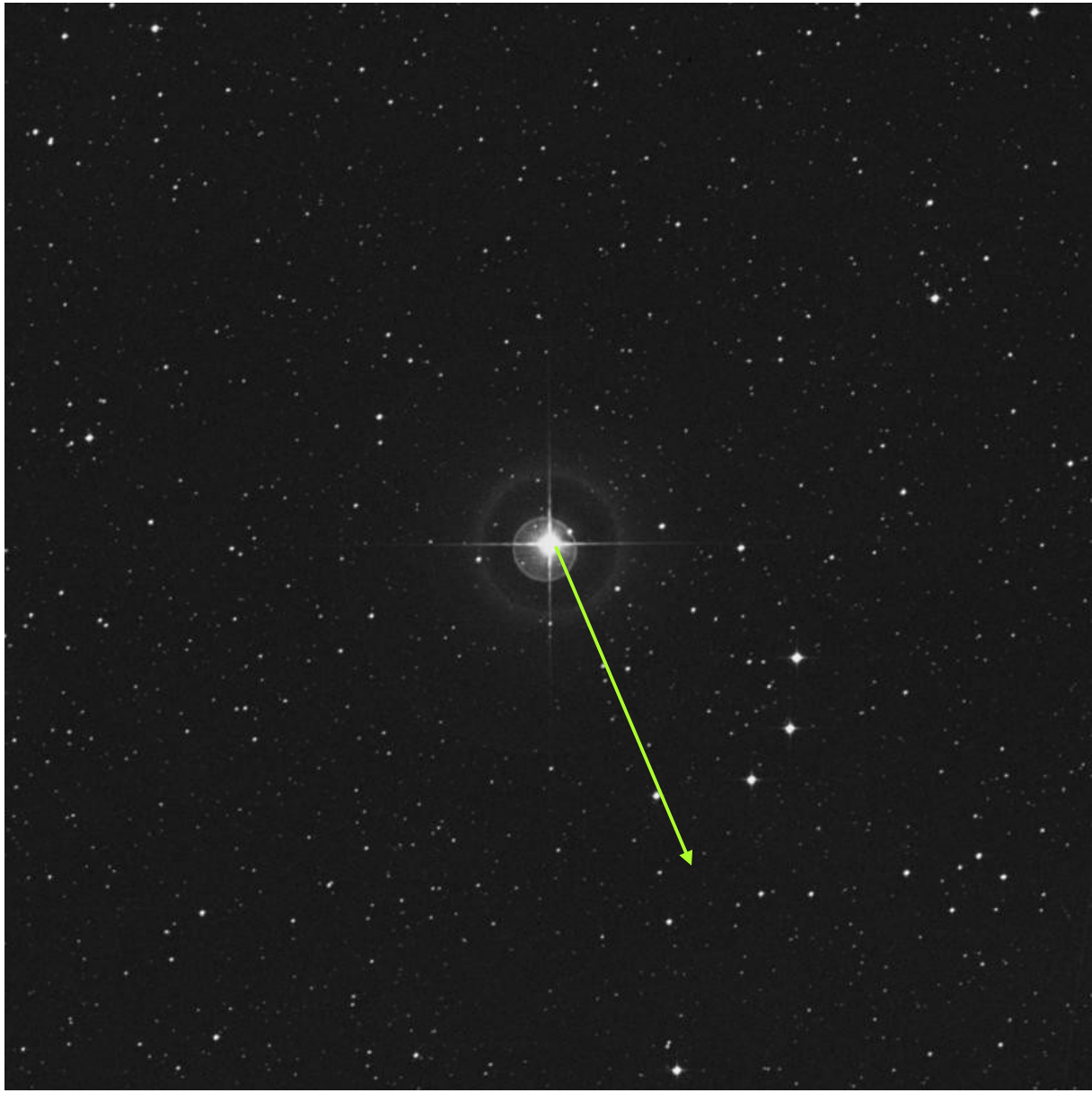

Chances de observar *microlensing* no bojo Galáctico ~ 10^{-6}

(c) Adaptação de imagem composta por Thiago Ferreira dos Santos

(c) NASA / JPL Caltech

Campo OGLE na direção do bojo Galáctico, mostrando a estrela do evento OGLE-2005-BLG-390

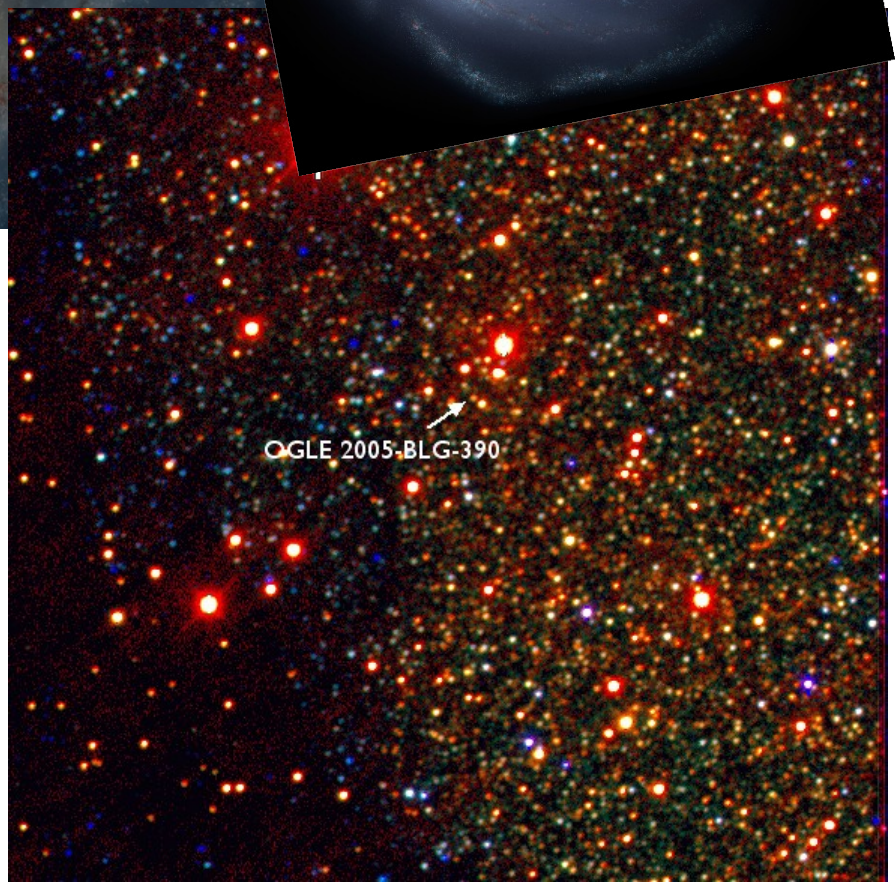

(c) Danish 1.54m telescope at ESO LaSilla

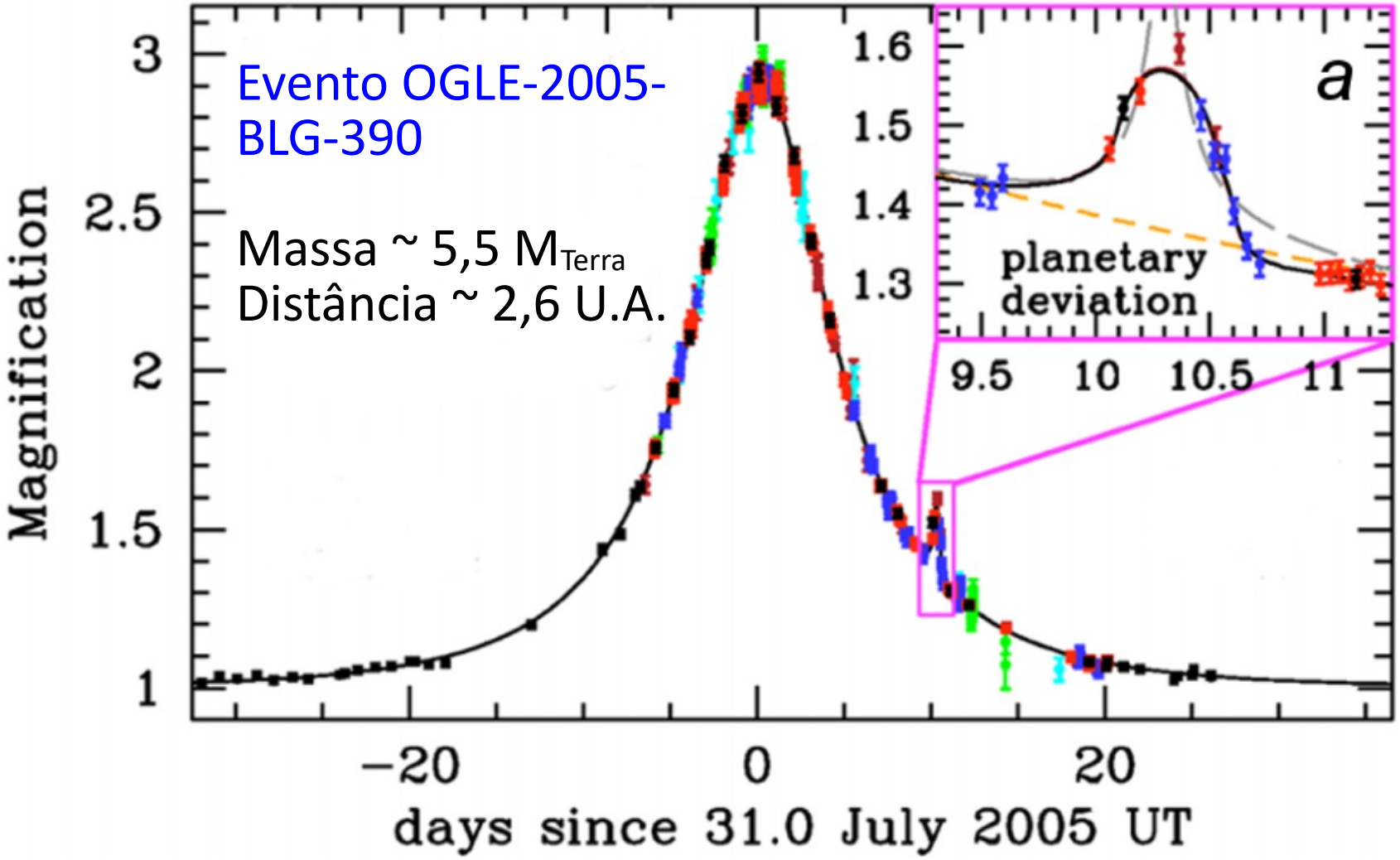

Figure 9. (**a**) The light curve of planetary microlensing event OGLE-2005-BLG-390. Six telescopes around the world participated in this discovery, with the individual contributions represented by the data points in different colors. The inset on the top right shows the planetary anomaly with the best-fit planetary model indicated by the solid black line. Single lens and binary source models, respectively represented by the orange and gray dashed lines, cannot account for the observed deviation. The planet has a mass of ~5.5 M_{Earth} and lies at a distance of ~2.6 AU from its host star. [*Figure adapted with permission from Beaulieu et al. [169], Figure 1*]; (**b**) The light curve of planetary microlensing event

Discovery of a Jupiter/Saturn Analog with Gravitational Microlensing

B.S. Gaudi[1,*], D.P. Bennett[2], A. Udalski[3], A. Gould[1],

Evento OGLE-2006-BLG-109

Estrela: 0,5 M_{Sol}
localizada a 1,5 kpc

2 planetas:
Massa ~ 0,7 e 0,3 M_{Jup}
Distância ~ 2,3 e 4,6 UA

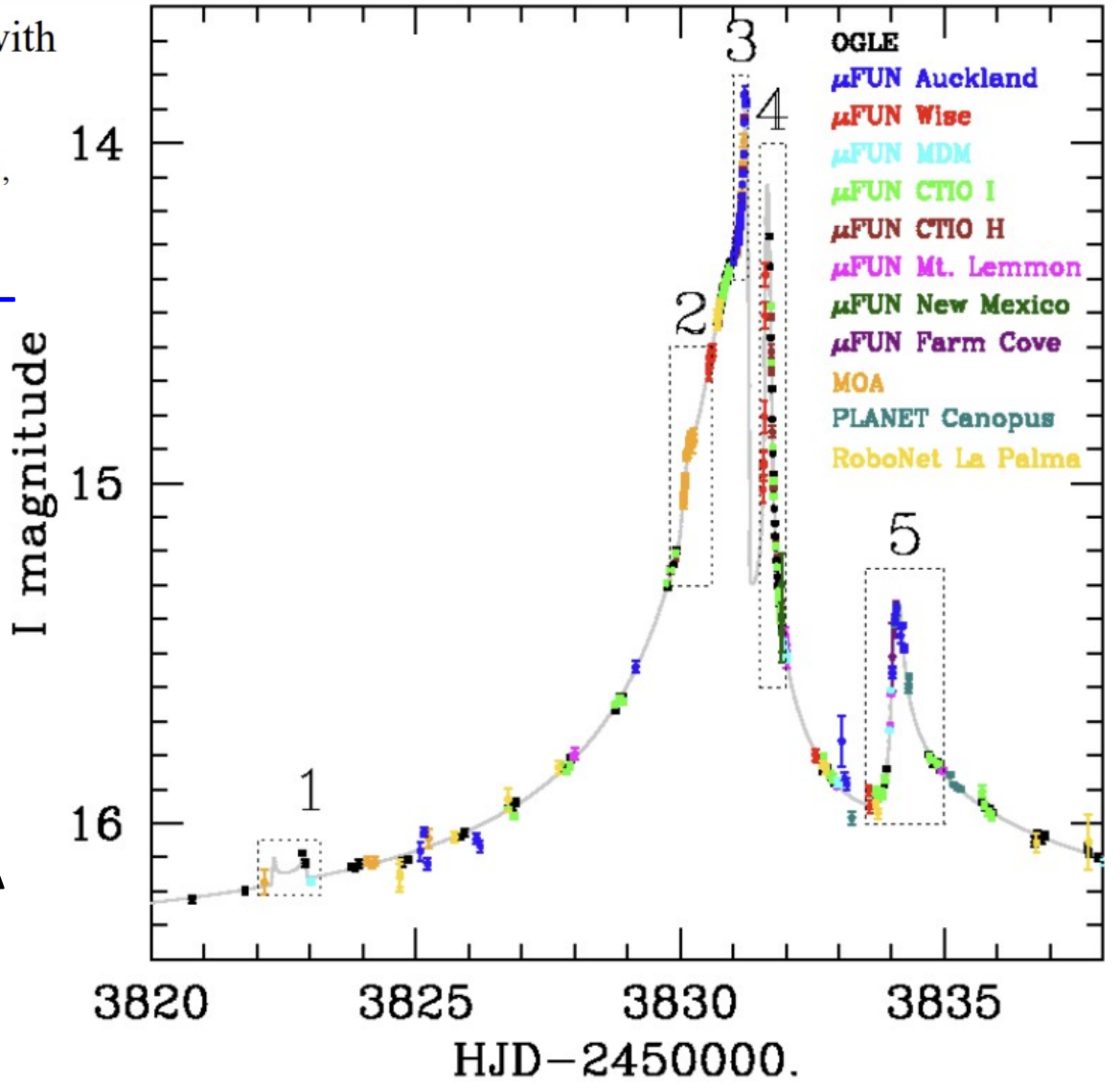

(**b**) The light curve of planetary microlensing event OGLE-2006-BLG-109. The event was observed from 11 different telescopes, represented by the data points in different colors. Five distinct anomalous features are apparent, produced by the source crossing the caustic of the two-planet system (shown in the inset on the left).

Técnica de microlensing é importante para estudar planetas além da linha de gelo.

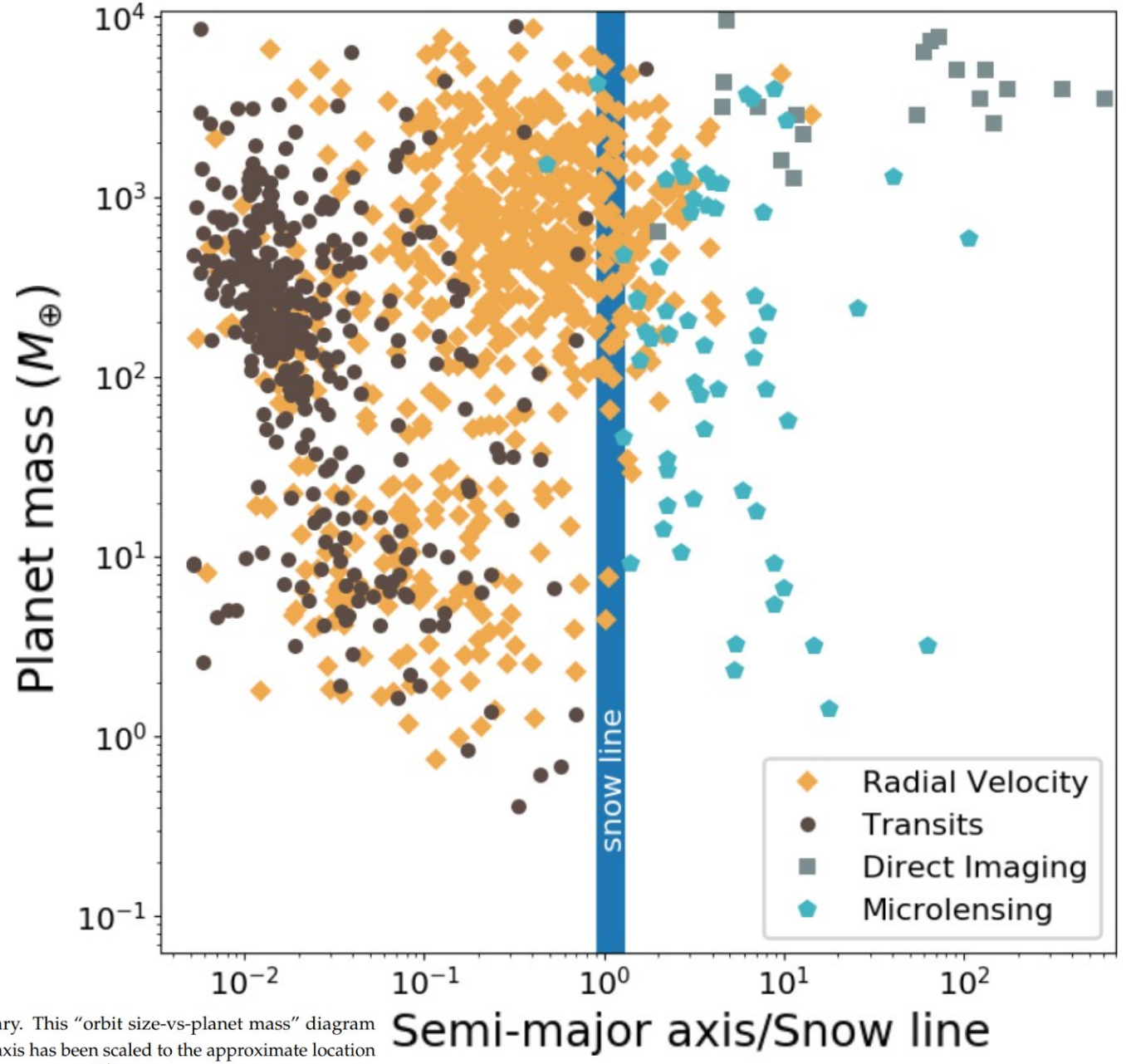

Figure 1. Planet-finding techniques are complementary. This "orbit size-vs-planet mass" diagram shows all reported exoplanets to-date. The semi-major axis has been scaled to the approximate location of the snow line of the planet-hosting star (assuming $a_{snow} \approx 2.85 M_*^{3/2}$AU). Transits and radial velocity are exceptionally good at finding "hot" planets close to their host stars, whereas microlensing and direct imaging are more efficient in discovering "cold" planets. *[Figure based on data from the NASA*

(c) Yiannis Tsapras, 2018

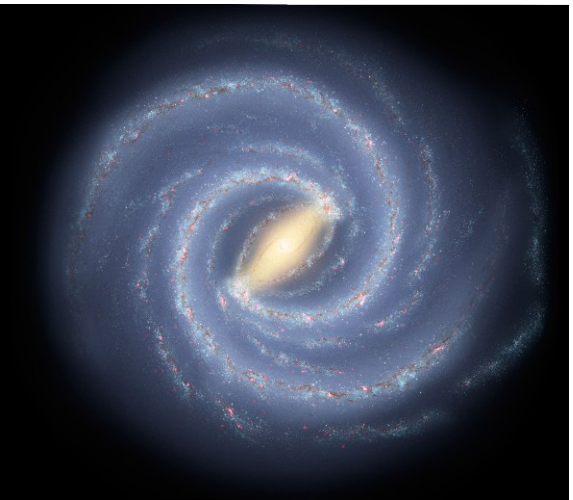

Técnica de microlensing é importante para estudar planetas em lugares distantes

Usando a técnica de microlente gravitacional, foi descoberto planeta tipo Júpiter orbitando uma anã branca a ~3UA → Júpiter deve sobreviver a evolução do Sol para as 2 fases de gigante

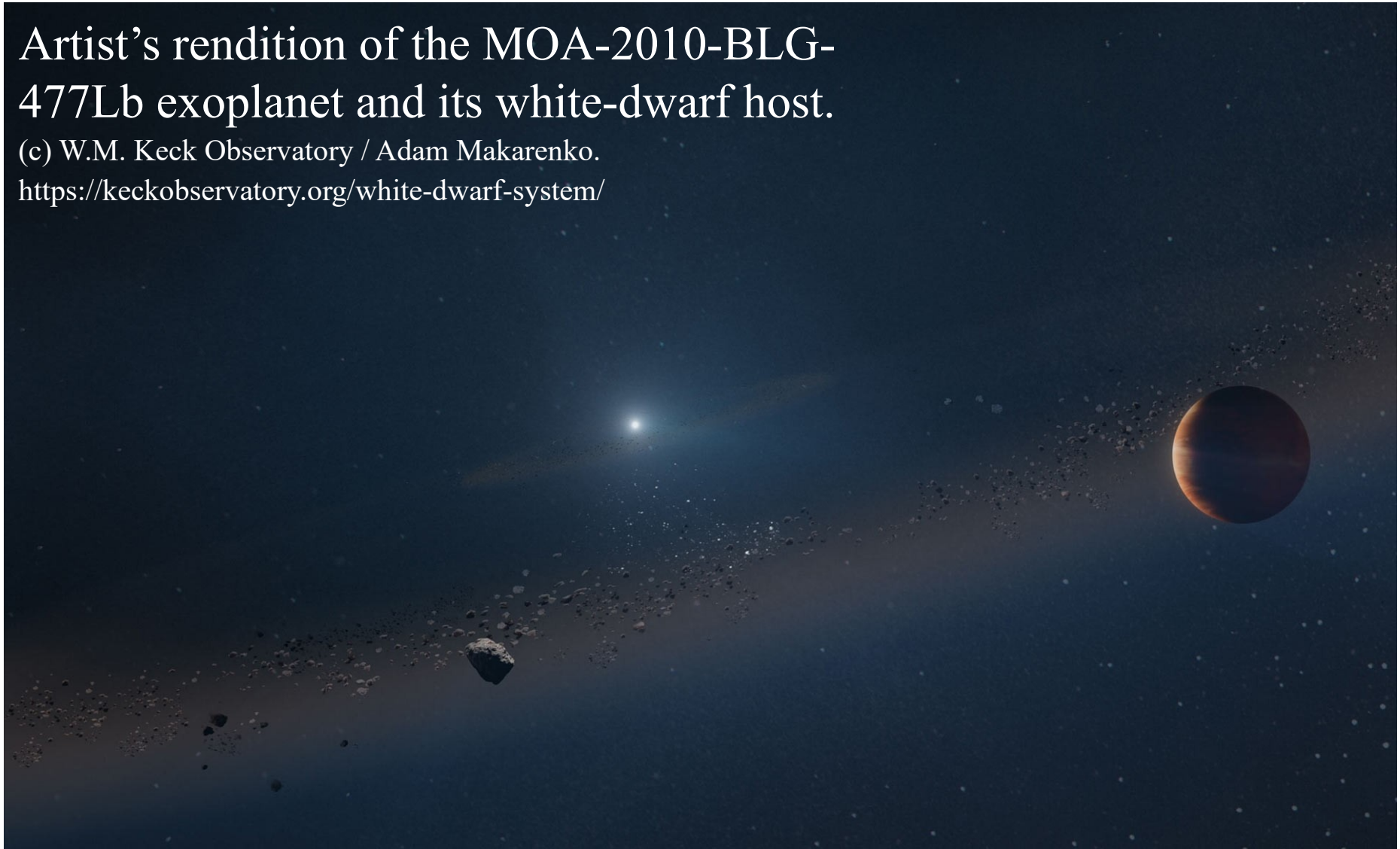

O futuro de exoplanetas via Microlensing:
Nancy Grace **Roman** Space Telescope (*former* WFIRST)

Kepler: D = 0,95m - optical
Stars: 100 thousand within 3000 light years

Nancy (WFIRST): D = 2,4 m – optical to IR. Launch: 5/2027 ?
Stars: 200 million within ~ 20000 light years (Galactic center)

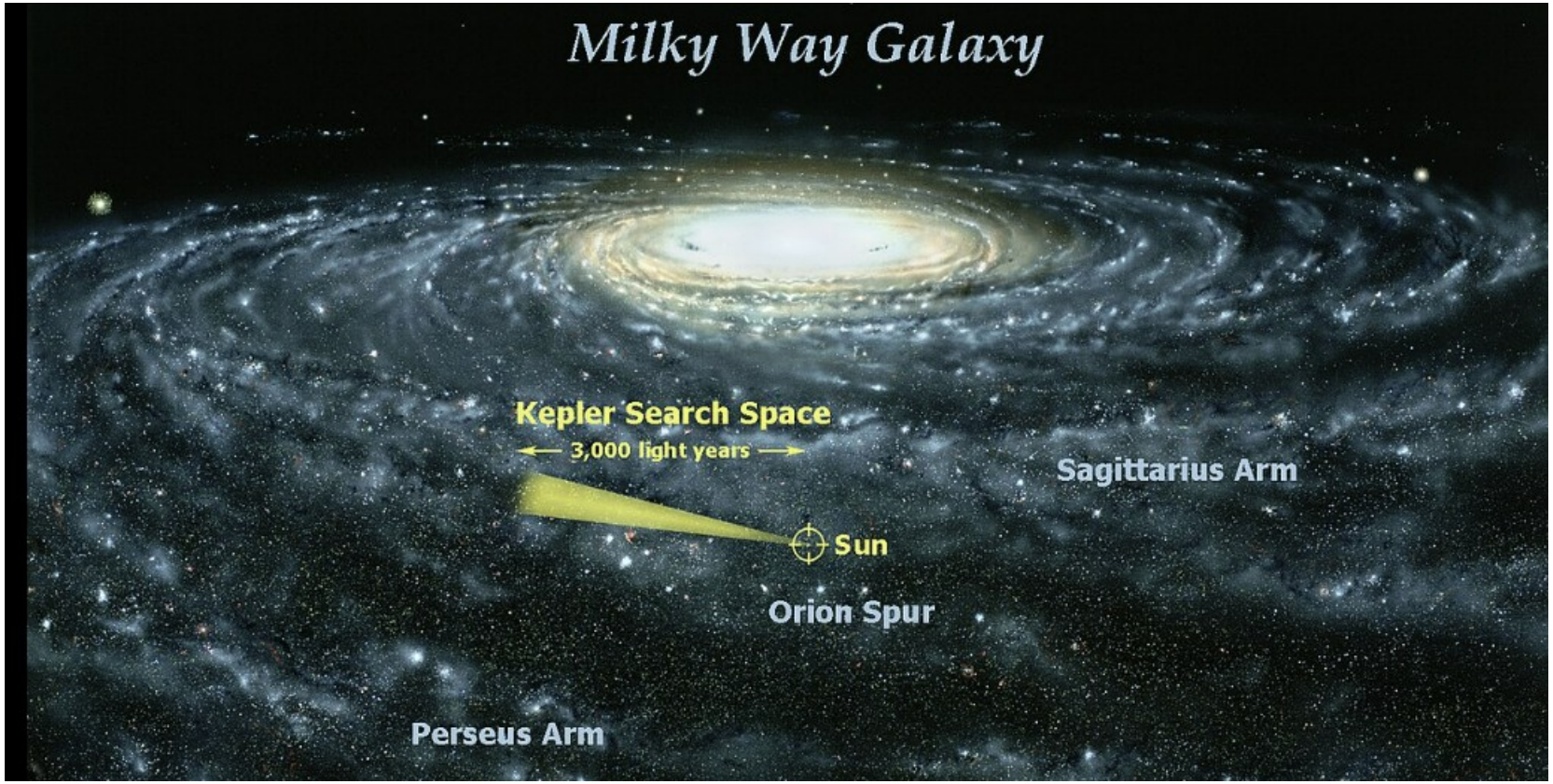

https://pt.wikipedia.org/wiki/Telesc%C3%B3pio_Espacial_Nancy_Grace_Roman

Instrumentos

O telescópio transportará dois instrumentos

Wide-Field Instrument (WFI)

O Wide-Field Instrument (WFI) é uma câmera de 300,8 megapixels que fornece multibanda visível para imagens até infravermelho próximo (0,48 a 2,30μm) [18] usando um filtro de banda larga e seis filtros de banda estreita. Uma matriz de plano focal baseada em HgCdTe captura um campo de visão de 0,28 graus quadrados com uma escala de pixels de 110 milissegundos de arco. A matriz de detectores é composta por 18 detectores H4RG-10 fornecidos pela Teledyne .[19] Este instrumento também carrega conjuntos de prismas de alta dispersão e de baixa dispersão para espectroscopia sem fenda de campo amplo.

Instrumento Coronagráfico (CGI)

O Instrumento Coronagráfico (CGI) é um coronógrafo de alto contraste que cobre comprimentos de onda mais curtos (575 nm a 825 nm) usando tecnologia de supressão de luz estelar de espelho duplo deformável. Pretende-se obter uma supressão de parte por bilhão da luz estelar para permitir a detecção e espectroscopia de planetas com uma separação visual de apenas 0,15 segundos de arco de suas estrelas hospedeiras.[20]

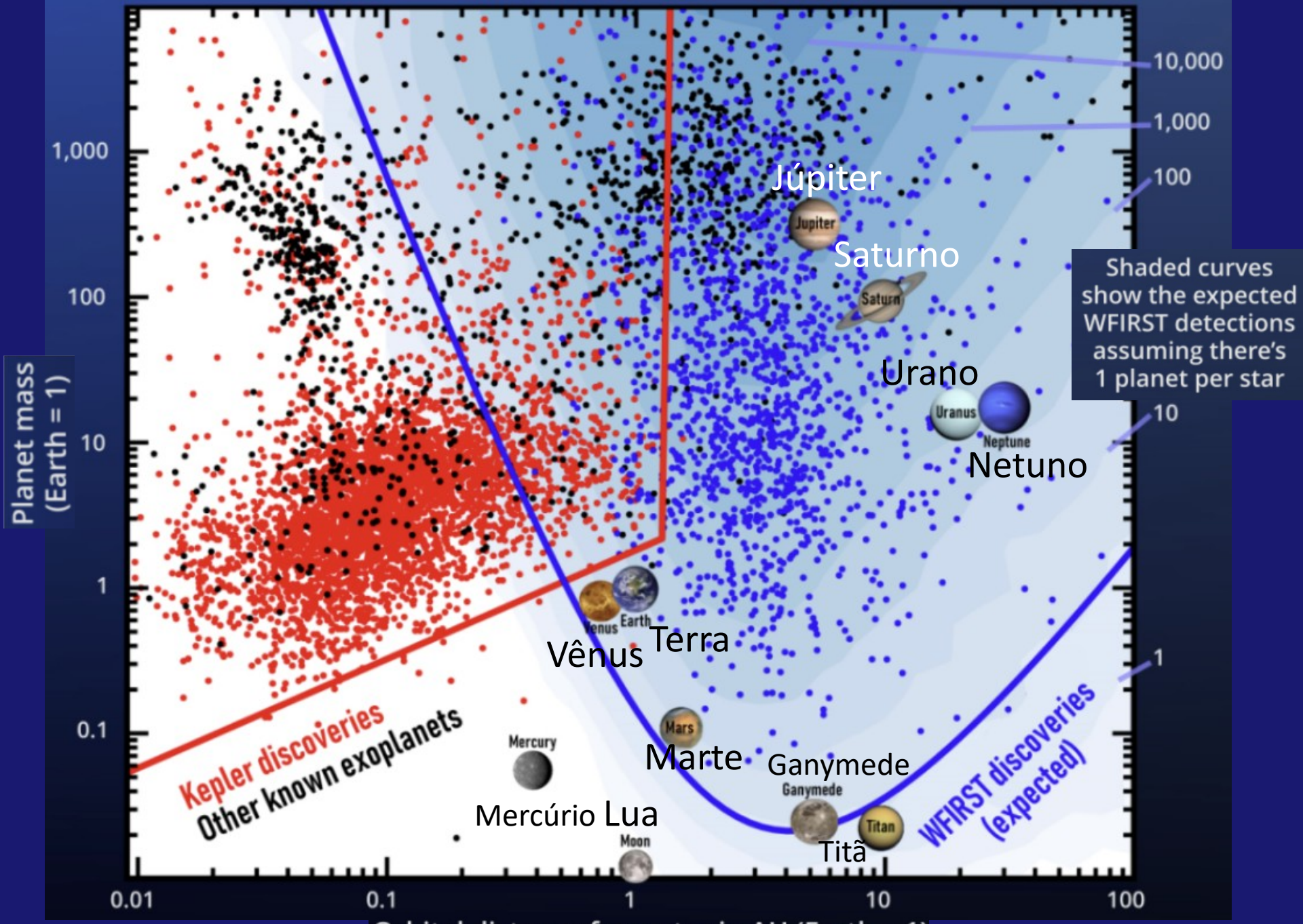

https://www.nasa.gov/missions/roman-space-telescope/warped-space-time-to-help-wfirst-find-exoplanets/

Método de detecção: imageamento

Planetas são muito fracos. A detecção só é possível bloqueando a luz da estrela-mãe: CORONOGRAFIA

Eclipse solar total de 2017

https://www.nasa.gov/centers-and-facilities/ames/how-scientists-predicted-coronas-appearance-during-aug-21-2017-total-solar-eclipse/

Finding the firefly next to the lighthouse

vagalume
luciernaga

http://w.astro.berkeley.edu/~gduchene/

Finding the firefly next to the lighthouse

http://w.astro.berkeley.edu/~gduchene/

Finding the firefly next to the lighthouse

http://w.astro.berkeley.edu/~gduchene/

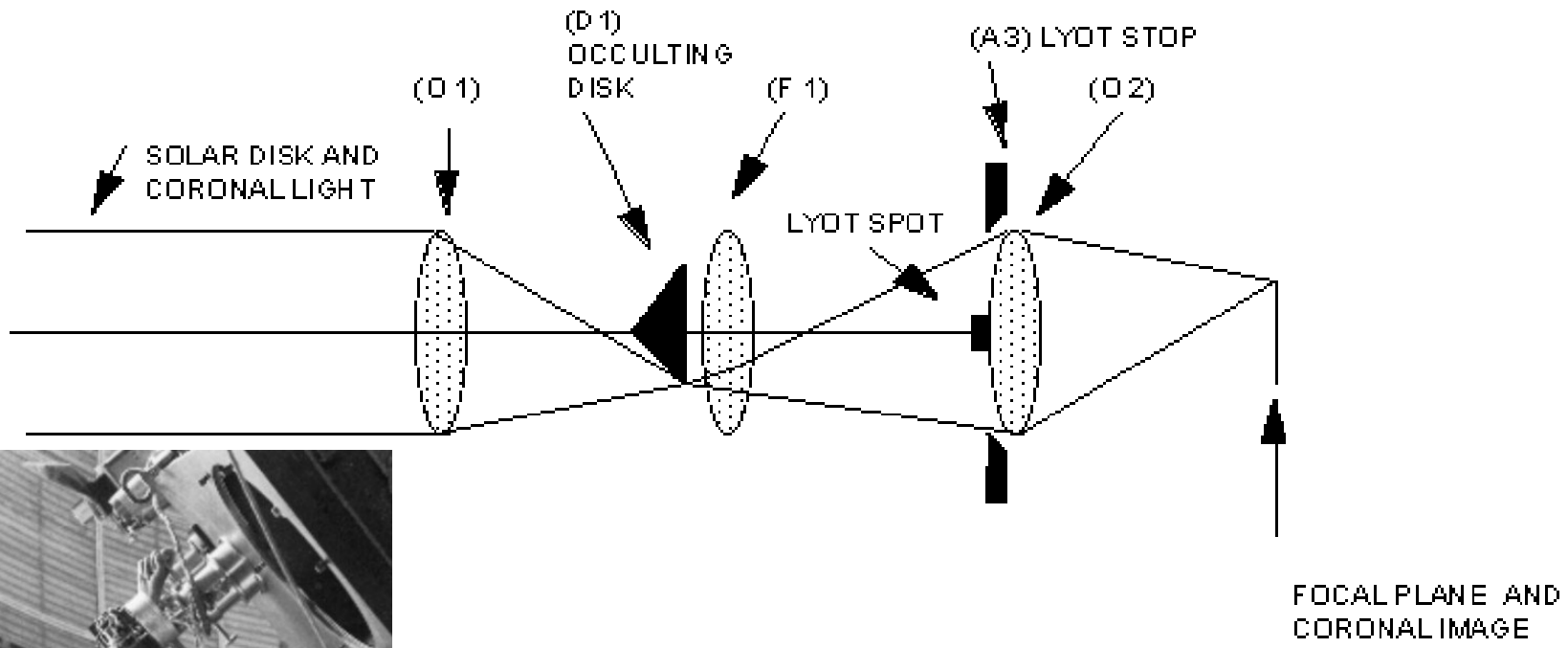

Lyot Coronograph

Os primeiros coronografos foram desenhados para estudar a coroa solar

Bernard Lyot at Pic du Midi (1939)

Solar corona, High Altitude Observatory, 30/5/2018

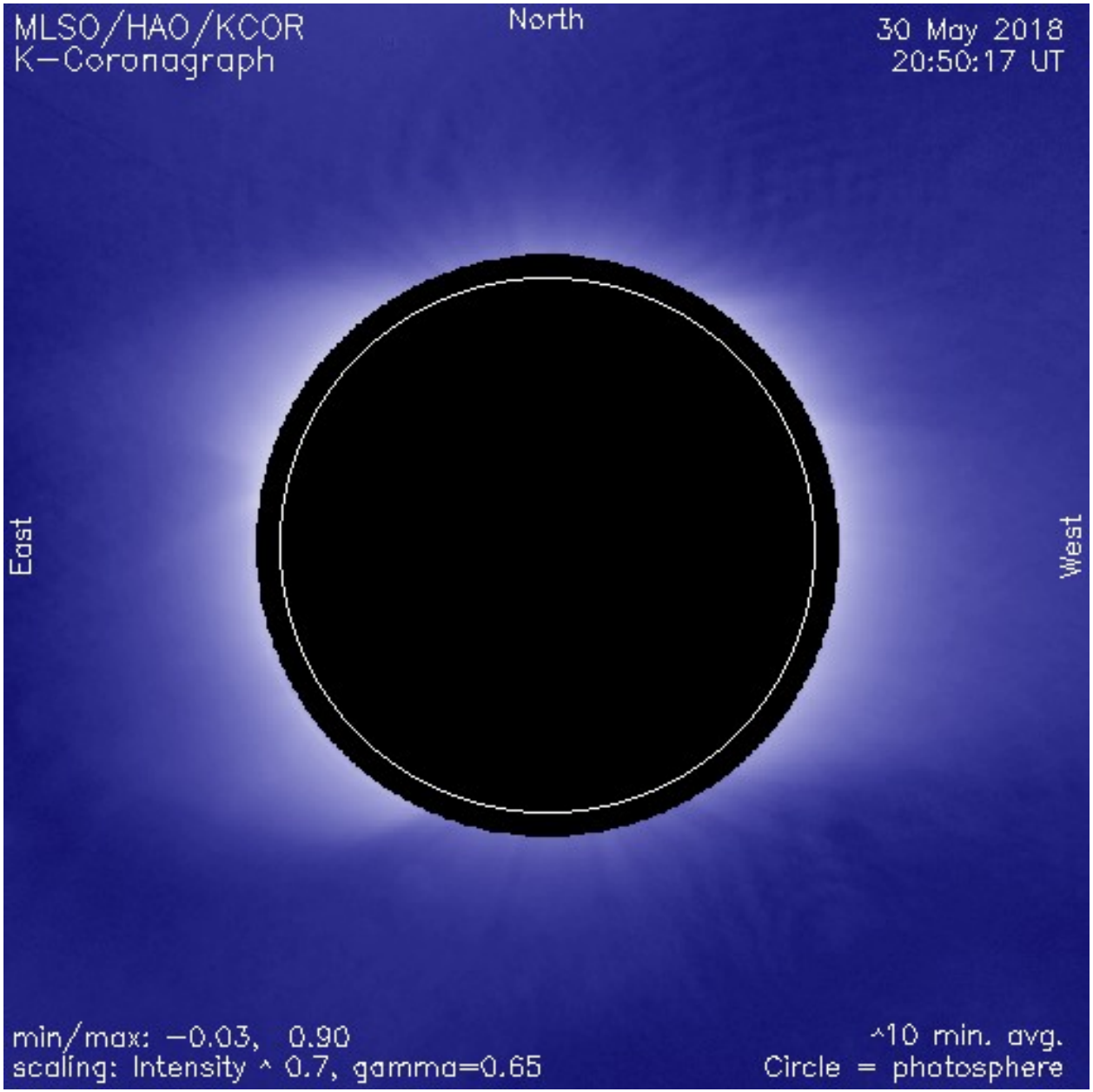

Ejeção de massa coronal

Besides the SDO images, the CME was also observed by SOHO using 2 coronagraphs where the bright sun is blocked by a disk so it does not overpower the fainter corona.

What about coronography in stars?

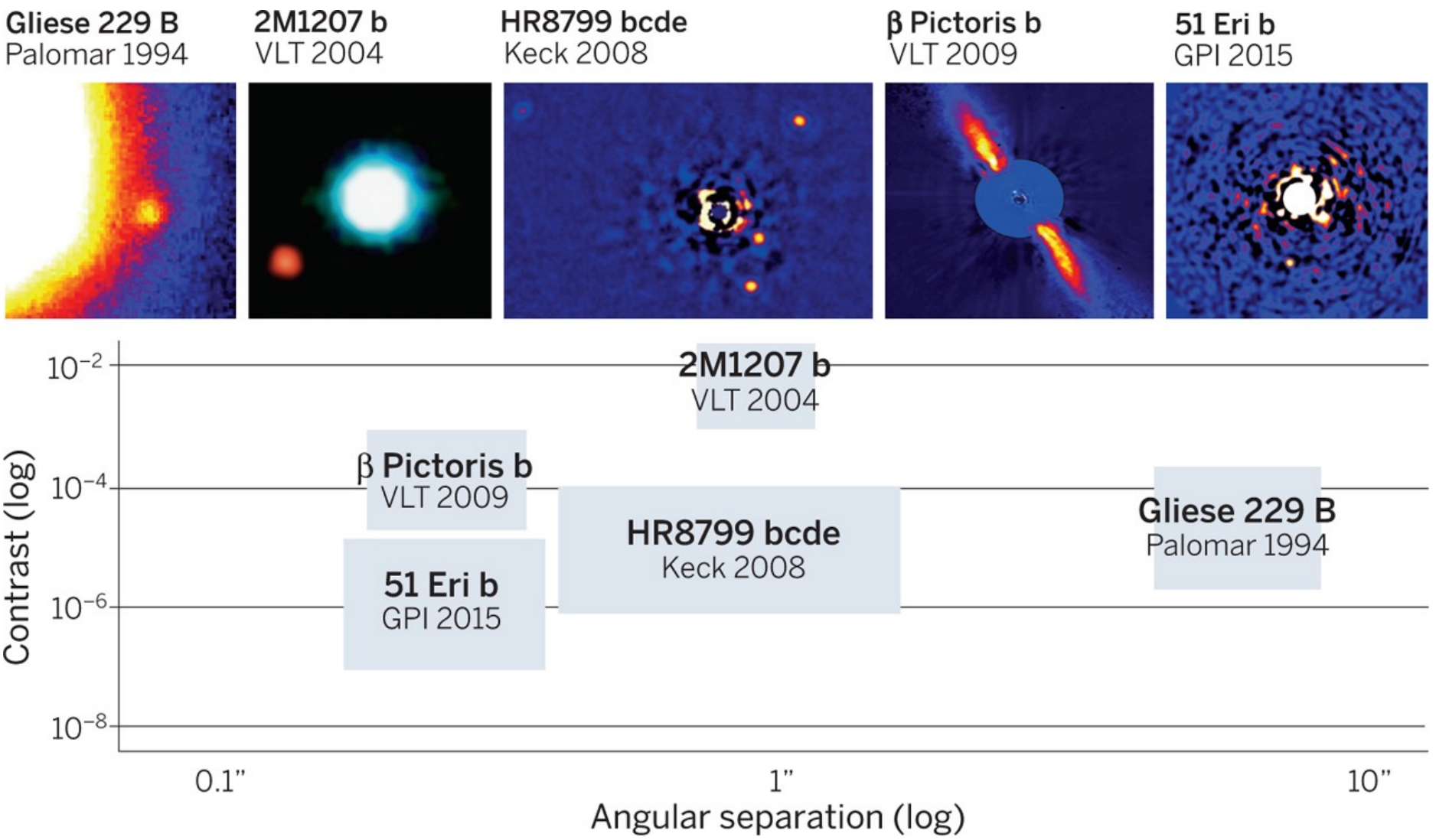

http://science.sciencemag.org/content/350/6256/39.full

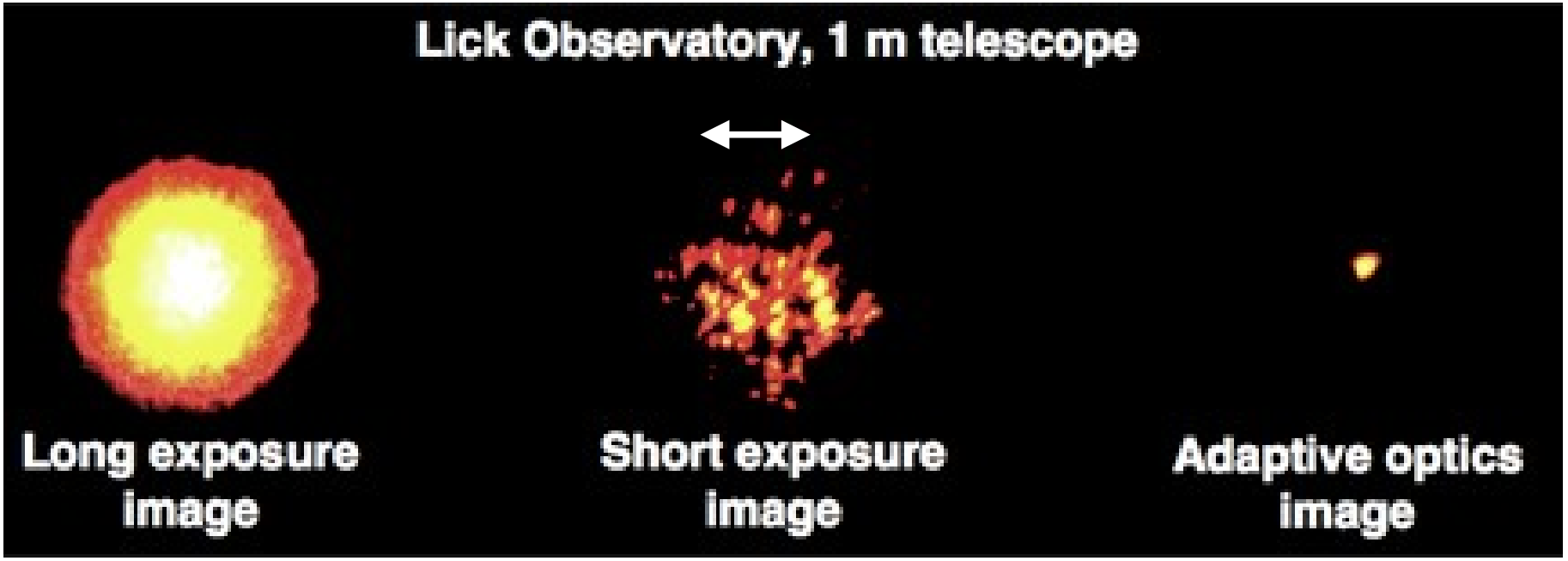

Bright Star (Arcturus) Observed with Lick Observatory's 1-m Telescope

A turbulência (“seeing” ~ 1 arcsec) da atmosfera terrestre não permite obter imagens muito nítidas

Efeito da turbulência atmosférica

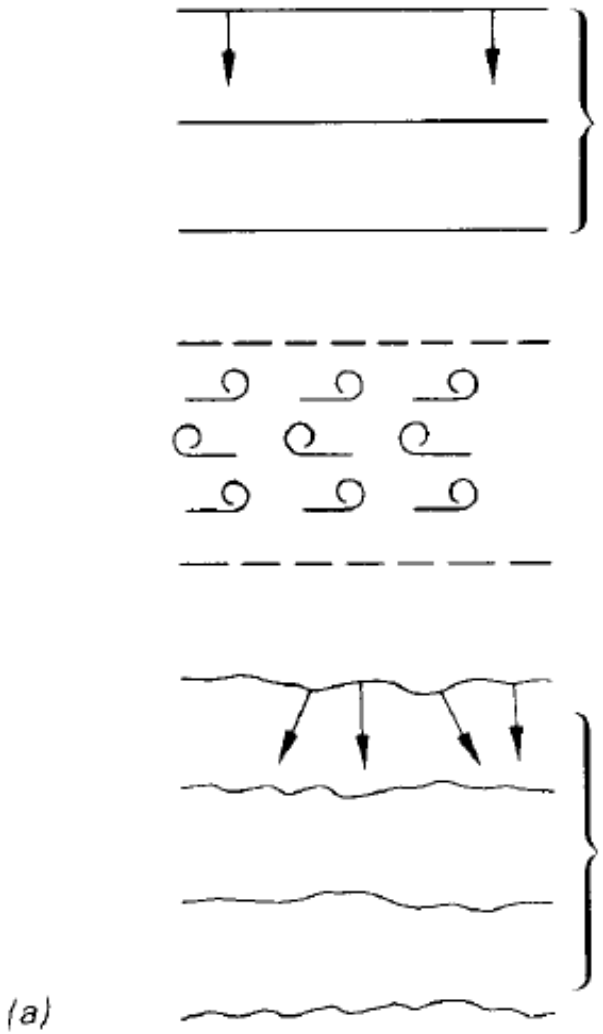

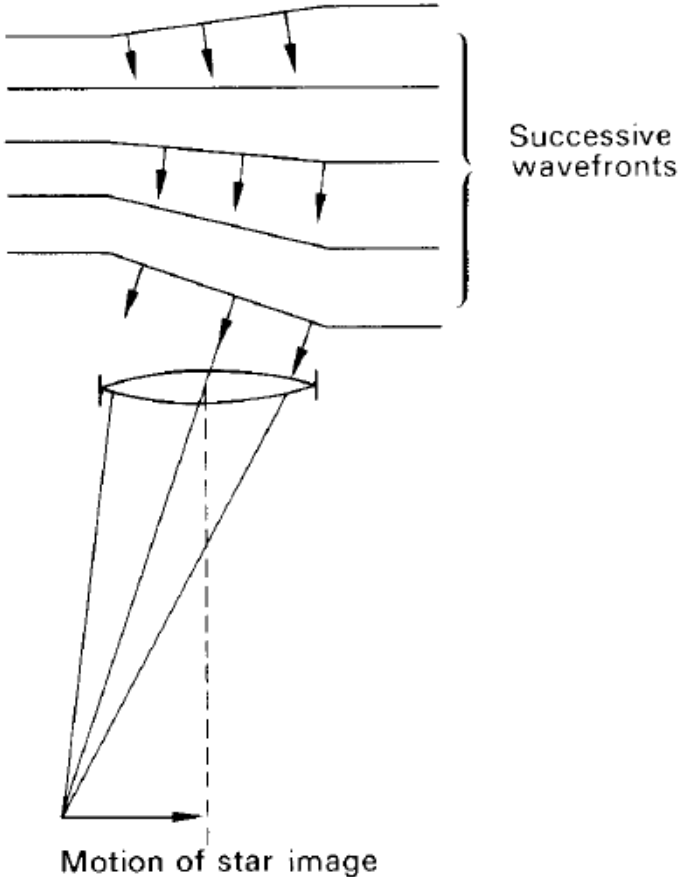

(*b*) The dancing effect of a star image when viewed with a telescope.

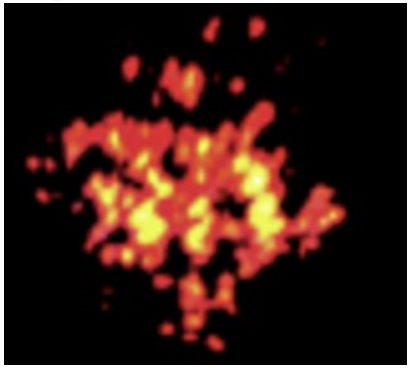

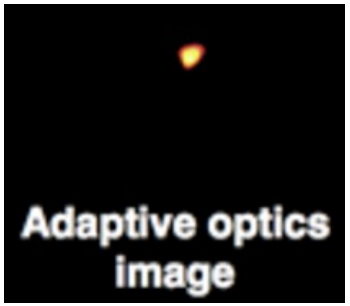

Figure 19.7. (*a*) The effect of atmospheric turbulence.

© Roy & Clarke

Seeing vs. Diffraction (angular resolution) limit

Airy disc, I_A. The ratio, $S = I_S/I_A$, is referred to as the **Strehl index** and it is not uncommon for it to be no greater than a few per cent.

Resolução angular (limite de **difração**) de telescópio de diâmetro d:

α [rad] = 1,2 λ /d

Para banda V (540nm):

α[”] = 0,136 /*d*[m]

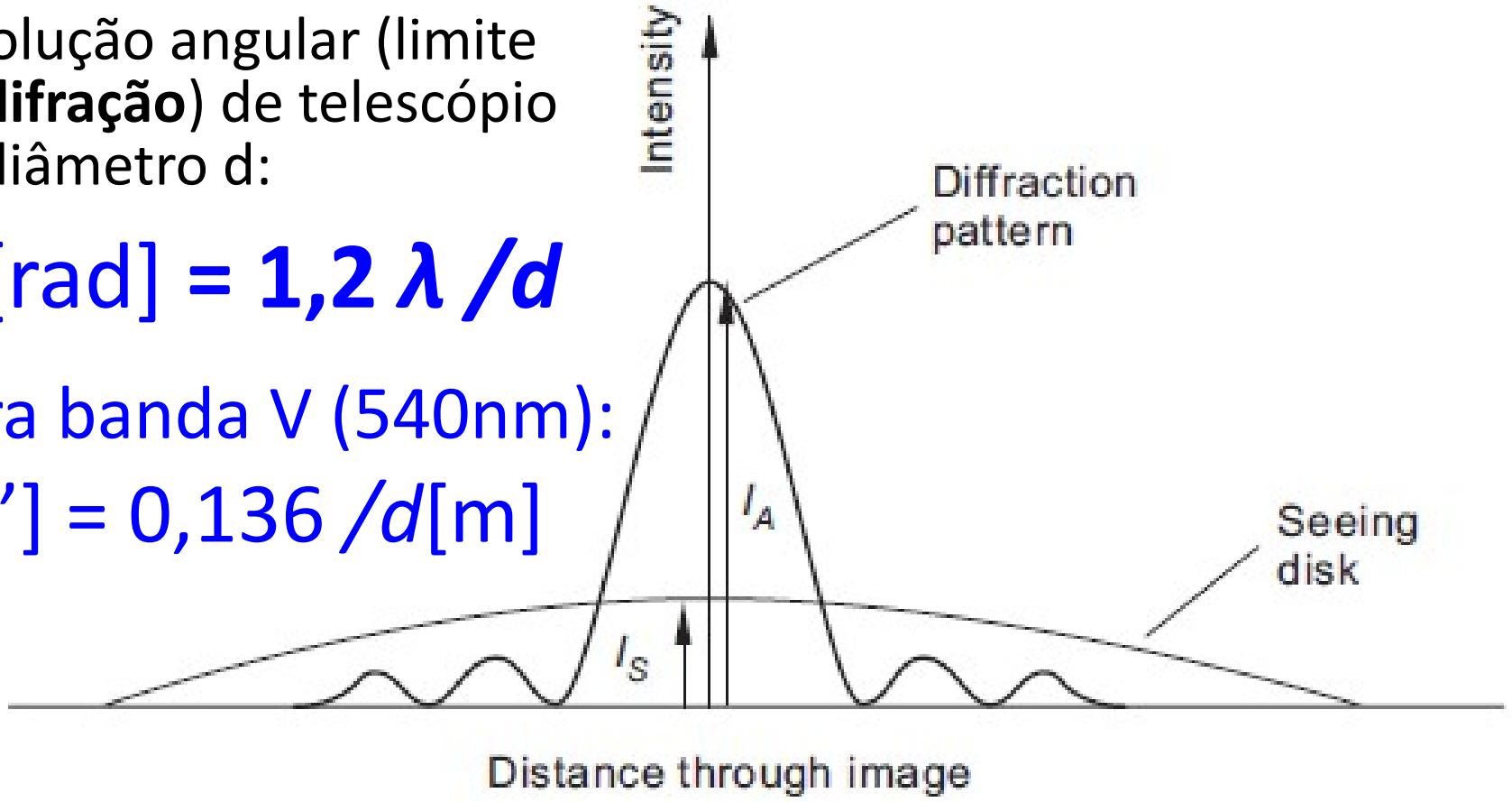

Figure 19.8. The seeing disc of a star is superposed in the theoretical diffraction pattern in the image plane. The ratio of the peak intensities, I_S/I_A is referred to as the Strehl index.

© Roy & Clarke

Image of a point source by a circular aperture (telescope) due to diffraction: Airy function

α [rad] = **1,2 λ /d**

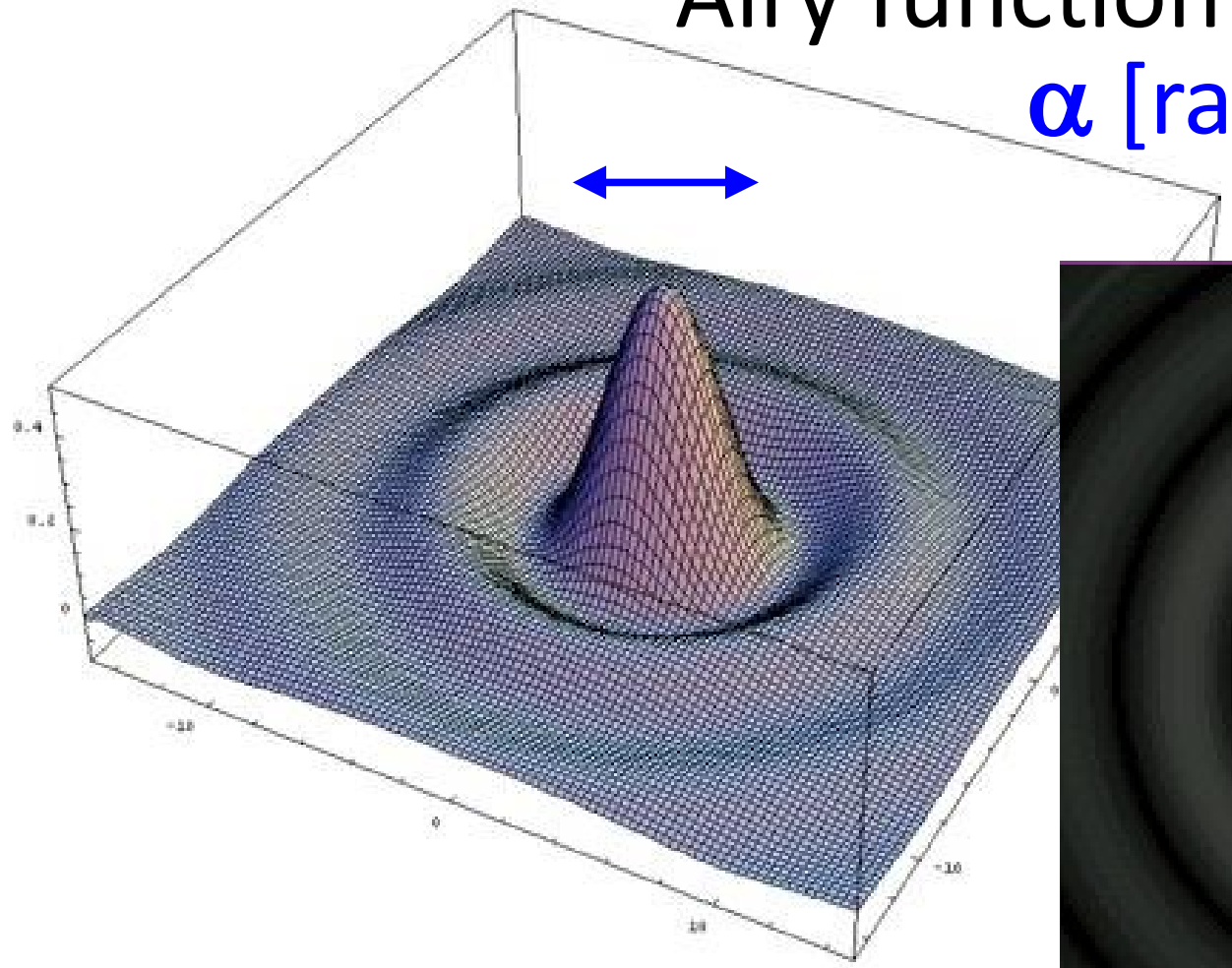

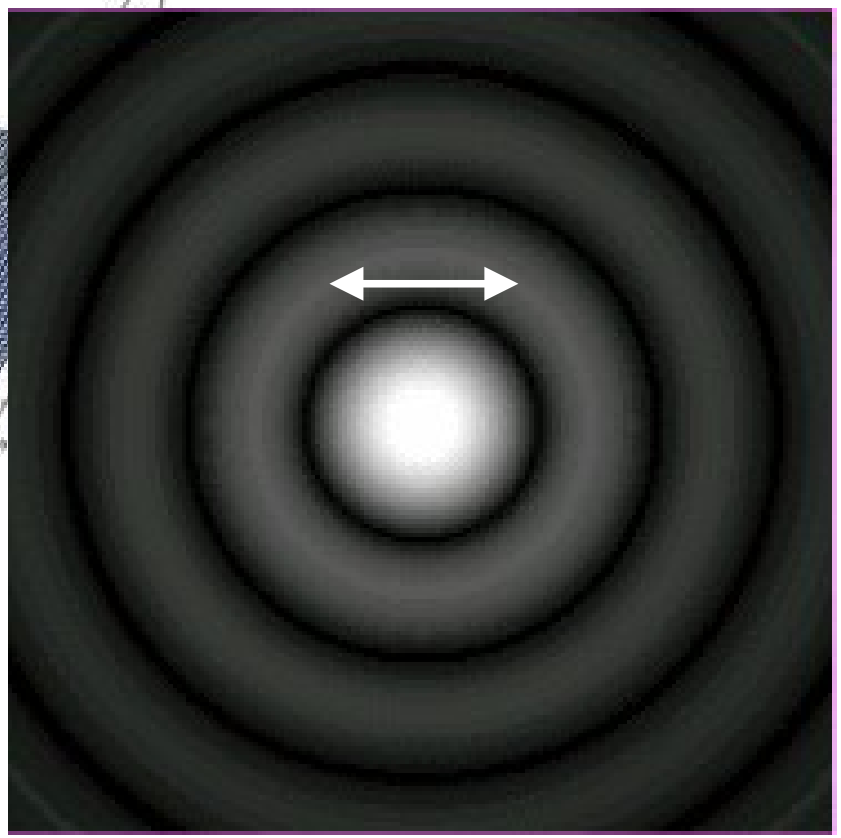

Adaptive optics

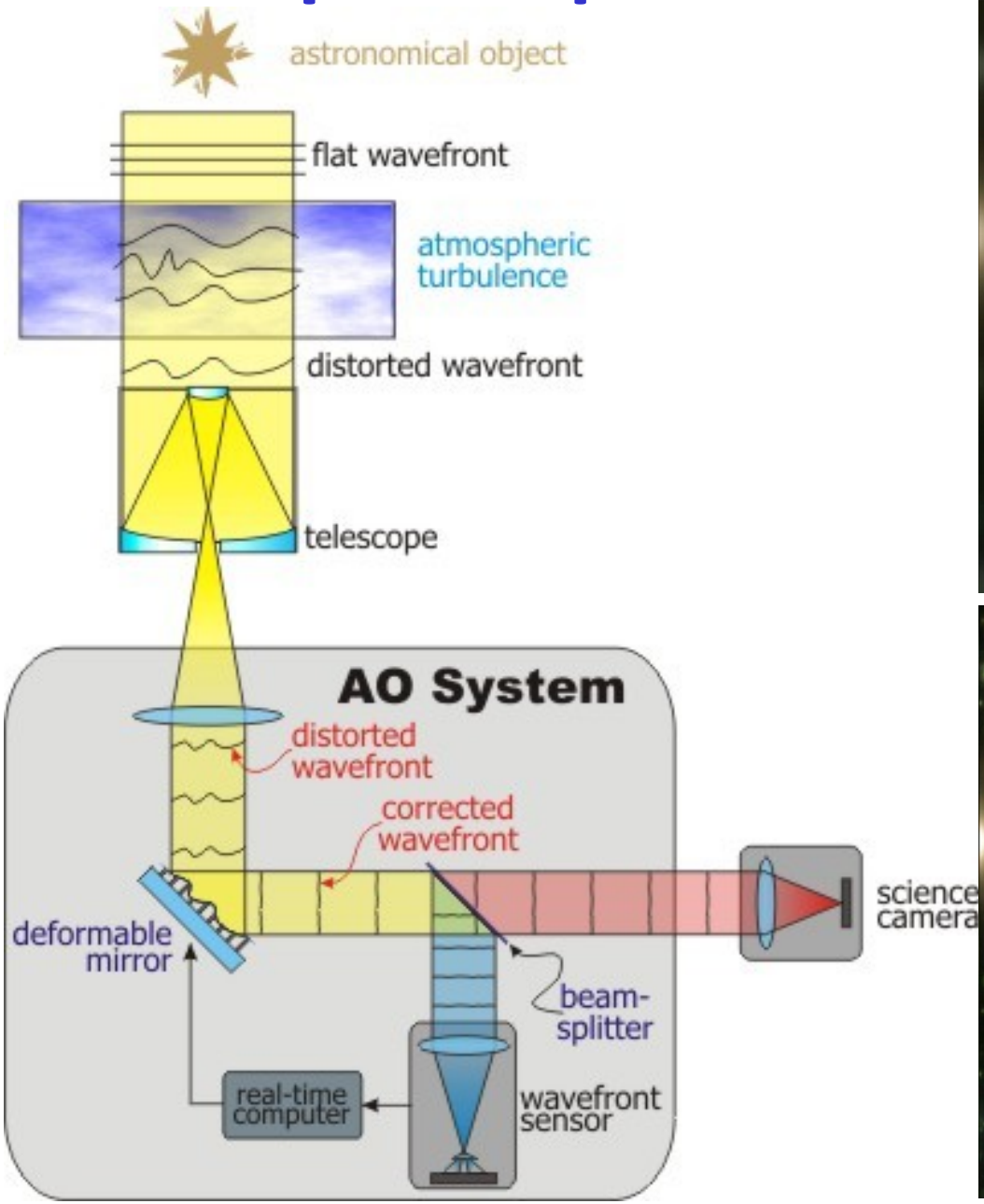

Center of our galaxy

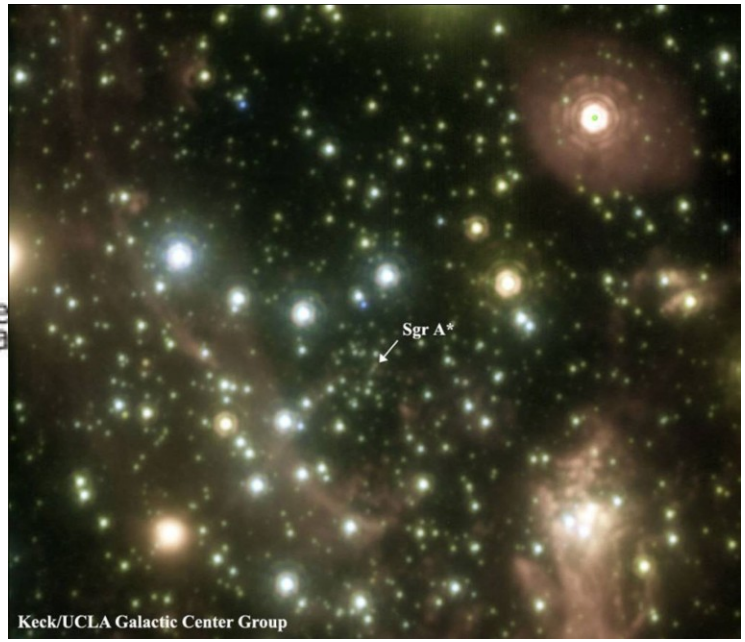

Corrections with Adaptive Optics

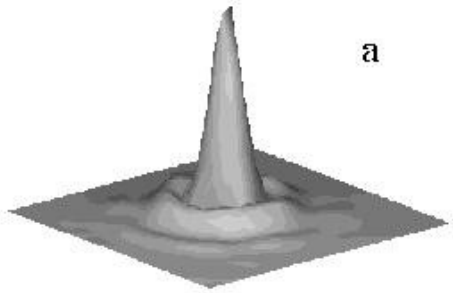

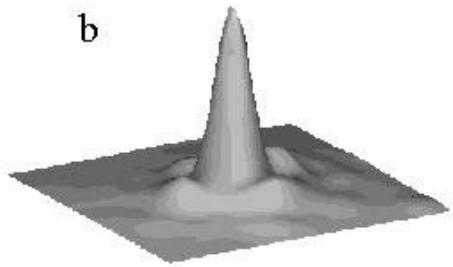

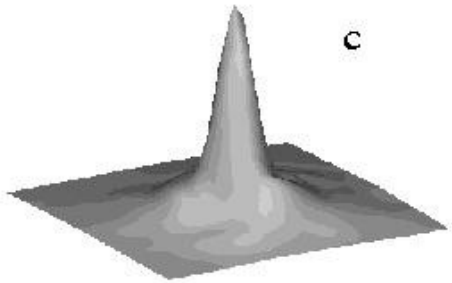

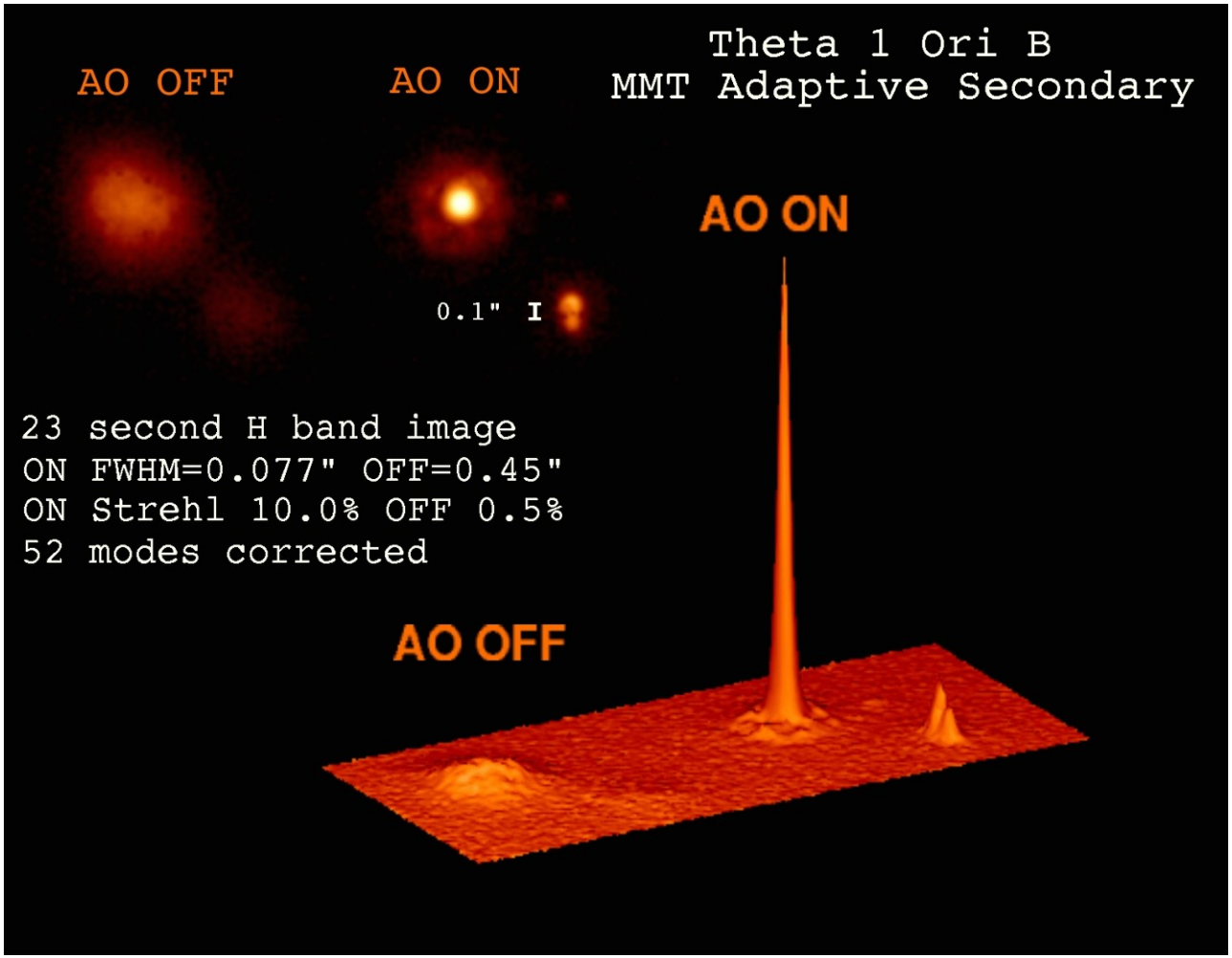

The state of the art

Gemini Planet Imager

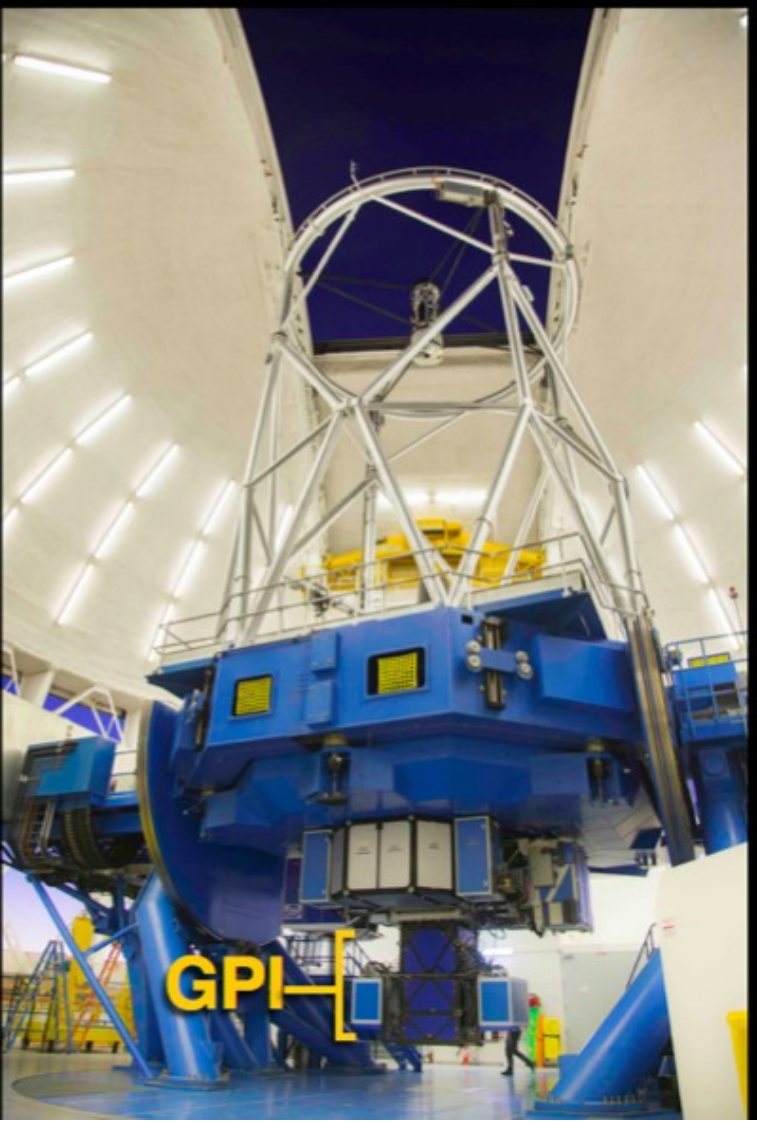

Gemini Planet Imager

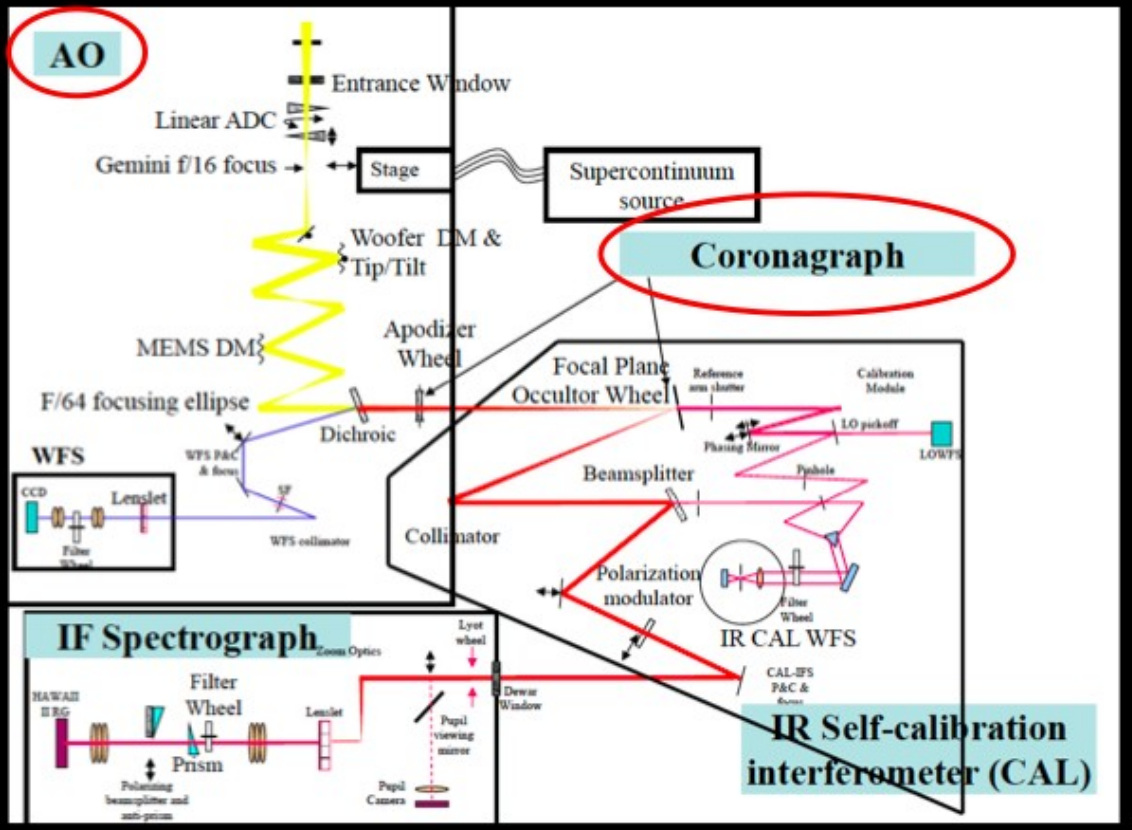

http://w.astro.berkeley.edu/~gduchene/

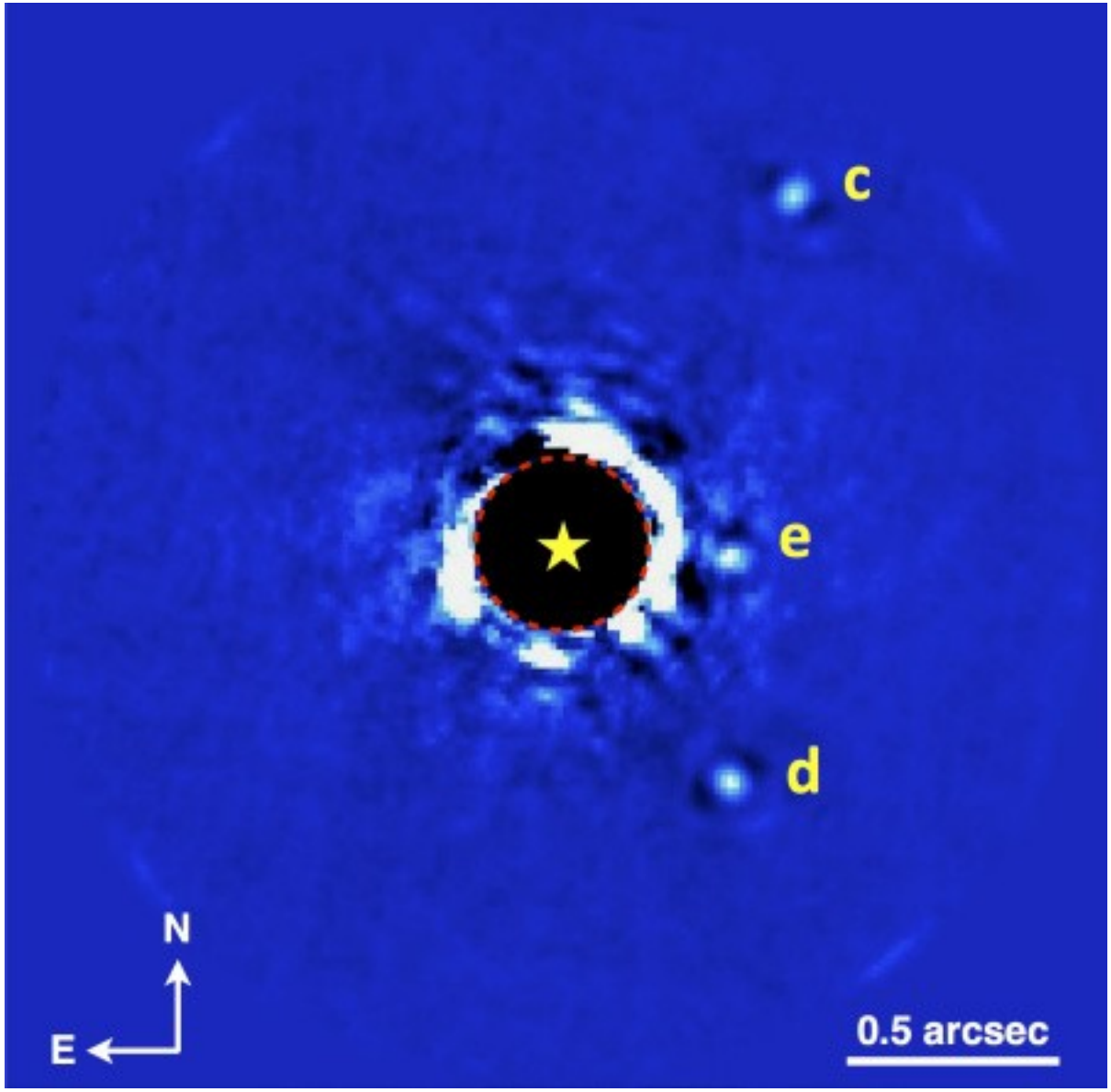

GPI imaging of the planetary system HR 8799 in the near-infrared K band, showing 3 of the 4 planets. (Planet b is outside the field of view shown here, off to the left.) These data were obtained on November 17, 2013 during the first week of operation of GPI and in relatively challenging weather conditions, but with GPI's advanced adaptive optics system and coronagraph the planets can still be clearly seen. Credit: Christian Marois (NRC Canada), Patrick Ingraham (Stanford University) and the GPI Team.

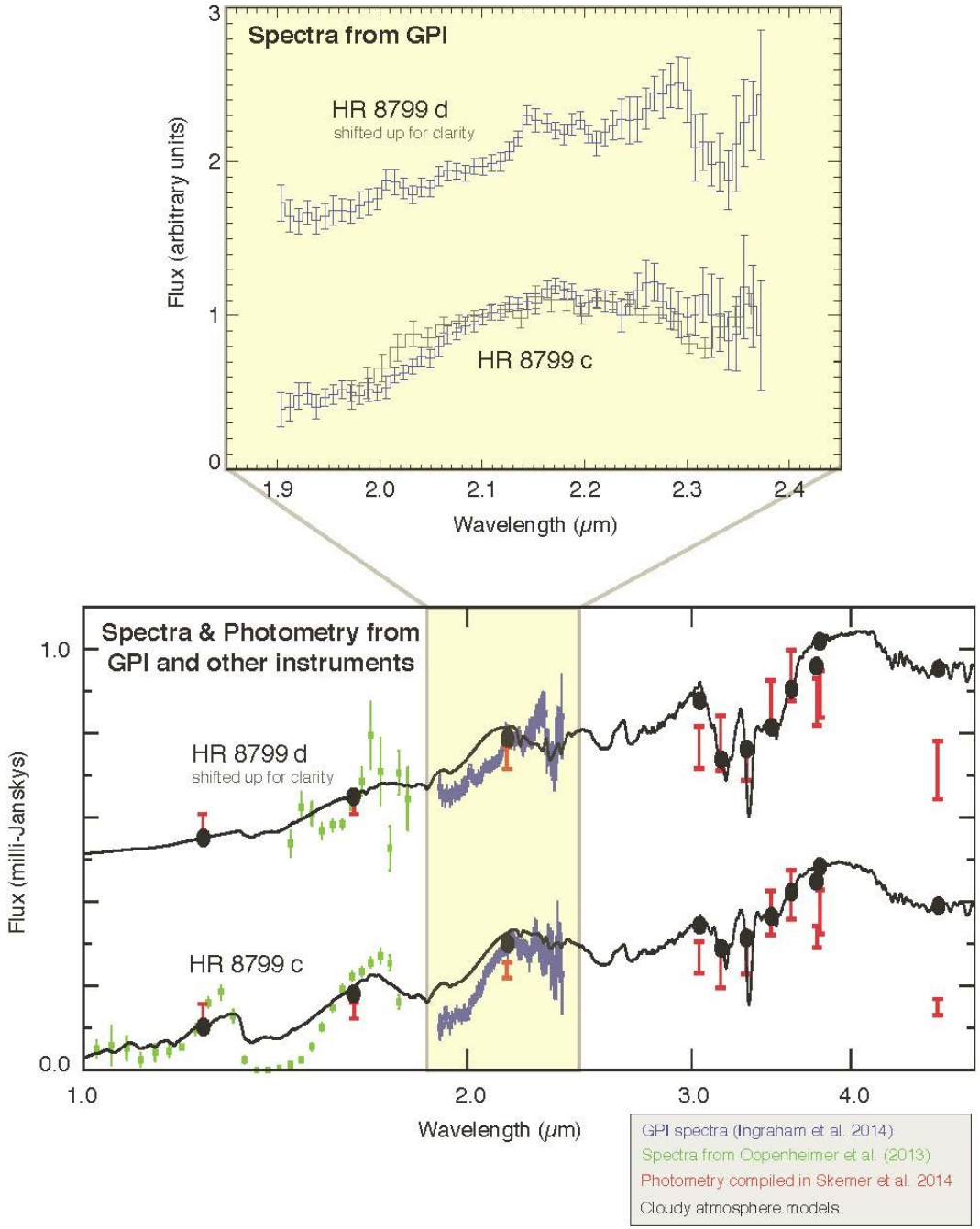

GPI spectroscopy of planets c and d in the HR 8799 system. While earlier work showed that the planets have similar overall brightness and colors, these newly-measured spectra show surprisingly large differences. The spectrum of planet d increases smoothly from 1.9-2.2 microns while planet c's spectrum shows a sharper kink upwards just beyond 2 microns. These new GPI results indicate that these similar-mass and equal-age planets nonetheless have significant differences in atmospheric properties, for instance more open spaces between patchy cloud cover on planet c versus uniform cloud cover on planet d, or perhaps differences in atmospheric chemistry. These data are helping refine and improve a new generation of atmospheric models to explain these effects. © Patrick Ingraham, Mark Marley, Didier Saumon and the GPI Team.

Sphere at the VLT

First light of the VLT planet finder SPHERE

III. New spectrophotometry and astrometry of the HR 8799 exoplanetary system ⋆

A. Zurlo[1,2,3,4], A. Vigan[3,5], R. Galicher[6], A.-L. Maire[4], D. Mesa[4], R. Gratton[4], G. Chauvin[7,8], M. Kasper[9,7,8], C. Moutou[3], M. Bonnefoy[7,8], S. Desidera[4], L. Abe[10], D. Apai[11,12,13], A. Baruffolo[4], P. Baudoz[6], J. Baudrand[6], J.-L. Beuzit[7,8], P. Blancard[3], A. Boccaletti[6], F. Cantalloube[7,8], M. Carle[3], J. Charton[8], R.U. Claudi[4], A. Costille[3], V. de Caprio[14], K. Dohlen[3], C. Dominik[15], D. Fantinel[4], P. Feautrier[8], M. Feldt[16], T. Fusco[3,18], E. Gascone[14], P. Gigan[6], J.H. Girard[5,7,8], D. Gissler[17], L. Gluck[7,8], C. Gry[3], T. Henning[16], E. Hugot[3], M. Janson[19,16], M. Jacquet[3], A.-M. Lagrange[7,8], M. Langlois[20,3], M. Llored[3], F. Madec[3], Y. Magnard[8], P. Martinez[10], D. Maurel[8], D. Mawet[21], M.R. Meyer[17], J. Milli[5,7,8], O. Moeller-Nilsson[16], D. Mouillet[7,8], A. Origné[3], A. Pavlov[16], C. Petit[18], P. Puget[8], S.P. Quanz[17], P. Rabou[8], J. Ramos[16], A. Roux[8], B. Salasnich[4], G. Salter[3], J.-F. Sauvage[3,18], H.M. Schmid[17], C. Soenke[5], E. Stadler[8], M. Suarez[5], M. Turatto[4], S. Udry[22], F. Vakili[10], Z. Wahhaj[5], F. Wildi[22]

Planetary system HR 8799

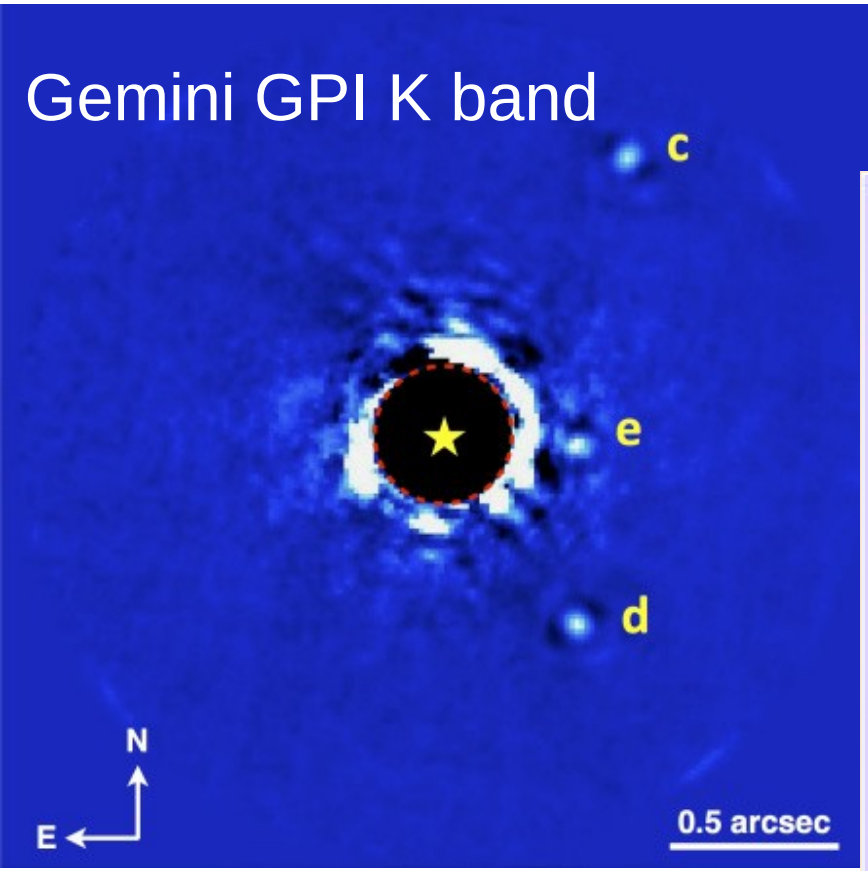

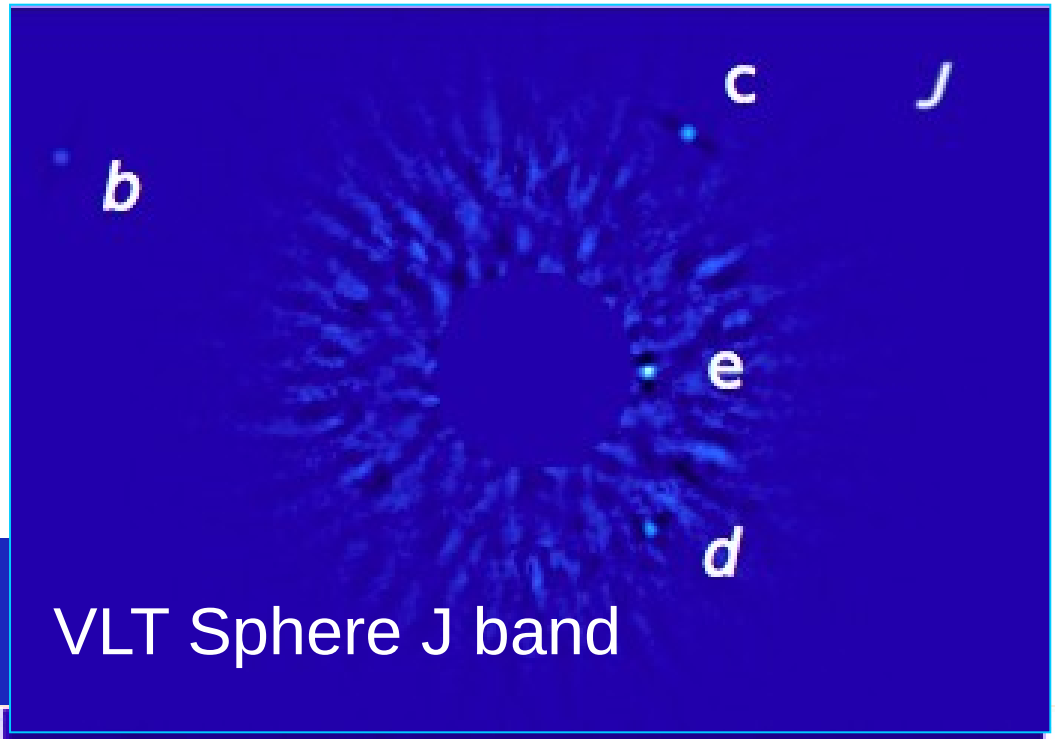

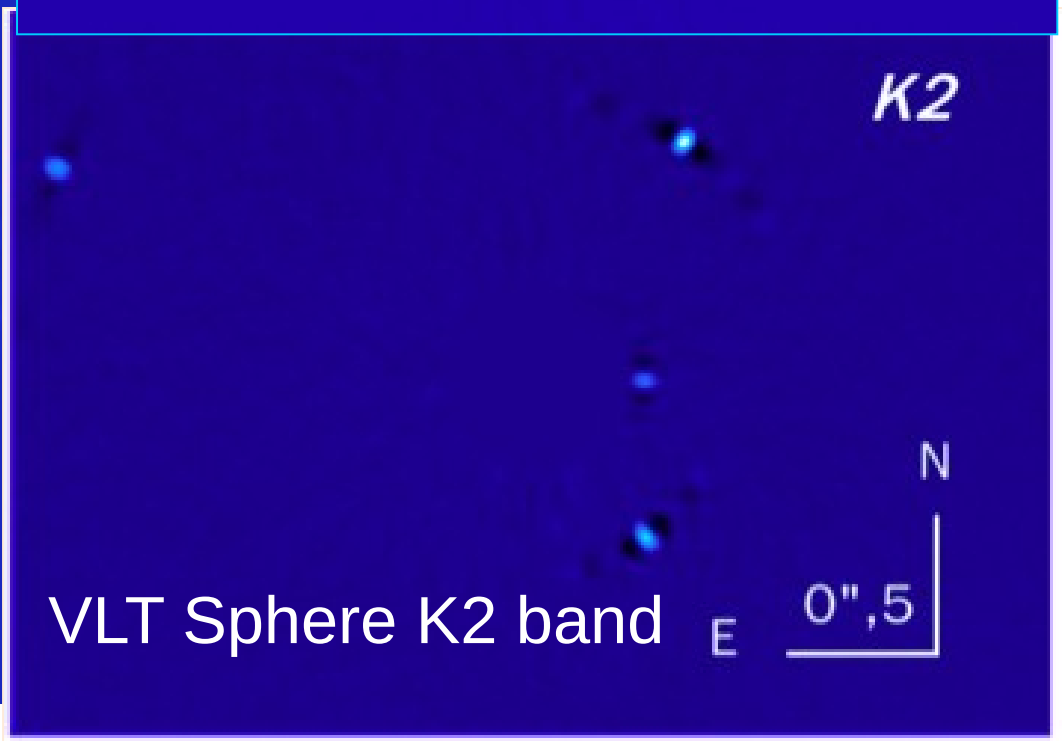

Spectrum of the planet HR 8799d (Y, J, H bands with Sphere/VLT; K band with GPI/Gemini)

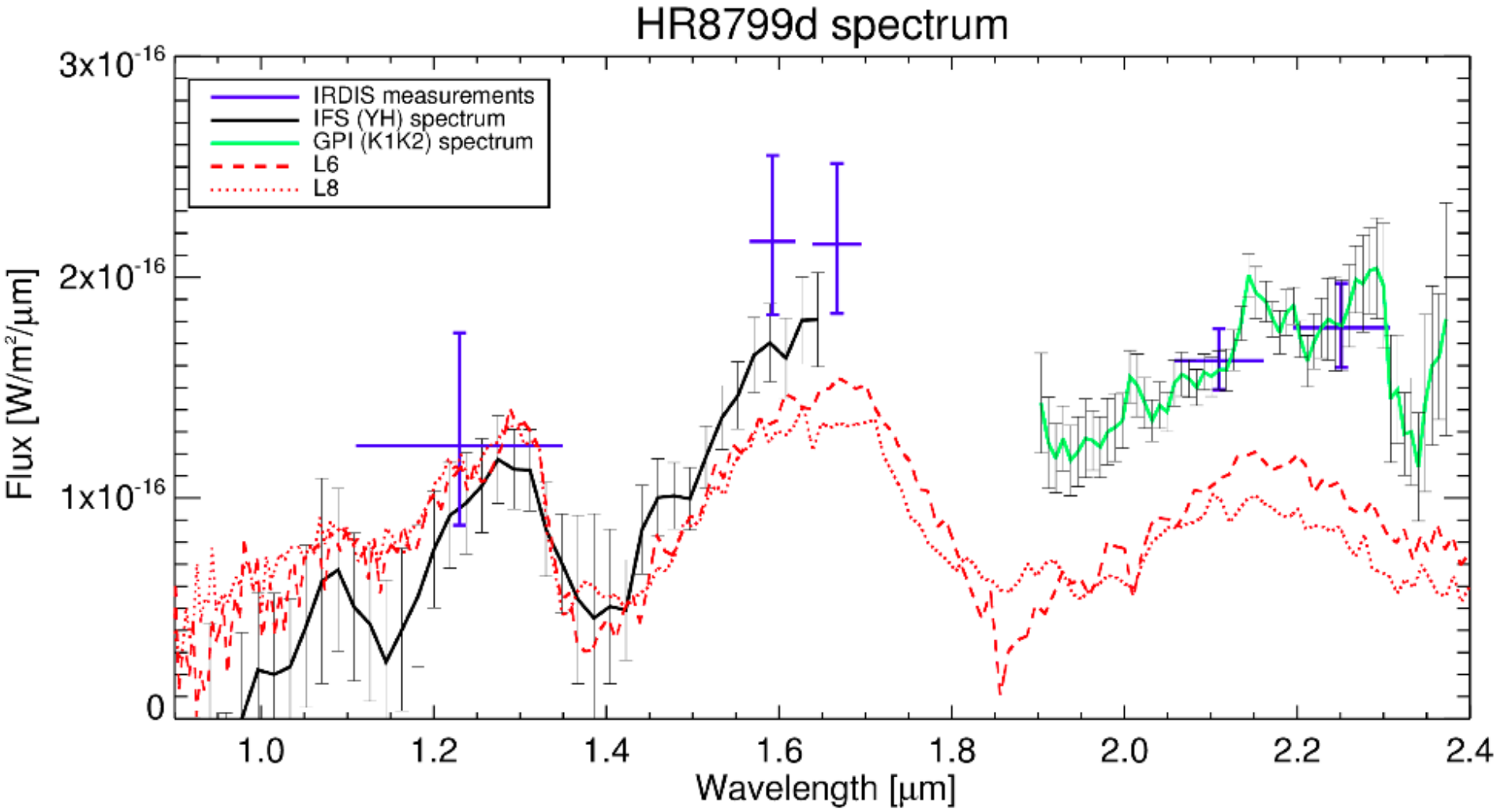

Title: **Characterization of solar twin blue straggler candidates: towards improved stellar ages for field stars**

Principal Investigator: **Thayse Pacheco**

GEMINI OBSERVATORY

observing time request summary

Partner	Lead	PI Request Time	Min
Brazil	Pacheco	4.0 hr	2.0 hr

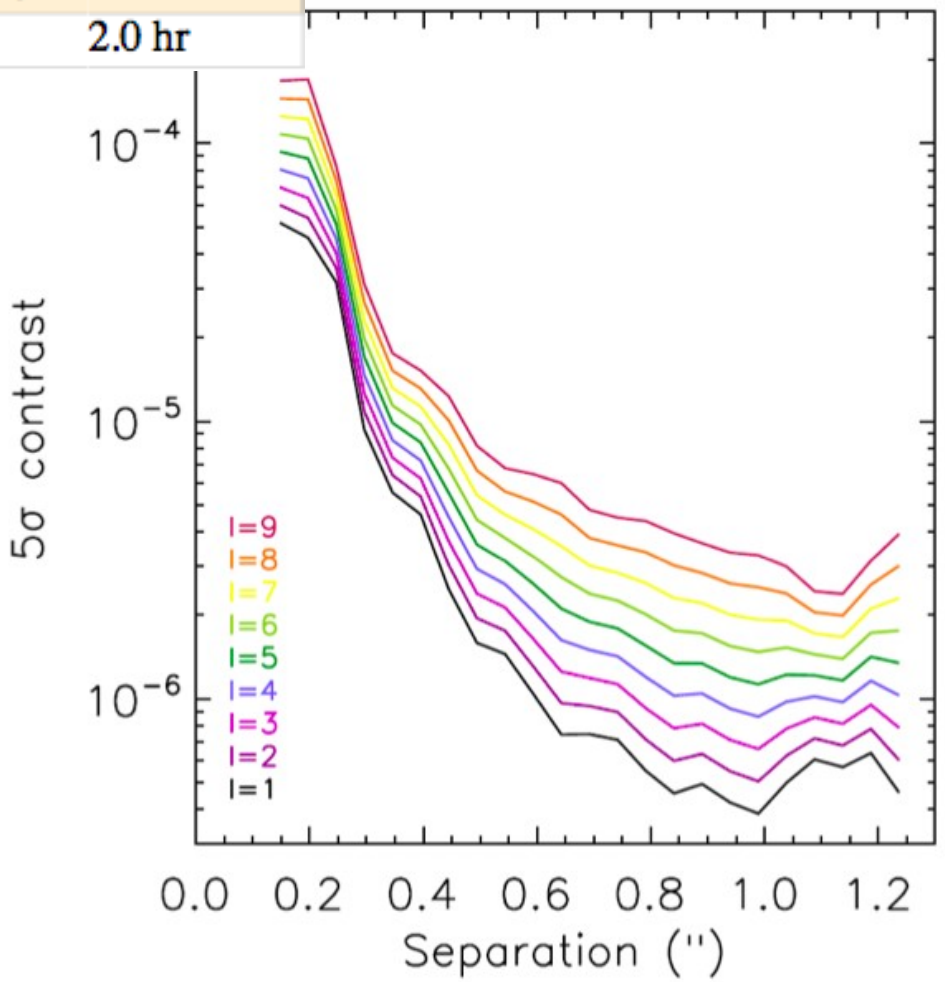

Figure 2: Typical GPI constrasts in function of target separation for different I magnitudes in a 1 hour exposure.

https://www.gemini.edu/sciops/instruments/gpi/instrument-performance/strehl-0

GPI Strehl

GPI PSFs

With coronagraph (top)
W/O coronagraph (bottom)

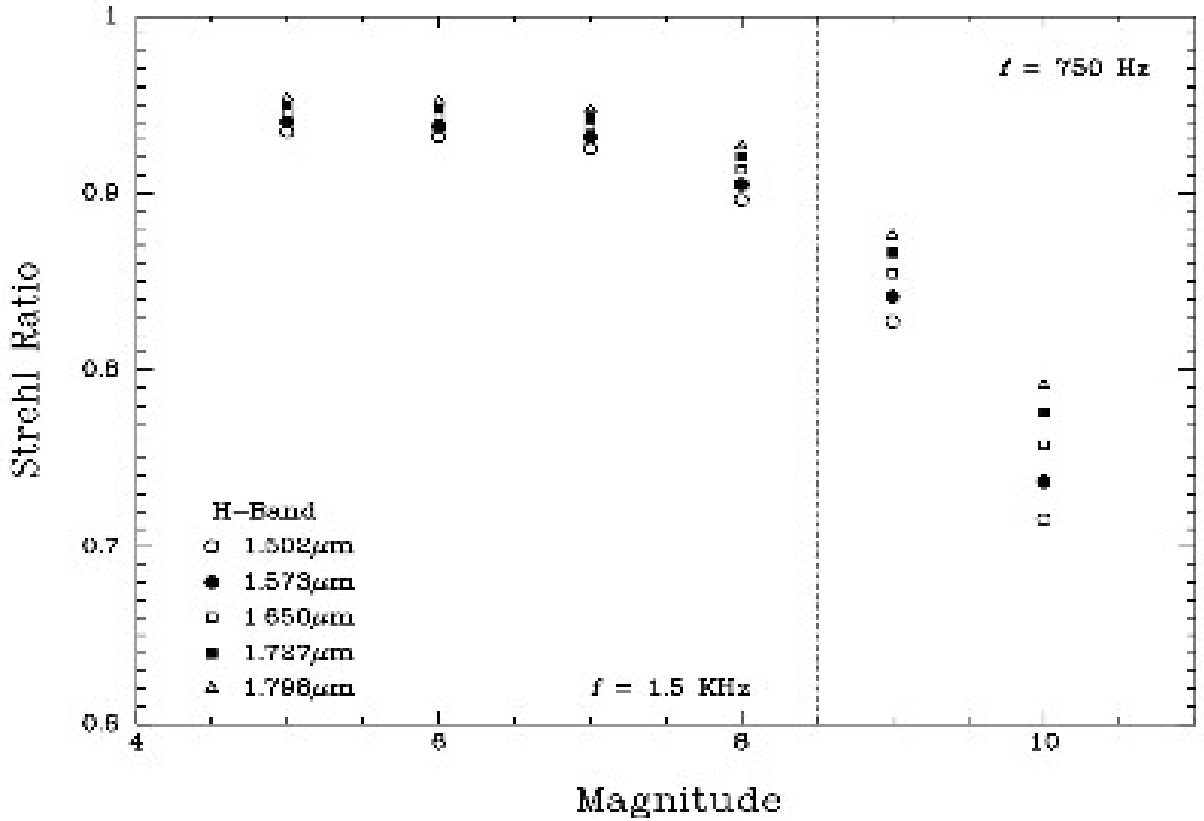

Plot of the simulated GPI H-Band Strehl performance as function of AO Guide Star I magnitude

Sphere at VLT: SAXO (Adaptive Optics), IFS (IFU spectroscopy in Y, J, H bands), IRDIS (imaging + spectroscopy), ZIMPOL (polarimetry)

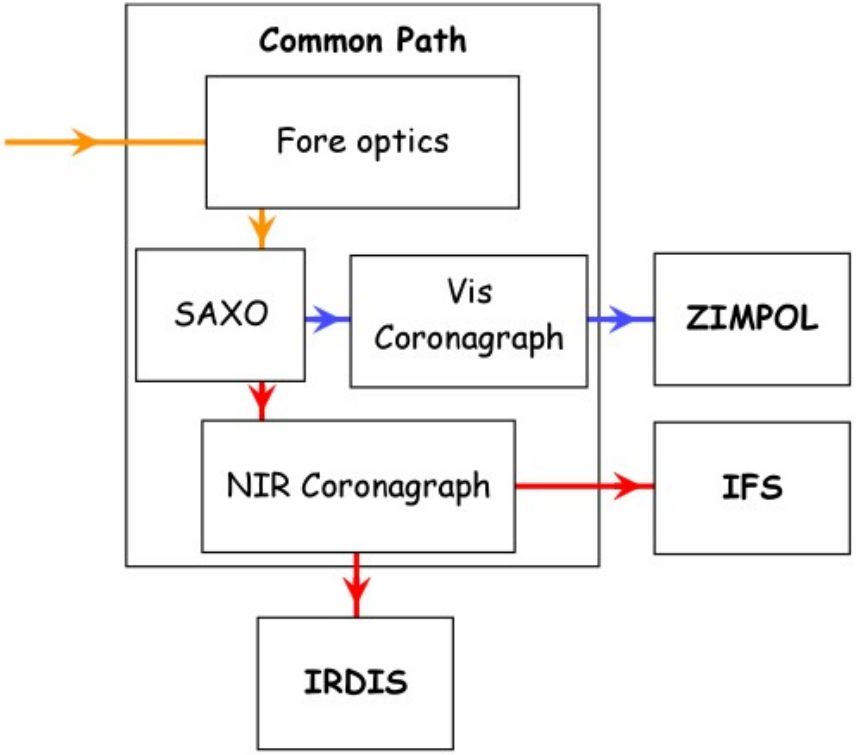

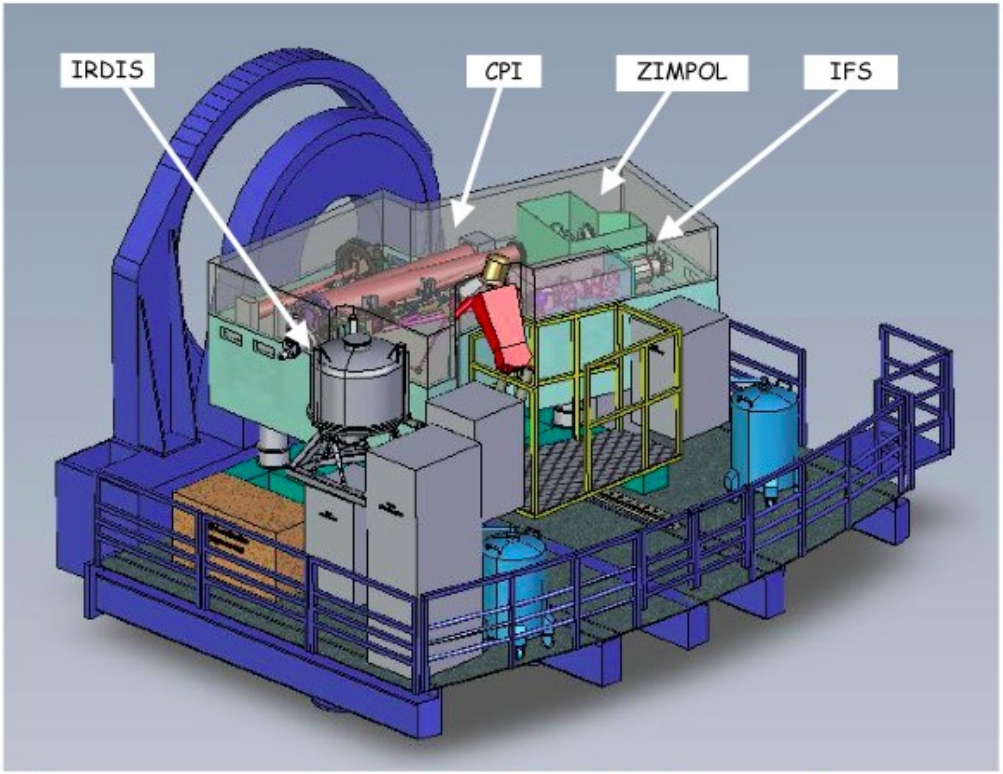

Figure 1: SPHERE sub-systems (left) including the common path (CPI) with adaptive optics system SAXO, coronagraphs, and sub-instruments IRDIS, IFS and ZIMPOL. Left: schematic view of the instrument on the Nasmyth platform.

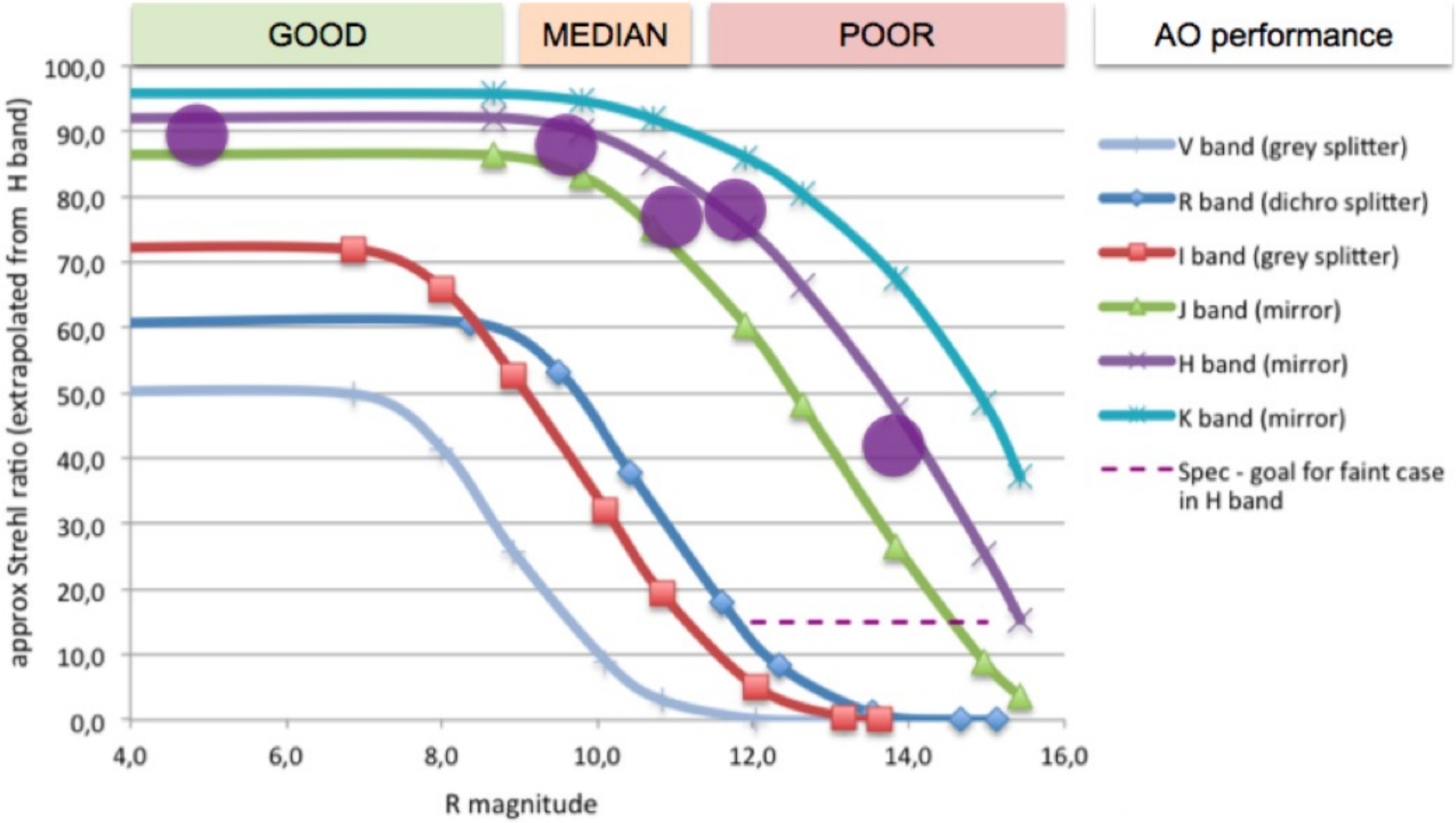

Figure 11: Theoretical and measured (purple circles) SPHERE-SAXO Strehl ratio as a function of R magnitude for good seeing conditions and different wavelength ranges from V to K (see Table 9 and Table 10 for details).

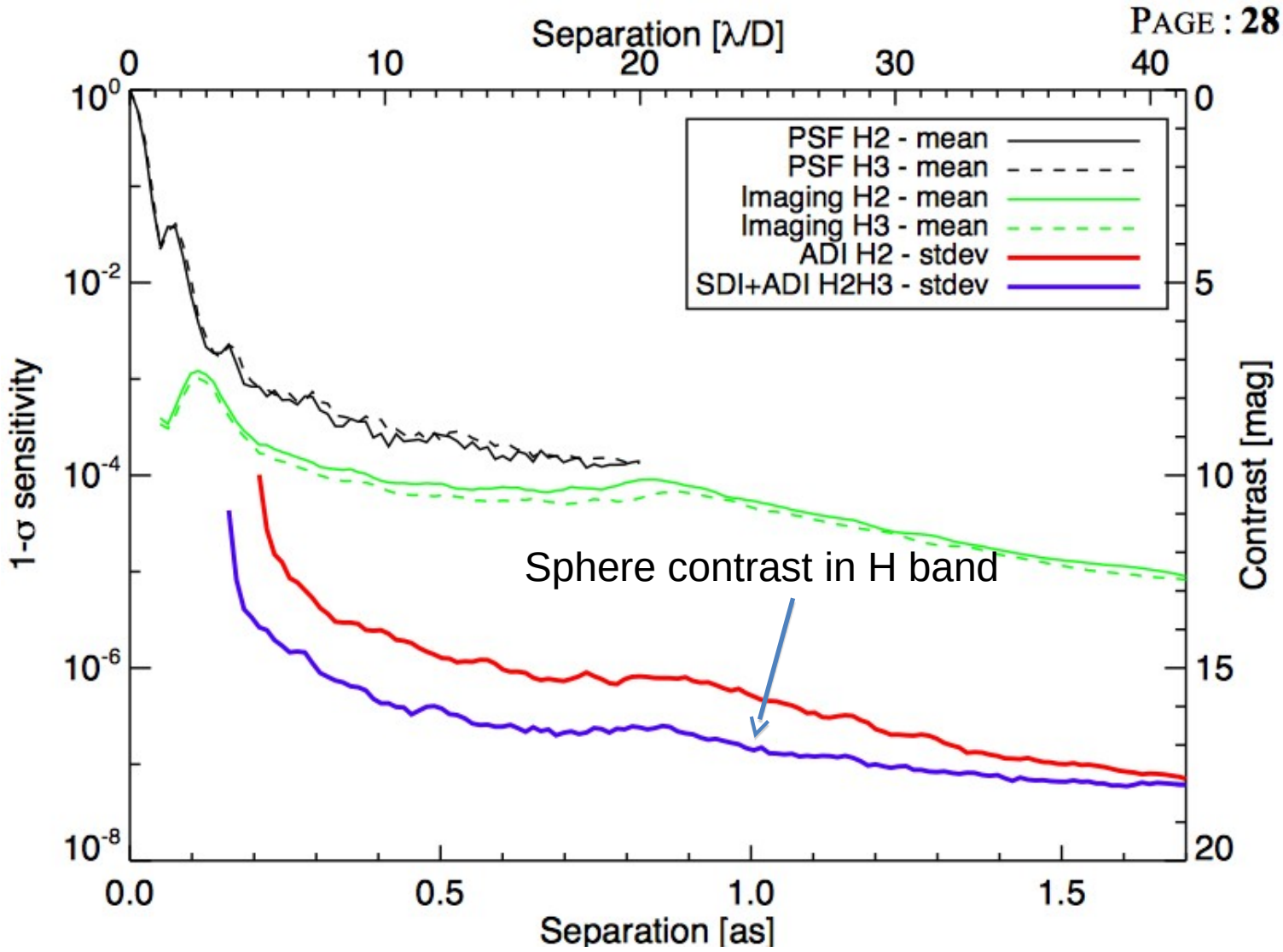

Figure 15: IRDIS DBI H2H3 contrast curves obtained on-sky for a bright target (H=0.2), in average conditions (seeing ~1.0”), with an ADI field rotation of 30 degrees. The plot shows the PSF profiles (black) and coronagraphic profiles (green) in the H2 and H3 filters, the 1σ contrast curve for ADI on the H2 data (red), and the 1σ contrast curve for SDI+ADI on the H2 and H3 data. For the ADI and SDI+ADI analysis, the algorithm throughput is taken into account and compensated, assuming a T8 spectral-type for the planet in SDI.

- Both are powerful instruments
- Sphere is faster (in 1 shot Y, J, H spectra & photometry in K)
- GPI can take spectra in K band

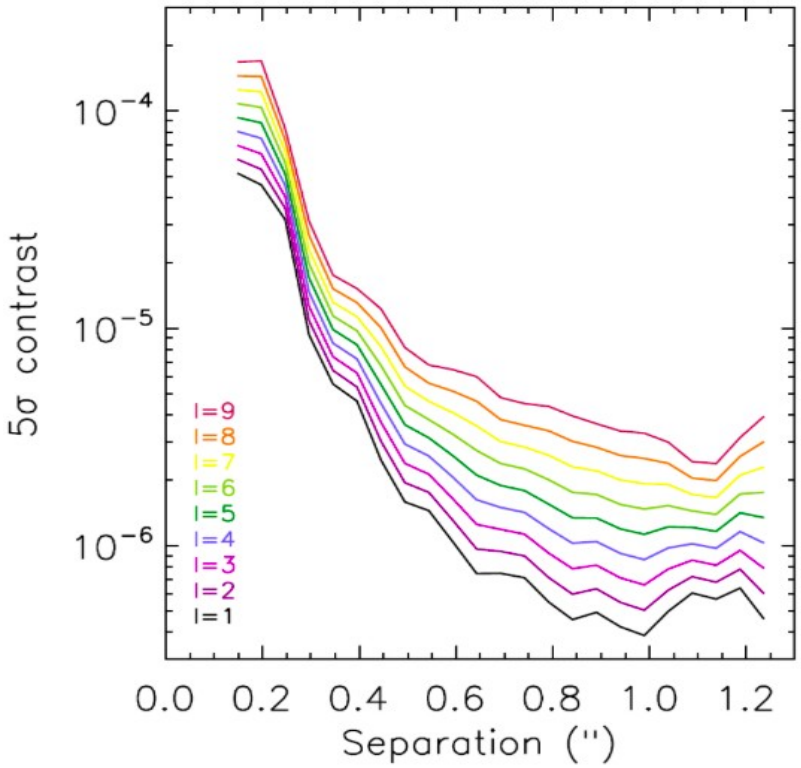

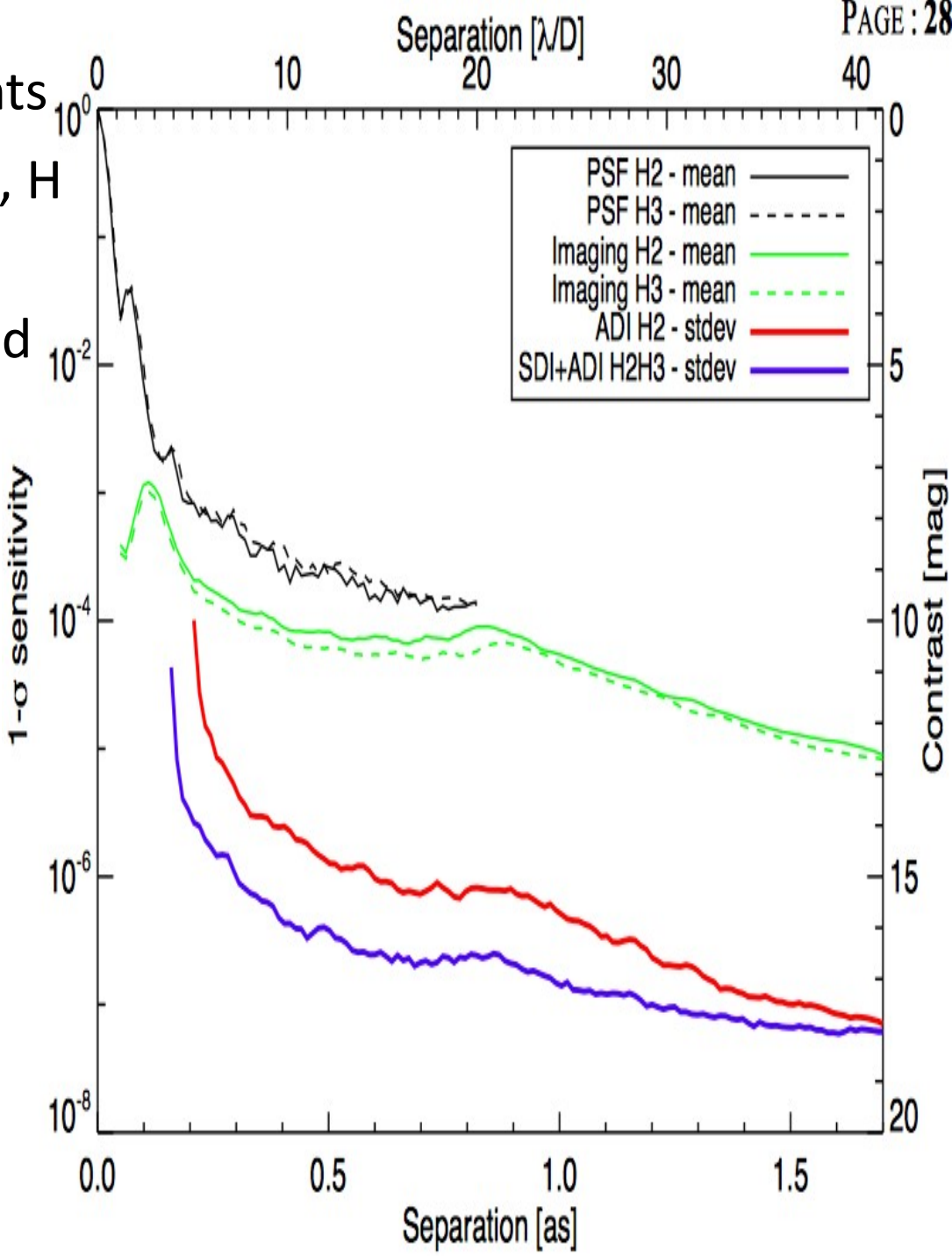

GPI 1.0 vs Sphere

http://www.gemini.edu/instrumentation/future-instruments/gpi2

Latest News

May 2022

GPI 1.0 has been shipped on May 6th to the University of Notre Dame in Indiana, where the upgrades will be taking place.

August 2020

GPI 1.0 is decommissioned at Gemini South, after being in nearly continuous operation since 2013.

What is GPI 2.0?

Gemini Planet Imager 2.0 (GPI 2.0) is an upgrade of the GPI instrument previously located at Gemini South. The upgrade includes an enhanced high-sensitivity wavefront sensor, newcoronagraph masks with smaller inner working angles or higher throughput, new spectrographic modes, and software/operability improvements. GPI 2.0 is an extreme adaptive-optics imaging polarimeter and integral-field spectrometer, which will provide diffraction-limited data between 0.97 and 2.4 microns with a Strehl Ratio in H-band of ~0.9 down to 12th magnitude stars and will continue to operate, albeit with a decreased performance, beyond the 14th magnitude. The system should provide contrast ratios of 10^7 for companions at separations of 0.2-1.0" in a 1-2 hour observation thanks to an upgrade of its coronagraph. The science instrument will also be upgraded to provide a single-shot YJHK spectroscopy at R~12 and higher spectral resolution in single bands (R~40 in H-band). The control software will be updated to significantly increase the efficiency and robustness of GPI operations. The dual-beam polarimetry will remain unchanged. GPI 2.0 will still be capable of detecting point sources down to H=20, with ≥5σ, in 1 hour in absence of photon noise from a bright companion.

- AO operable 0-14th mag, with a graceful degradation after 13th mag
- Strehl ratio 0.9 for stars brighter than H=12
- contrast ratio 10^7 at separations 0.2-1.0"
- wavelength range 0.97-2.4μm
- plane options
  - coronagraphy (APLC)
  - direct (no APLC)
  - non-redundant mask (NRM)
- IFU spectroscopy
  - single-shot YJHK at R~12
  - single-band at R~40
  - 2.7" square field of view
  - 0.014" per lenslet spatial sampling
- polarimetry
  - dual-channel polarimetry
  - Y, J, H and K bands

With this configuration, GPI will become competitive:

- lower mass planets in younger stars
- higher mass planets in older stars
- closer (4 - 10 AU) orbits
- distribution peak of giant planets around solar-type stars
- differentiate between cold-start (core accretion) and hot-start (disk collapse) formation models
- very young stars & transitional disks
- planet variability and abundances
- AGN jets, both spectroscopic and polarimetric
-asteroids & other solar system bodies

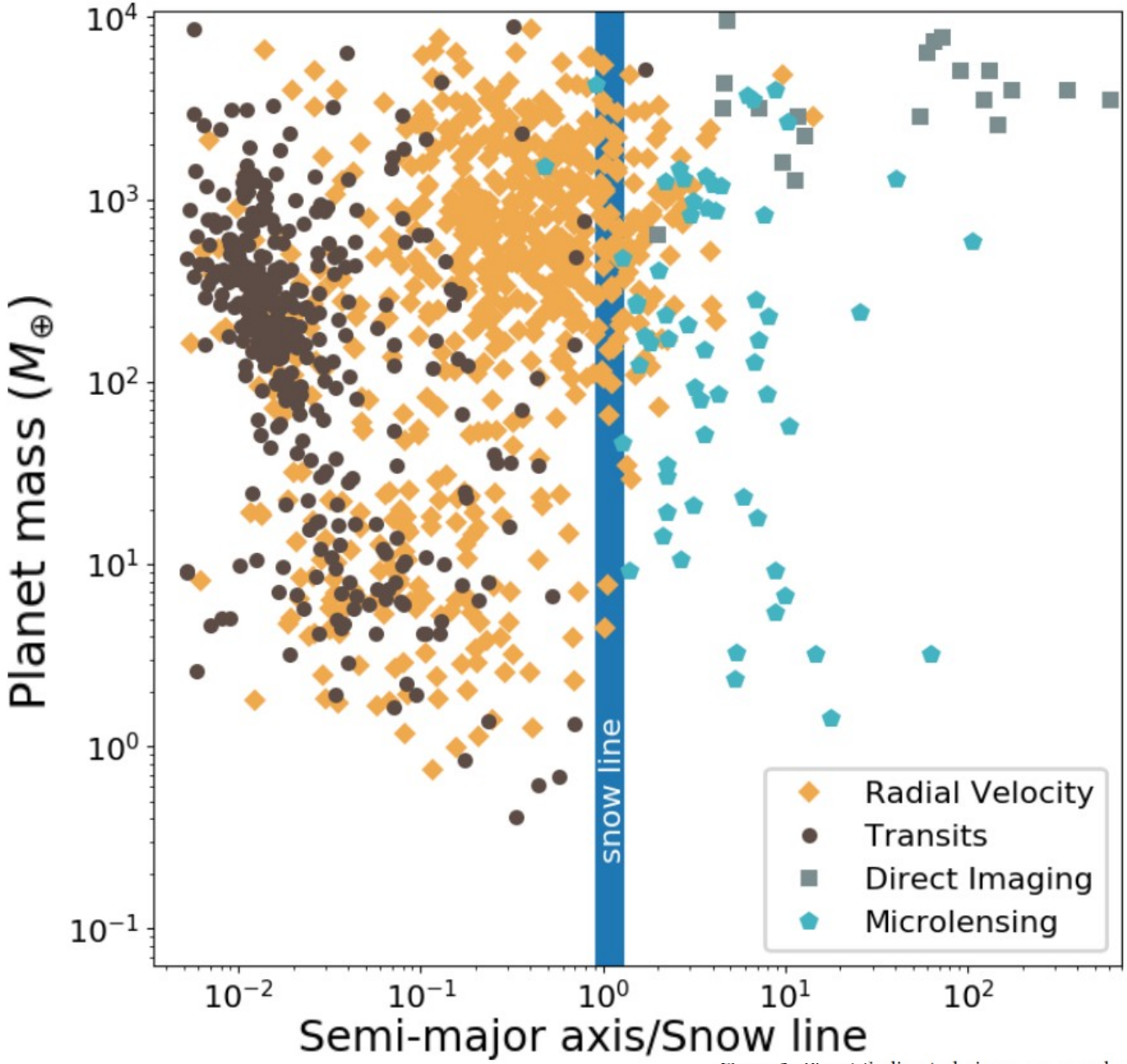

Técnica de **imageamento** é importante para estudar planetas jovens e distantes

Figure 1. Planet-finding techniques are complementary. This "orbit size-vs-planet mass" diagram shows all reported exoplanets to-date. The semi-major axis has been scaled to the approximate location of the snow line of the planet-hosting star (assuming $a_{snow} \approx 2.85 M_*^{3/2}$AU). Transits and radial velocity are exceptionally good at finding "hot" planets close to their host stars, whereas microlensing and direct imaging are more efficient in discovering "cold" planets. *[Figure based on data from the NASA*

(c) Yiannis Tsapras, 2018

Método de detecção: imageamento

- Método funciona bloqueando a luz da estrela central.
- É usado a região do infravermelho, pois o contraste é melhor (estrela brilha menos e planeta brilha mais).
- Funciona geralmente em objetos jovens, pois planetas jovens são mais brilhantes.

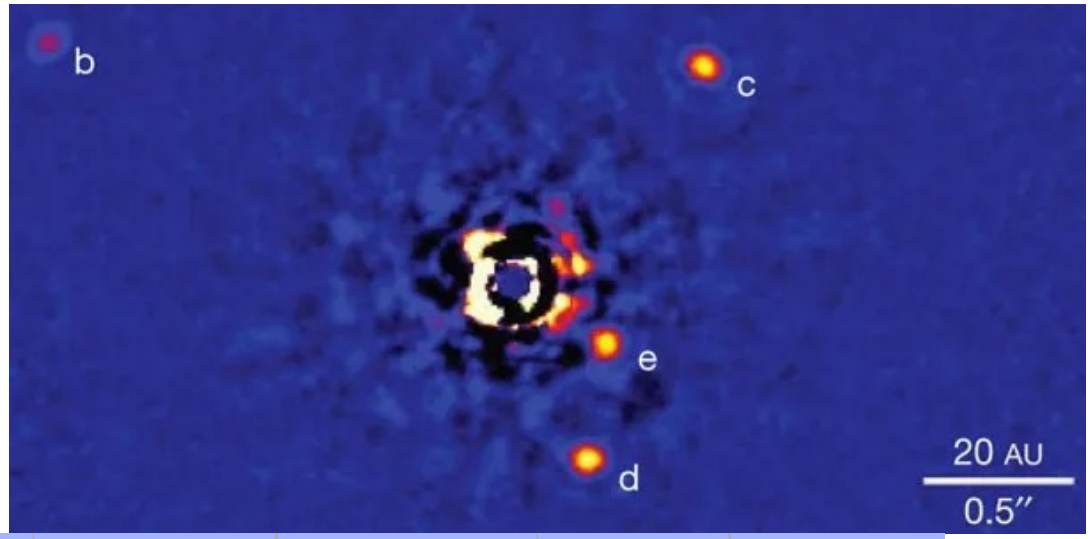

Exoplanetas da estrela jovem HR 8799 (30 Myr)

(c) Marois et al (2010)

Observatório Keck

Companion (in order from star)	Mass	Semimajor axis (AU)	Orbital period (years)	Eccentricity	Inclination	Radius
e	7.4 ±0.6 M_J	16.25 ±0.04	~45	0.1445 ±0.0013	25 ± 8°	1.17 $^{+0.13}_{-0.11}$ R_J
d	9.1 ±0.2 M_J	26.67 ±0.08	~100	0.1134 ±0.0011	28°	1.2 $^{+0.1}_{-0}$ R_J
c	7.8 ±0.5 M_J	41.39 ±0.11	~190	0.0519 ±0.0022	28°	1.2 $^{+0.1}_{-0}$ R_J
b	5.7 ±0.4 M_J	71.6 ±0.2	~460	0.016 ±0.001	28°	1.2 $^{+0.1}_{-0.1}$ R_J

Método de detecção: imageamento

Imagem infravermelha do Observatório Europeu do Sul, mostrando o disco de detritos ao redor da estrela jovem Beta Pictoris (23 Myr) e o planeta Beta Pictoris b, descoberto inicialmente em 2008.

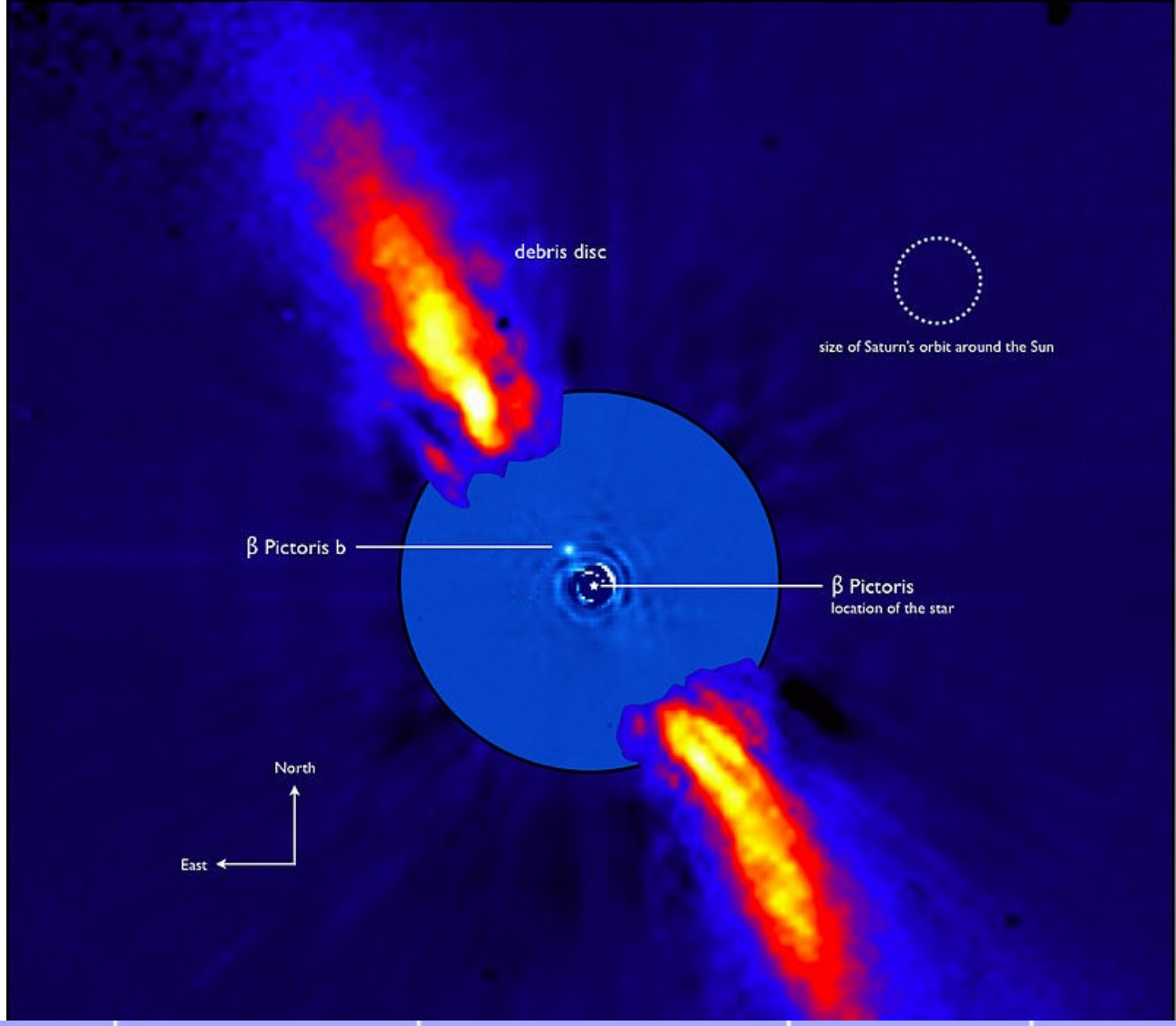

Planeta (a partir da estrela)	Massa	Semieixo maior (UA)	Período orbital (d)	Excentricidade orbital	Inclinação (°)	Raio
b	$12^{+4}_{-3}\ M_J$	$9{,}2^{+0{,}4}_{-1{,}5}$	7890 ± 1000	~0,1	89,01 + 0,36	1,65 R_J

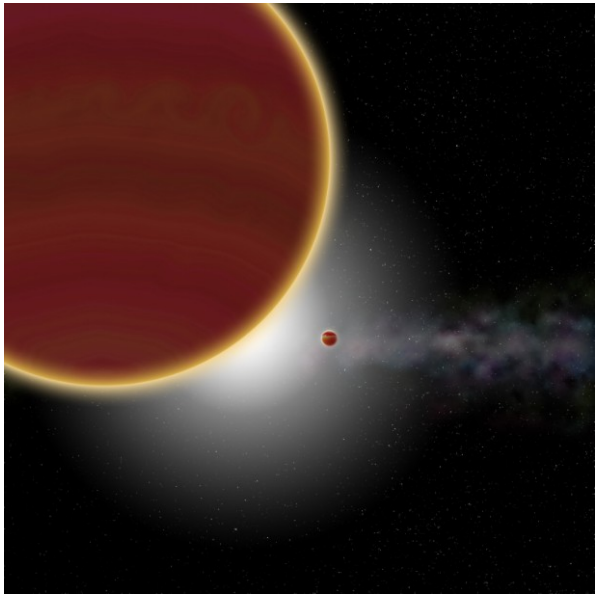

Imagem artística do planeta Beta Pictoris c

(c) Pascal Rubini / A-M Lagrange

nature astronomy

Article | Published: 19 August 2019

Evidence for an additional planet in the β Pictoris system

A.-M. Lagrange ✉, Nadège Meunier, Pascal Rubini, Miriam Keppler, Franck Galland, Eric Chapellier,

Novo planeta descoberto em Agosto de 2019, Beta Pictoris c, usando o método de velocidades radiais, com 10 anos de observações obtidas com o HARPS/ESO

The Beta Pictoris planetary system

Companion (in order from star)	Mass	Semimajor axis (AU)	Orbital period (days)	Eccentricity	Inclination	Radius
c	$9\ M_J$	2.7	1200	0.24	—	—
Inner belt	6.4 AU				~89°	—
b	$12^{+4}_{-3}\ M_J$	$9.2^{+0.4}_{-1.5}$	7890 ± 1000	~0.1	89.01 + 0.36°	$1.65\ R_J$
secondary disk	130+ AU				89 ± 1°	—
main disk	16–1450/1835 AU				89 ± 1°	—

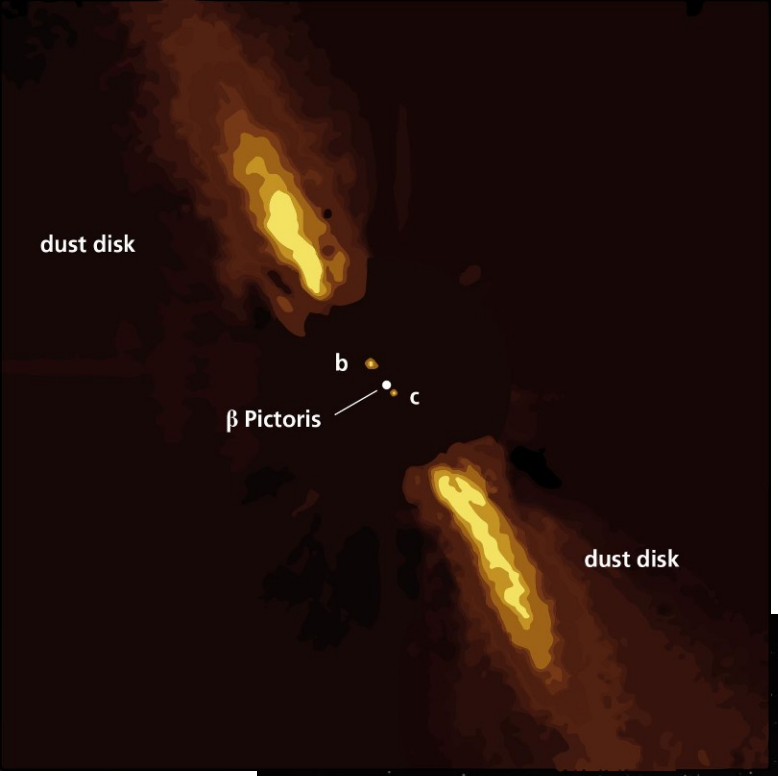

Published online 02 October 2020

A&A 642, L2 (2020)

Letter to the Editor

Direct confirmation of the radial-velocity planet β Pictoris c

M. Nowak[1,2], S. Lacour[3,7], A.-M. Lagrange[4], P. Rubini[24], J. Wang[10], T. Stolker[27], R. Abuter[7], A. Amorim

Atualização (2020) para as massas:

β Pictoris c: 8.2 ± 0.8 M_{jup},

β Pictoris b: 9.0 ± 1.6 M_{Jup}

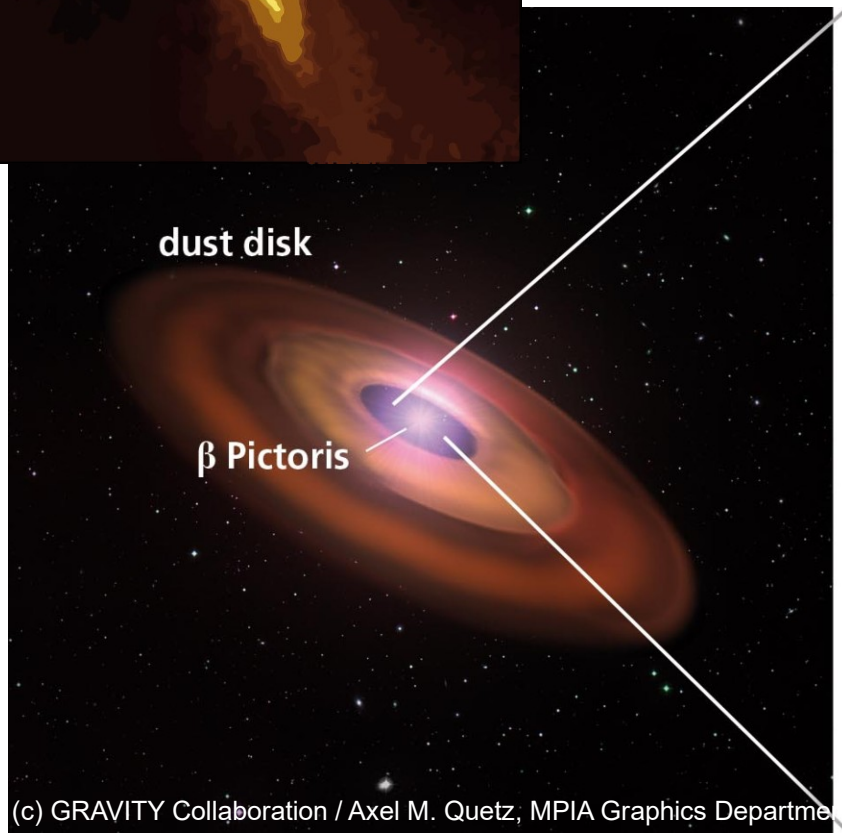

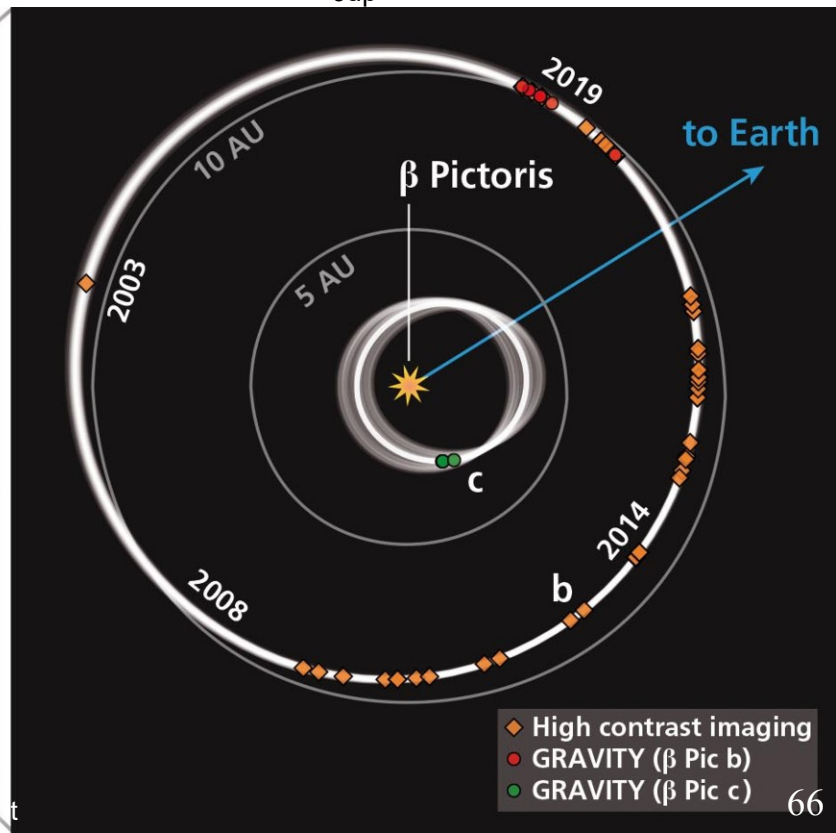

(c) GRAVITY Collaboration / Axel M. Quetz, MPIA Graphics Department

Futuro: Roman Space Telescope (WFIRST), 2027

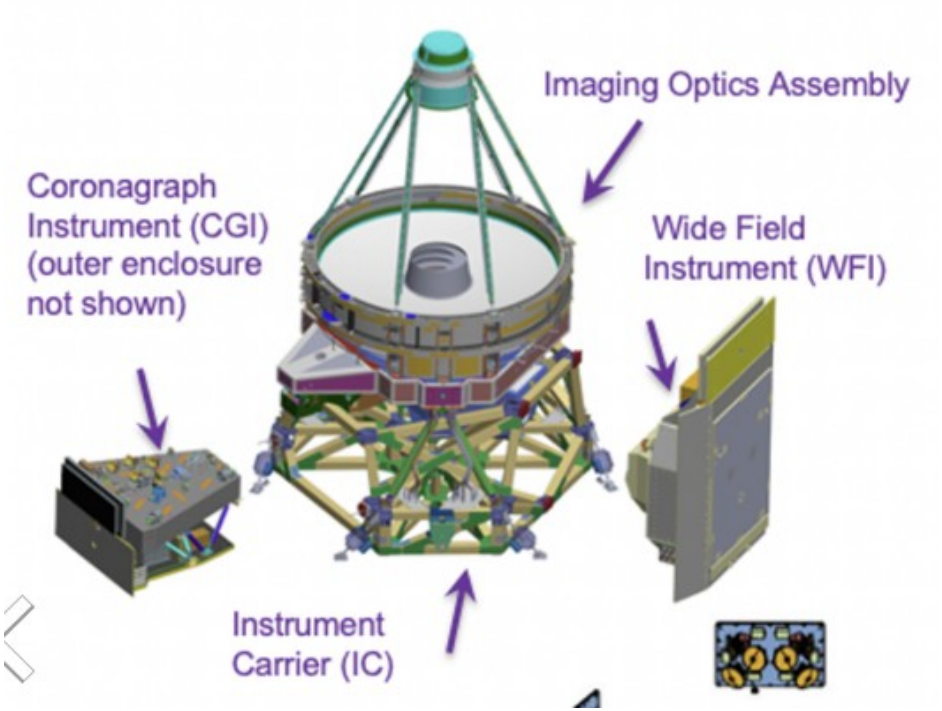

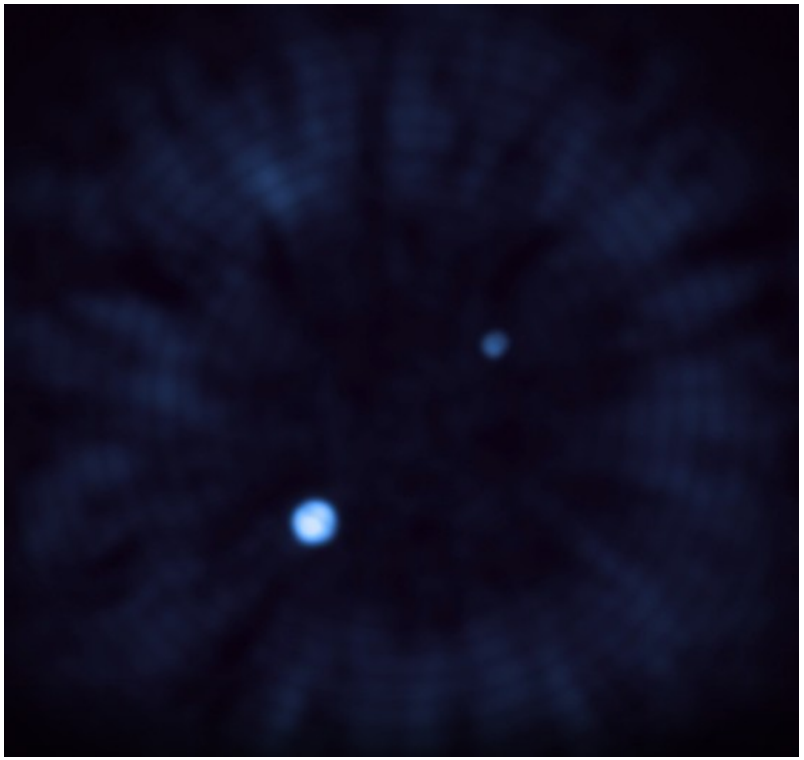

Futuro: Habitable Worlds Observatory (HWO), 2040?

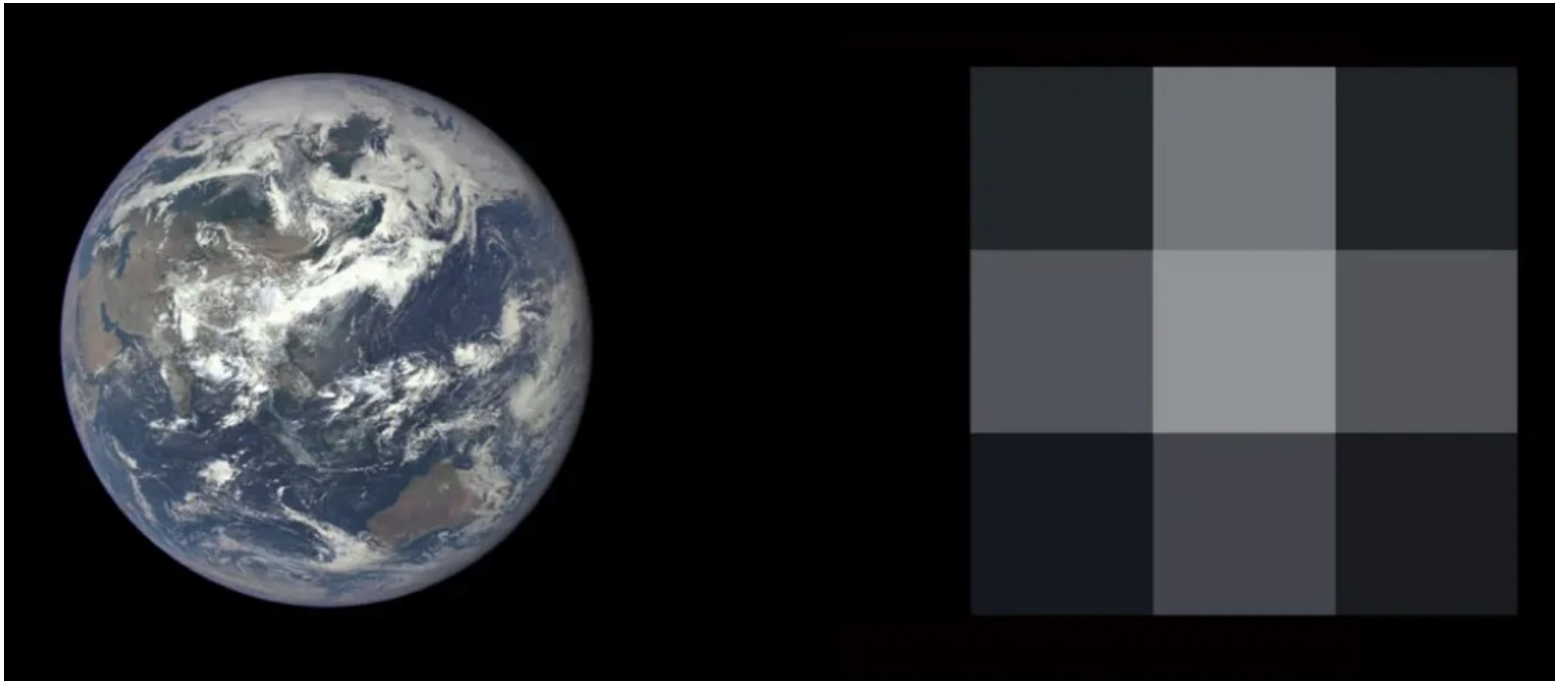

- 9 star systems within 10 light-years of Earth,
- 22 star systems within 12 light-years of Earth,
- 40 star systems within 15 light-years of Earth,
- and 95 star systems within 20 light-years of Earth.

Futuro: Habitable Worlds Observatory (HWO), 2040?

- that launches as early as the late 2030s/early 2040s,
- that's on-budget and on-time,
- that possesses the necessary architecture to achieve its observational goals without needing a starshade,
- that's fully refuellable and whose instruments are fully serviceable and replaceable,
- that could have a starshade added to it at any point in the future,
- and that quite possibly images enough "Earth-like" planets to discover at least one (and maybe even more than one) exoplanet that's actually inhabited.

Futuro: Habitable Worlds Observatory (HWO), 2040?

Sample	F	G	K	M
Tier A	14	15	17	1
Tier B	15	23	11	2
Tier C	37	17	12	0
Total (A+B+C)	66	55	40	3

Serão observadas principalmente estrelas de tipo solar (F, G, K).
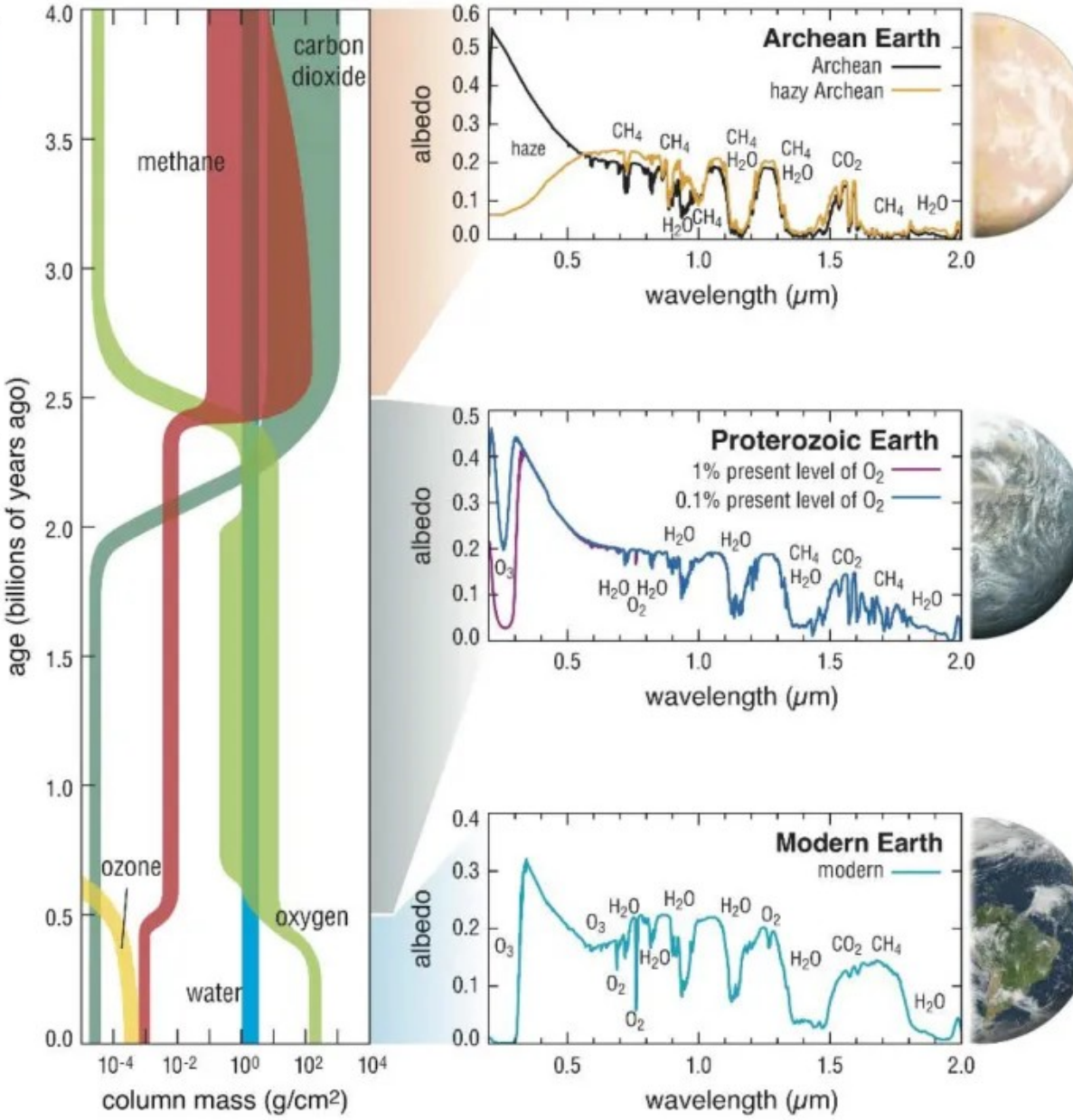
Grupo SAMPA/IAG-USP deve ajudar a caracterizar as propriedades das estrelas *target* do HWO